



NTNU – Trondheim
Norwegian University of
Science and Technology

Analysis of the Trilateral Flash Cycle for Power Production from low Temperature Heat Sources

Stian Trædal

Master of Science in Mechanical Engineering

Submission date: June 2014

Supervisor: Trygve Magne Eikevik, EPT

Co-supervisor: Daniel Rohde, SINTEF Energy Research
Brede Hagen, SINTEF Energy Research

Norwegian University of Science and Technology
Department of Energy and Process Engineering

EPT-M-2014-121

MASTER THESIS

for

Student Stian Trædal

Spring 2014

Analysis of the Trilateral Flash Cycle for power production from low temperature heat sources*Analyse av "Trilateral Flash Cycle" for kraftproduksjon fra varmekilder ved lav temperatur***Background and objective**

Utilizing renewable heat sources for electricity production is an important part of meeting the world's energy demand. This includes industrial heat at low to medium temperature which is often released to the ambient and therefore wasted.

The Organic Rankine Cycle (ORC) is now a well-established technology for power production from low to medium temperature heat sources. This technology is challenged by the Trilateral Flash Cycle (TFC), which is still in a state of technical development. It has been known to be efficient for a long time, but the two-phase expansion has been a barrier to realization. Lately, two-phase expanders have been developed which reach efficiencies up to 80% and thus make the TFC economically interesting for many applications.

Identifying possible applications by a thorough thermodynamic analysis of the cycle and its characteristics will be the main objective of the thesis.

The following tasks are to be considered:

1. Literature survey on the TFC and its components
2. Further development of an in house calculation tool (Excel), including
 - a. Pressure drop and heat transfer correlations in the heat exchanger models
 - b. Improved heat exchanger size estimates
 - c. Improved expander efficiency calculation
 - d. Advanced cycle configurations
3. Evaluate working fluids for the TFC
4. Make a scientific paper of the main results from the work
5. Make proposal for further work

-- " --

Within 14 days of receiving the written text on the master thesis, the candidate shall submit a research plan for his project to the department.

When the thesis is evaluated, emphasis is put on processing of the results, and that they are presented in tabular and/or graphic form in a clear manner, and that they are analyzed carefully.

The thesis should be formulated as a research report with summary both in English and Norwegian, conclusion, literature references, table of contents etc. During the preparation of the text, the candidate should make an effort to produce a well-structured and easily readable report. In order to ease the evaluation of the thesis, it is important that the cross-references are correct. In the making of the report, strong emphasis should be placed on both a thorough discussion of the results and an orderly presentation.

The candidate is requested to initiate and keep close contact with his/her academic supervisor(s) throughout the working period. The candidate must follow the rules and regulations of NTNU as well as passive directions given by the Department of Energy and Process Engineering.

Risk assessment of the candidate's work shall be carried out according to the department's procedures. The risk assessment must be documented and included as part of the final report. Events related to the candidate's work adversely affecting the health, safety or security, must be documented and included as part of the final report. If the documentation on risk assessment represents a large number of pages, the full version is to be submitted electronically to the supervisor and an excerpt is included in the report.

Pursuant to "Regulations concerning the supplementary provisions to the technology study program/Master of Science" at NTNU §20, the Department reserves the permission to utilize all the results and data for teaching and research purposes as well as in future publications.

The final report is to be submitted digitally in DAIM. An executive summary of the thesis including title, student's name, supervisor's name, year, department name, and NTNU's logo and name, shall be submitted to the department as a separate pdf file. Based on an agreement with the supervisor, the final report and other material and documents must be given to the supervisor in digital format. All relevant data collected and produced during the project shall be delivered to the supervisor on a CD at the end of the project.

- Work to be done in lab (Water power lab, Fluids engineering lab, Thermal engineering lab)
 Field work

Department of Energy and Process Engineering, January 14th 2014



Prof. Olav Bolland
Department Head



Prof. Trygve M. Eikevik
Academic Supervisor

Research Advisor:

Daniel Rohde, SINTEF Energy Research, e-mail: daniel.rohde@sintef.no


Brede Hagen, SINTEF Energy Research, e-mail: brede.hagen@sintef.no

Preface

This is the written work of my Master thesis at the Norwegian University of Science and Technology (NTNU), Department of Energy and Process Engineering. The work is a continuation of the work done in my project thesis in the fall 2013.

The purpose of this study is to analyze the Trilateral Flash Cycle and the Partially Evaporating Cycle for power production from low temperature heat sources, and compare the performance with today's leading technology, the Organic Rankine Cycle.

I would like to thank my supervisor Prof. Trygve M. Eikevik (NTNU), and co-supervisor Daniel Rohde (SINTEF Energy Research) for the help they have given me during this work.



Stian Trædal

08.06.2014

Summary

In this study, the Trilateral Flash Cycle (TFC) and the Partially Evaporating Cycle (PEC) have been analyzed and compared to the Organic Rankine Cycle (ORC) for power production from low temperature heat sources. This study is a continuation of the work done in my project thesis fall 2013.

The ORC is a well-known technology that is in use in several plants today. The TFC and PEC on the other hand are still in a state of technical development. The biggest challenge for the TFC and PEC is the required two-phase expansion. Lately, two-phase expanders with high efficiencies have been developed, which makes the TFC and PEC economically interesting.

Currently, only a few studies on the TFC and PEC can be found, and most of them are theoretical considerations. All of these studies finds the TFC promising for low temperature heat sources, which was also the findings of my project thesis. The PEC is found to be promising for smaller systems where the working fluid pump efficiency is low.

The TFCs main difference from the ORC is that the heating process ends at the boiling point of the working fluid, i.e. there is no evaporation and superheating. This leads to a better temperature match between the working fluid and the heat source, such that more heat can be transferred to the working fluid. Power is produced in a two-phase expander after the heating process. The cost pr. kWh for TFC systems have been estimated to be lower than for ORC systems due to the elimination of the evaporator, separator drum, gear box, lube oil system and the fact that simpler heat exchangers can be used.

In the PEC, the working fluid is allowed to be partially evaporated during the heating process. This is done in an attempt to combine the advantages of the TFC and the ORC.

The ORC, TFC and PEC have been simulated in a Microsoft Excel calculation tool, using Visual Basic for Applications. The simulations include detailed heat exchanger models to calculate heat transfer coefficients and pressure losses, and two-phase expander efficiency models for the TFC and PEC. The three cycles have been simulated and optimized for maximum net power production for three cases using different heat source temperatures. Air with a mass flow of 10 kg/s and temperatures of 100, 150 and 200 °C are used for Case I, Case II and Case III respectively. Water at 20 °C is used as the heat sink. The three cases are simulated with eight different working fluids, R123, R134a, R245fa, R1234ze(E), butane, pentane, isopentane and propane with maximum heat exchanger areas of 1000, 1500, 2000,

2500, 3000, 3500 and 4000 m². Different performance parameters are calculated and used to compare the performance of the ORC, TFC and PEC, and the different working fluids.

The results show that the TFC has the lowest power production for all cases, and the largest estimated system size. Both the total heat exchanger area and expander outlet volume flow are generally higher for the TFC systems, especially for the lower heat source temperature cases. For the 100 °C and 150 °C cases the power production for the TFC and ORC is in the same range. Since TFC systems are estimated to have a lower cost than ORC systems, they can be suitable for systems with heat sources in this range when system size is not a critical factor.

The PEC does not show any advantage over the ORC for the cases analyzed here.

This study shows less promising results for the TFC than my project thesis and other published studies. This is mainly due to the variable two-phase expander efficiency used here, and that none of the other studies considers pressure losses in the system or calculation of heat transfer coefficients for each working fluid.

A scientific paper on the main results from the study before the simulation of the PEC and inclusion of the heat exchanger models is given in Appendix C. This paper has been submitted to the journal *Energy*. A scientific paper on the final results of the study is given in Appendix D. This paper has been submitted to the *Gustav Lorentzen Conference*.

Sammendrag

I denne studien blir Trilateral Flash Cycle (TFC) og Partially Evaporating Cycle (PEC) analysert og sammenlignet med Organic Rankine Cycle (ORC) for kraftproduksjon fra varmekilder ved lav temperatur. Denne studien er en fortsettelse på arbeidet gjort i prosjektarbeidet mitt høst 2013.

ORC er en velkjent teknologi som er i bruk i mange kraftverk i dag. TFC og PEC er på den andre siden fortsatt i et teknisk utviklingsstadium. Den største utfordringen i TFC og PEC er to-fase ekspansjonen som kreves. To-fase ekspandere med høy virkningsgrad har nylig blitt utviklet, hvilket gjør TFC og PEC økonomisk interessante.

Det finnes så langt bare noen få studier av TFC og PEC i litteraturen, og de fleste er teoretiske. Felles for disse studiene er at de alle gir lovende resultater for TFC for varmekilder ved lave temperaturer, hvilket også var resultatet i prosjektarbeidet mitt. Resultatene for PEC er lovende for mindre systemer der arbeidsmediepumpen har lav virkningsgrad.

Hovedforskjellen mellom TFC og ORC er at for TFC ender oppvarmingen ved kokepunktet til arbeidsmediet, slik at det ikke er noen fordampning og overhetning. Dette fører til en bedre temperatur match mellom arbeidsmediet og varmekilden, slik at varmekilden utnyttes bedre. Kraft produseres i en to-fase ekspander etter oppvarmingen. TFC systemer er estimert til å koste mindre pr. kWh produsert på grunn av eliminering av fordamper, separator, girkasse, smøreoljesystem, og det faktum at enklere varmevekslere kan benyttes.

I PEC blir arbeidsmediet delvis fordampet i oppvarmingsprosessen. Dette blir gjort i et forsøk på å kombinere fordelene ved TFC og ORC.

De tre kraftsyklusene er simulert i et Microsoft Excel beregningsverktøy som benytter Visual Basic for Applications. Simuleringene inneholder detaljerte varmeveksler modeller for beregning av varmeovergangskoeffisienter og trykktap, samt to-fase ekspander virkningsgradmodeller for TFC og PEC. Syklusene er simulert og optimalisert for maksimal netto kraftproduksjon for tre caser med forskjellig varmekilde temperatur. Luft med massestrøm 10 kg/s og temperaturene 100, 150 og 200 °C blir brukt for henholdsvis Case I, Case II og Case III. Vann ved 20 °C blir brukt som varmesluk. De tre casene er simulert med åtte forskjellige arbeidsmedier, R123, R134a, R245fa, R1234ze(E), butan, pentan, isopentan og propan med maksimalt varmeveksler areal på 1000, 1500, 2000, 2500, 3000, 3500, og

4000 m². Forskjellige ytelses parametere blir beregnet og brukt til å sammenligne ORC, PEC og TFC, og de forskjellige arbeidsmediene.

Resultatene av denne studien viser at TFC har lavest kraftproduksjon for alle de undersøkte casene, mens system størrelsen er estimert å være størst for TFC. Både totalt varmeveksler areal og volumstrøm ved ekspander utløpet er generelt høyere for TFC, spesielt for de laveste varmekilde temperatur casene. For 100 °C og 150 °C casene er kraftproduksjonen for TFC og ORC i samme størrelsesorden. Siden TFC systemer er estimert til å ha lavere kostnader enn ORC systemer kan de være passende for systemer med varmekilder i dette området der systemstørrelse ikke er en kritisk faktor.

PEC viser ingen fordel over ORC for casene som er analysert i denne studien.

Denne studien gir mindre lovende resultater for TFC enn prosjektarbeidet mitt og andre publiserte studier. Dette er hovedsakelig på grunn av den variable to-fase ekspander virkningsgraden brukt her, og at ingen av de andre studiene tar hensyn til trykktap i systemet eller beregner varmeovergangskoeffisient for hvert arbeidsmedium.

En vitenskapelig artikkel med hovedresultatene fra studiet før simuleringen av PEC og inkluderingen av varmeveksler modellen er gitt i Appendix C. Denne artikkelen er sendt inn til journalen *Energy*. En vitenskapelig artikkel med de endelige resultatene fra studiet er gitt i Appendix D. Denne artikkelen er sendt inn til *Gustav Lorentzen konferansen*.

Table of contents

1	Introduction.....	1
2	Objectives	3
3	Theory of ORC, TFC, PEC, heat exchangers and two-phase expanders.....	4
3.1	Description of the Organic Rankine Cycle	4
3.2	Description of the Trilateral Flash Cycle	5
3.3	Description of the Partially Evaporating Cycle.....	6
3.4	Supply and removal of heat to the cycles.....	7
3.5	Working fluids.....	8
3.6	Heat exchangers	9
3.6.1	Plate finned-tube heat exchangers	9
3.6.2	Plate heat exchangers	10
3.7	Two-phase expanders	12
3.7.1	Screw expanders	12
3.7.2	Variable Phase Turbine.....	13
4	Literature review	16
4.1	Studies of the TFC and PEC	16
5	Methodology	21
5.1	Software	21
5.2	Cycle simulations	21
5.2.1	Simulation of the ORC.....	23
5.2.2	Simulation of the TFC	27
5.2.3	Simulation of the PEC	30
5.3	Macros.....	32
6	Heat exchanger models	33
6.1	Heating process	33
6.1.1	Heat transfer coefficients and pressure losses	33

6.1.2	Heater geometry.....	39
6.2	Condensing process.....	40
6.2.1	Heat transfer coefficients and pressure losses	41
6.2.2	Condenser geometry	44
7	Case Studies.....	46
7.1	Case definition.....	46
7.2	Working fluid selection.....	48
8	Results.....	50
8.1	Case I, heat source: 10 kg/s air at 100 °C	50
8.2	Case II, heat source: 10 kg/s air at 150 °C	52
8.3	Case III, heat source: 10 kg/s air at 200 °C.....	53
8.4	Discussion	54
9	Conclusions.....	58
10	References.....	60
11	Appendix A: Results for all working fluids.....	1
12	Appendix B: Working fluid properties	10
13	Appendix C: Scientific paper submitted to Energy	11
14	Appendix D: Scientific paper submitted to the Gustav Lorentzen conference.....	28
15	Appendix E: Important macros.....	37

List of figures

Figure 1: Ts – diagram for ORC with propane as working fluid.....	4
Figure 2: Configuration of a TFC system	5
Figure 3: Ts – diagram for TFC. State 4 is in the wet vapor region with butane (left), and in the dry vapor region with isopentane (right) as working fluid	6
Figure 4: Ts-diagram for PEC with R245fa as working fluid	6
Figure 5: Variation in stream temperature during heat addition for ORC (left) and TFC (right).	8
Figure 6: Finned tube heat exchanger, left: (lv-soft.com), right (Incropera, DeWitt et al. 2007)	10
Figure 7: Principle schematic of a plate heat exchanger, (deltathx.com).	11
Figure 8: Plate heat exchanger, two-/two-pass arrangement (Andresen 2009)	11
Figure 9: Schematic of a screw expander (Smith, Stosic et al. 2005)	12
Figure 10: Schematic of two-phase VPT nozzle (Welch and Boyle 2009)	14
Figure 11: Schematic of flow path in two-phase VPT blades (left), and rotor (right) (Welch and Boyle 2009).....	14
Figure 12: TFC geothermal power plant, 1 MW, (Welch, Boyle et al. 2010).....	18
Figure 13: Th-diagram for ORC with propane as working fluid	23
Figure 14: Th-diagram for a TFC with propane as working fluid	28
Figure 15: Th-diagram for PEC with R245fa as working fluid	30
Figure 16: Condenser geometry	44
Figure 17: Case I, Net power for TFC, PEC and ORC for the five best working fluids	50
Figure 18: Case II, Net power for TFC, PEC and ORC for the five best working fluids.....	52
Figure 19: Case III, Net power for TFC, PEC and ORC for the five best working fluids	53

List of tables

Table 1: Fischer's results for the comparison between TFC and ORC for the five cases.....	17
Table 2: Zamfirescu and Dincer's results.....	19
Table 3: Calculation parameters	22
Table 4: Overview of the three cases	46
Table 5: Input data for the ORC, TFC and PEC simulations.....	46
Table 6: Input and output data for the heater and condenser calculations.....	47
Table 7: Properties of selected working fluids (Calm and Hourahan 2011, Fukuda, Kondou et al. 2014)	49
Table 8: Case I, Performance parameters and details for the two best ORCs, TFCs and PECs	51
Table 9: Case II, Performance parameters and details for the two best ORCs, TFCs and PECs	52
Table 10: Case III, Performance parameters and details for the two best ORCs, TFCs and PECs.....	54
Table 11: Average values over all working fluids for system size estimation for Case I, II and III.....	55

Nomenclature

Nomenclature		VBA	Visual Basic for Applications
$a, b, B_1, c, C_1, E,$	Constants	VLE	Vapor – Liquid Equilibrium
F, Fr_H, H, K_1, n		VPT	Variable Phase Turbine
A	Area, m ²	W	Width, m
b	Channel spacing, m	We	Weber number
D	Diameter, m	\dot{W}	Power, kW
d_v	Vapor density, kg/m ³	x	Vapor quality
f	Friction factor		
F	Forced convection enhancement factor	Greek letters	
F_p	Fin pitch, m	α	Dimensionless parameter
G	Mass flux, kg/m ²	Δ	Difference of quantities
g	Gravitational acceleration, m/s ²	ε	Exergy efficiency
$Ge_1 - Ge_4$	Functions of heat exchanger geometry, constants	η	Energy efficiency
GWP	Global Warming Potential	μ	Viscosity, Pa-s
H	Height, m	Φ_{fr}^2	Two-phase multiplier
h	Enthalpy kJ/kg and Heat Transfer Coefficient W/m ² K	σ	Surface tension, N/m
HRHE	Heat Recovery Heat Exchanger	ρ	Density, kg/m ³
j	Colburn j-factor	Φ	Fin efficiency (and heat transfer area enhancement ratio)
K	Dimensionless parameter	φ	Chevron angle
k	Conductivity, W/mK	Subscripts	
L	Length, m	0	At 0° Chevron angle
L_D	Depth, m	1	At 90° Chevron angle
LMTD	Logarithmic Mean Temperature Difference, °C	1, 2, 2', 2'', 3,	State points of working fluid in TFC and ORC
m	Quantity characterizing fin geometry	4, 4'	TFC and ORC
M	Molecular weight, kg/kmol	2r, 4r	State points of working fluid in ORC with recuperator
\dot{m}	Mass flow rate, kg/s	a	Acceleration
N	Number of tubes	Air	Air side
NP	Net Power, kW	c	Minimum flow area
Nu	Nusselt number, $Nu = \frac{h \cdot D_h}{k}$	cond	Condenser
ODP	Ozone Depleting Potential	desup	Desuperheater
ORC	Organic Rankine Cycle	Eq	Equivalent
P	Pressure, MPa	Exp	Expander
		F	Fin
		fg	Difference between saturated vapor and saturated liquid

PEC	Partially Evaporating Cycle	front	Heat exchanger front
Pr	Prandtl number, $Pr = \frac{c_p \mu}{k}$	g	Gas
P_r	Reduced pressure	h	Hydraulic
\dot{Q}	Heat extracted from the heat source, kW	H hs	Homogenous Heat sink
R	Resistance (and bend radius)	i	State point (and inside)
Re	Reynolds number, $Re = \frac{G \cdot D}{\mu}$	L	Longitudinal
R123	2,2-Dichloro-1,1,1-trifluoroethane	l	Liquid
R1234ze(E)	1,3,3,3-Tetrafluoropropene	m	Mean
R134a	1,1,1,2-Tetrafluoroethane	max	Maximum
R245fa	1,1,1,3,3-Pentafluoropropane	min	Minimum
s	Entropy, kJ/kgK	mo	motor
S	Distance between tubes, m (and pool boiling suppression factor)	O Optimum	Outside Found in optimization
T	Temperature, °C	P	Ports
t	Thickness, m	PC	Channels per pass
TFC	Trilateral Flash Cycle	pool	Pool boiling
Th	Temperature-enthalpy	T	Transverse
Ts	Temperature-entropy	t	Tube
U	Overall heat transfer coefficient, W/m ² K	TP	Two-phase
\dot{V}	Volume flow rate, m ³ /s	W	Wall
		water	Water side
		wf	Working fluid

1 Introduction

The world's energy demand is rising and the emission of greenhouse gases like CO₂ is increasing as an effect. It is therefore necessary to search for alternate energy sources, and improve existing methods for power production. In this study, the possibility of improving the power production from low temperature heat sources, such as geothermal, biomass, solar or waste heat, by using the Trilateral Flash Cycle (TFC) or the Partially Evaporating Cycle (PEC) instead of the Organic Rankine Cycle (ORC) is investigated.

The ORC is a well-established technology for power production from low to medium temperature heat sources, and is in use in several existing power plants (Fischer 2011). The TFC and PEC on the other hand are still in a state of technical development. The TFC has been known to be efficient for a long time, but the two-phase expansion has been a barrier to realization. Lately, two-phase expanders with high efficiency have been developed, like the screw expander and the Variable Phase Turbine (VPT) (see section 3.7.1 and 3.7.2), making the TFC economically interesting for many applications.

The TFCs main difference from the ORC is that the heating process ends at the boiling point of the working fluid, i.e. there is no evaporation and superheating. This leads to the possibility of a much better temperature matching between the heat carrier and the working fluid. Power is produced in a two-phase expander after the heating process.

In the PEC, the working fluid is allowed to be partially evaporated before it is expanded in a two-phase expander. It can be seen as a hybrid between the TFC and the ORC. The advantage of the PEC is that it requires lower mass flow rates of working fluid than the TFC, and hence yields a smaller system and requires less working fluid pump work. The temperature matching is however not as good as for the TFC.

Currently, only a few studies of the TFC have been published (see chapter 4.), but the ones that are published looks very promising for low temperature heat sources. The TFC was also found to be promising for low temperature heat sources in my project thesis. Even fewer studies are published on the PEC.

In this study, the ORC, TFC and PEC have been simulated in a Microsoft Excel calculation tool that uses Visual Basic for Applications. The simulation is done for three different cases, defined by different heat source temperatures. Air with a mass flow of 10 kg/s and temperatures of 100, 150 and 200 °C are used for Case I, Case II and Case III, respectively.

Water at 20 °C is used as the heat sink. The three cases are all simulated with eight different working fluids. Different performance parameters are calculated and used to compare the performance of the three cycles, and the different working fluids.

This report begins with theory of the ORC, TFC, PEC, working fluids, heat exchangers and two-phase expanders. A literature review of the published studies of the TFC, PEC and components are then given. This is followed by the methodology, model description, and the cases we have studied. Results, discussion, and conclusions are then presented.

2 Objectives

The TFC is found to be promising for power production from low temperature heat sources in my project thesis (Trædal 2013), and several other published studies (see chapter 4).

However, all of these studies neglect the pressure losses in the system and calculation of heat transfer coefficients for each fluid. Most of the published studies also assume constant and equal expander efficiencies for the TFC and ORC. In my project thesis, a simple two-phase expander (VPT) efficiency model that only depended on the vapor quality at the nozzle exit was used. The system size and necessary heat exchanger areas are also not considered in most existing studies.

This study takes aim to make an improved and more detailed model of the TFC and ORC, to obtain a more accurate analysis and comparison between the TFC and ORC, and better size and heat exchanger area estimations. This should be done by further development and improvement of the existing calculation tool from my project thesis.

The improved model should include heat exchanger models to calculate pressure losses and heat transfer coefficients. A two-phase expander efficiency model that includes the main influencing properties should also be implemented to allow a more realistic comparison between the different cycles and working fluids.

More complex configurations of the TFC has been proposed to improve the power production, one of them being the PEC. A calculation tool for the PEC should be made, and the cycle analyzed and compared to the TFC and ORC.

An evaluation of different working fluids, including natural working fluids, for the TFC and PEC should be included in the study.

A scientific paper should be made on the main results from the study.

3 Theory of ORC, TFC, PEC, heat exchangers and two-phase expanders

In this chapter, a description of the Organic Rankine Cycle (ORC), Trilateral Flash Cycle (TFC), Partially Evaporating Cycle (PEC) and the heat supply to the cycles are given. The heat exchangers used in the model, a plate finned-tube heat exchanger and a plate heat exchanger are then described. A description of two promising two-phase expanders, the screw expander and the Variable Phase Turbine (VPT) are then given.

3.1 Description of the Organic Rankine Cycle

The ORC, shown in a Ts – diagram in Figure 1, consists of a pump, a heater, an expander and a cooler-condenser. At state 1, the working fluid is saturated liquid at pressure P_1 and temperature T_1 . The pressure is increased to P_2 by the pump, to state 2. The liquid is then heated at constant pressure to state 3. If $P_2 = P_3$ is lower than the critical pressure P_c , the heating from state 2 to state 3 involves a phase change such that the working fluid is saturated or superheated vapor at state 3. The vapor is then expanded to pressure P_1 at state 4. Work is produced during this expansion. The fluid is then cooled and condensed at constant pressure back to state 1. If T_4 is significantly higher than T_1 , an internal heat exchanger can be used to recover some of the heat.

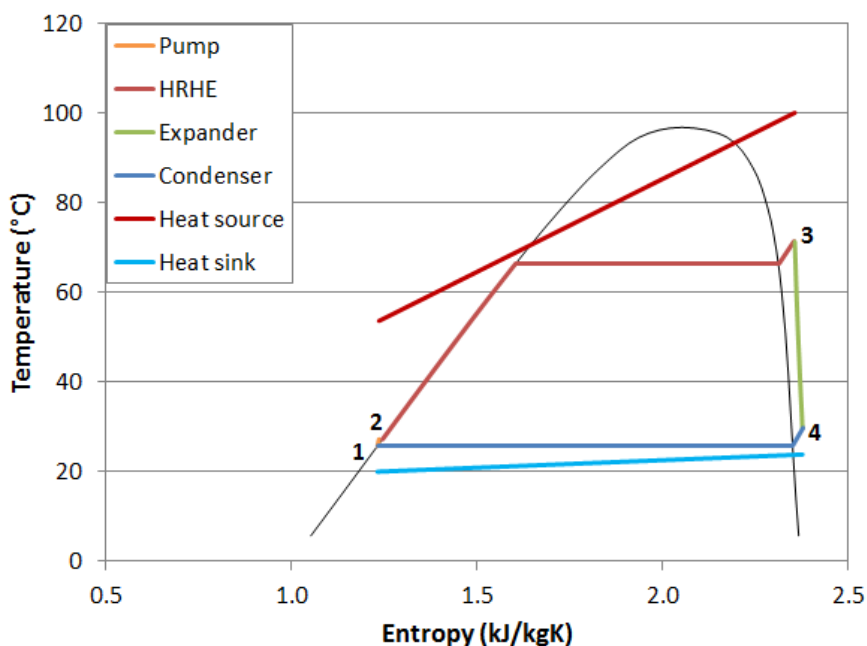


Figure 1: Ts – diagram for ORC with propane as working fluid

3.2 Description of the Trilateral Flash Cycle

The TFC consists of a pump, a heater, a two-phase expander and a condenser or a cooler-condenser as shown in Figure 2.

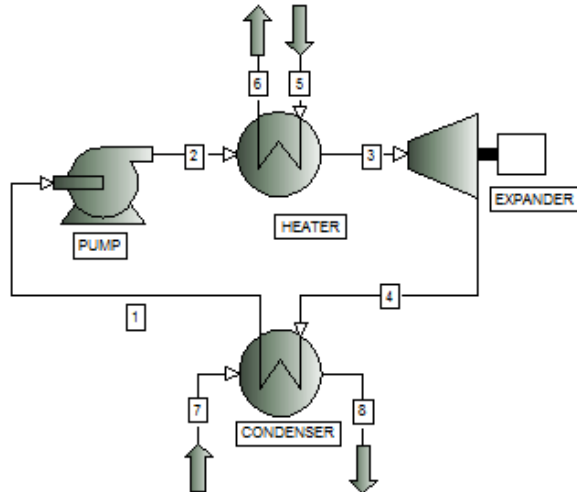


Figure 2: Configuration of a TFC system

The cycle is shown in a Ts -diagram in Figure 3. At state 1, the working fluid is saturated liquid at temperature T_1 and pressure P_1 . The pressure of the liquid is then increased to P_2 by the pump, to state 2. From state 2 the liquid is heated to its boiling point at pressure P_2 . This is state 3. The fluid is then expanded through the two-phase expander. The liquid expands into the wet vapor region, to pressure P_1 , and arrives at state 4. Work is produced during this expansion. State 4 may be in either the wet or the dry vapor region, depending on the working fluid. If state 4 is in the wet vapor region (Figure 3 (left)), T_4 is equal to T_1 . The wet vapor is then condensed back to state 1 in a condenser. If state 4 is in the dry vapor region (Figure 3 (right)), T_4 is higher than T_1 . In this case, the working fluid is cooled and then condensed back to state 1. If T_4 is significantly higher than T_1 , an internal heat exchanger can be used to recover some of the heat. (Fischer 2011) can be looked at for more details about the TFC.

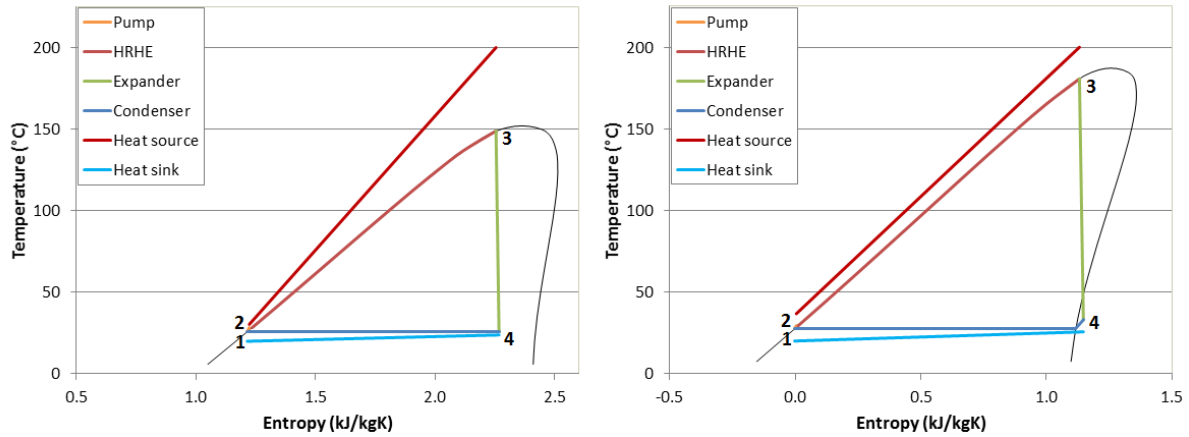


Figure 3: Ts – diagram for TFC. State 4 is in the wet vapor region with butane (left), and in the dry vapor region with isopentane (right) as working fluid

The technically most challenging component of the cycle is the two-phase expander, which may be a turbine, a scroll expander, a screw expander or a reciprocating engine (Lai and Fischer 2012). Two promising two-phase expanders, the screw expander and the Variable Phase Turbine, are discussed in section 3.7.1 and 3.7.2.

3.3 Description of the Partially Evaporating Cycle

The PEC consists of a pump, a heater, a two-phase expander and a condenser or a cooler-condenser. The cycle is shown in a Ts -diagram in Figure 4.

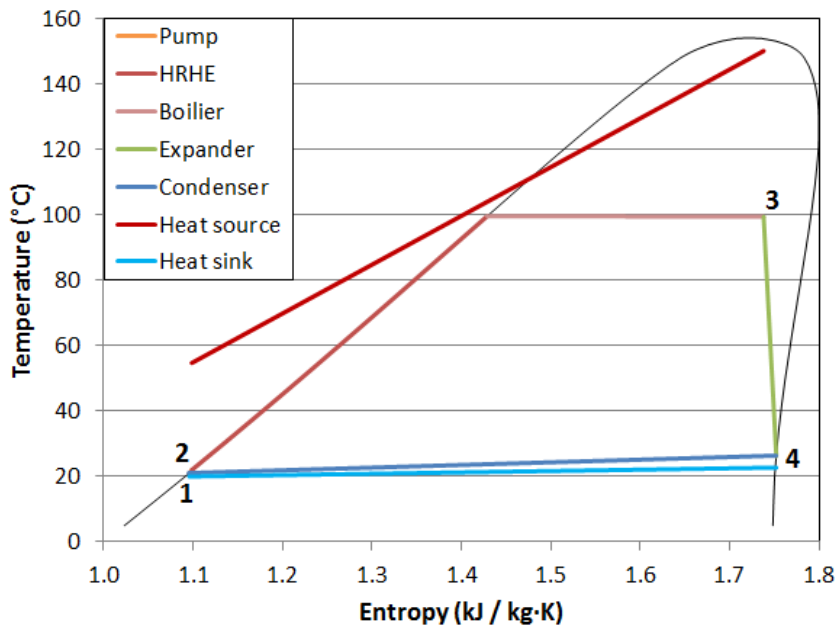


Figure 4: Ts -diagram for PEC with R245fa as working fluid

At state 1, the working fluid is saturated liquid at temperature T_1 and pressure P_1 . The pressure of the liquid is then increased to P_2 by the pump, to state 2. From state 2 the liquid is heated to its boiling point at pressure P_2 . The fluid is then partially evaporated to state 3, before it is expanded through the two-phase expander. The mixture expands in to the wet vapor region, to pressure P_1 , and arrives at state 4. Work is produced during this expansion. State 4 may be in either the wet or the dry vapor region, depending on the working fluid. If state 4 is in the wet vapor region, T_4 is equal to T_1 . The wet vapor is then condensed back to state 1 in a condenser. If state 4 is in the dry vapor region, T_4 is higher than T_1 . In this case, the working fluid is cooled and then condensed back to state 1. If T_4 is significantly higher than T_1 , an internal heat exchanger can be used to recover some of the heat.

The purpose of the PEC is to obtain a higher thermal efficiency, a reduction in required heat transfer area, and a lower mass flow rate of working fluid than for a pure TFC, but still obtain a higher net power output than for an ORC.

3.4 Supply and removal of heat to the cycles

The efficiency of the heat to power conversion is highly dependent on the heat transfer to the cycle, and to a minor extent on the heat removal from the cycle.

For the operation of a system such as the ORC, TFC or PEC, one usually has a heat carrier available with a given inlet temperature, mass flow rate and heat capacity. On the heat removal side, one has a cooling agent with an inlet temperature that can be close to environmental, or higher if the removed heat is used in another process.

The cooling of the heat carrier is limited by the occurrence of a pinch point between the heat carrier and the working fluid, illustrated in Figure 5. This is where the minimum temperature difference between the hot and the cold stream reaches some minimum value, below which closer temperature matching of the streams is not economically feasible.

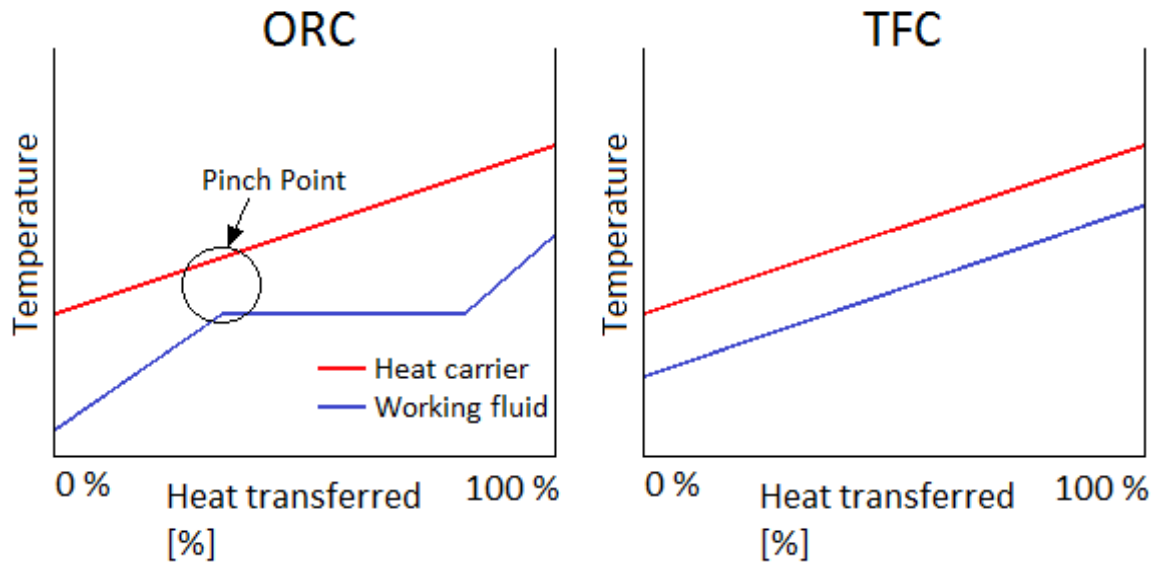


Figure 5: Variation in stream temperature during heat addition for ORC (left) and TFC (right).

In the TFC, the working fluid stays liquid during the heat addition process such that the temperature profile is approximately linear. This means that a better temperature matching is possible in TFC systems than in other systems where there is a phase change during the heat addition, like ORC and PEC. This is illustrated in Figure 5, where the left figure shows the variation in stream temperature during the heat addition process for ORC and the right shows the variation for TFC. The temperature matching for the PEC may be close to the TFC or worse than for ORC depending on the vapor quality at the expander inlet.

To improve the temperature matching in cycles that involves a phase change, the use of zeotropic working fluid mixtures or supercritical pressures have been suggested which leads to a gliding and thus better temperature profile. This is discussed in for example (Ho, Mao et al. 2012) and (Chan, Ling-Chin et al. 2013). Zeotropic working fluid mixtures could also be used in the TFC to improve the temperature matching in the condenser (Zamfirescu and Dincer 2008).

For more details about the heat transfer to the cycles the reader is referred to (Fischer 2011).

3.5 Working fluids

Several factors have to be considered to select the appropriate working fluid for a given cycle with given boundary conditions. The efficiency and/or power output should be as high as possible for the given heat source and sink. This is dependent on several properties of the

working fluid, like critical point, acentric factor, specific heat, density, etc. The working fluid should have a high conductivity such that the heat transfer coefficients in the heat exchangers are high, and low viscosity such that the friction losses are low. The fluid must also have high chemical stability such that it does not deteriorate under the conditions in the cycle. (Quoilin, Van Den Broek et al. 2013) can be consulted for a more thorough review of the properties that should be considered.

Factors concerning safety and environment, such as flammability, toxicity, Ozone Depleting Potential (ODP) and Global Warming Potential (GWP) should be taken into account.

The working fluid should be readily available. Fluids already in use in refrigeration or chemical industry are easier to obtain and less expensive.

For the TFC it is important that the working fluid has an acceptable vapor pressure at lower temperatures. The reason for this is that if the vapor pressure is too low the volume ratios required for two-phase expansion is enormous (Fischer 2011). This means that water is not suitable when the heat is rejected at typical ambient temperatures.

The critical temperature should also be close to the heat source inlet temperature for the TFC. If the critical temperature is too low, a good temperature match is not possible.

The shape of the vapor – liquid equilibrium (VLE) curve in the Ts-diagram is also important. The VLE curve may be either bell shaped or overhanging (wet or dry) (Lai and Fischer 2012). A TFC using a working fluid with an overhanging VLE can have state 4 in the dry vapor region like in Figure 3(right). If the VLE is bell shaped, state 4 will be in the wet vapor region, like in Figure 3(left). This can be important for the cycle efficiency.

3.6 Heat exchangers

In this section, the heat exchangers used in the model are described. A plate finned-tube heat exchanger is used for the heating process and a plate heat exchanger is used for the condensing process.

3.6.1 Plate finned-tube heat exchangers

Plate finned-tube heat exchangers are often used in gas-to-liquid heat exchange. The heat transfer coefficients on the gas side are generally much lower than those on the liquid side,

and fins are therefore required on the gas side. The heat exchanger consists of a tube bundle with continuous plate-fin sheets fixed on the outside as shown in Figure 6. The tube rows may be arranged either staggered or aligned in the direction of the external fluid velocity.

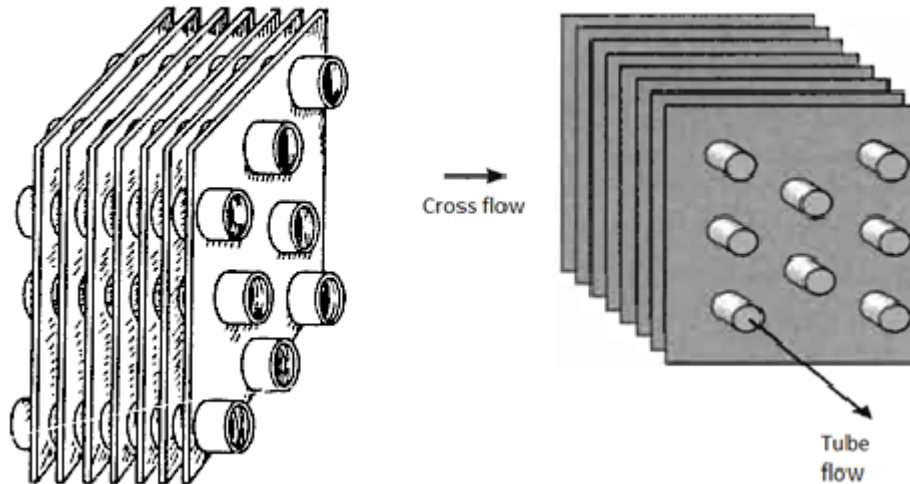


Figure 6: Finned tube heat exchanger, left: (lv-soft.com), right (Incropera, DeWitt et al. 2007)

The gas is blown across the banks of finned tubes, and for the case of a heater, it delivers heat to the stream on the tube side while the gas itself is cooled. The gas is usually blown or drawn across the tube banks at relatively low velocities by large fans. Plate finned-tube heat exchangers are commonly used in heating, ventilation, refrigeration and air conditioning systems. The reader is referred to (Kaka and Liu 2002) for more information about finned tube heat exchangers.

3.6.2 Plate heat exchangers

Plate heat exchangers consists of plates that are clamped together in a frame with rubber gaskets between each plate. Alternatively, the plates are welded or brazed together. The gasket position on each plate determines the flow arrangement through the plates, which allows the heat exchanging fluids to flow in alternate plate channels. Different pass arrangements may be controlled in a similar manner. A principle schematic of a plate heat exchanger is shown in Figure 7.

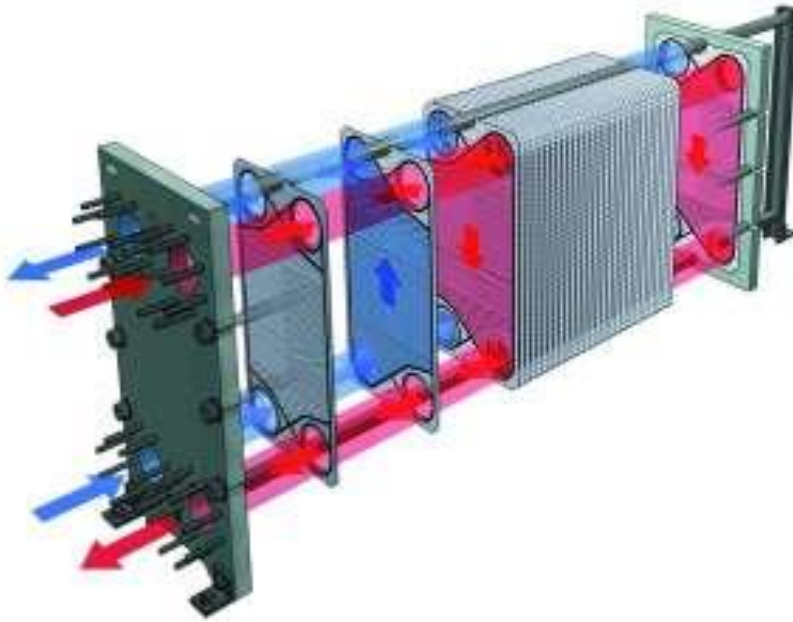


Figure 7: Principle schematic of a plate heat exchanger, (deltathx.com).

The plates are usually 0.4 – 0.6 mm thick, and are pressed with a pattern, most commonly chevrons. Good structural rigidity and turbulence conditions are often obtained by stacking alternate plates with reversed chevron angle.

Arrangements of fluid stream passes can be made to enhance the performance. Figure 8 shows an example of a two-/two-pass arrangement.

More information about plate heat exchangers can be found in (Andresen 2009), which this section is based on.

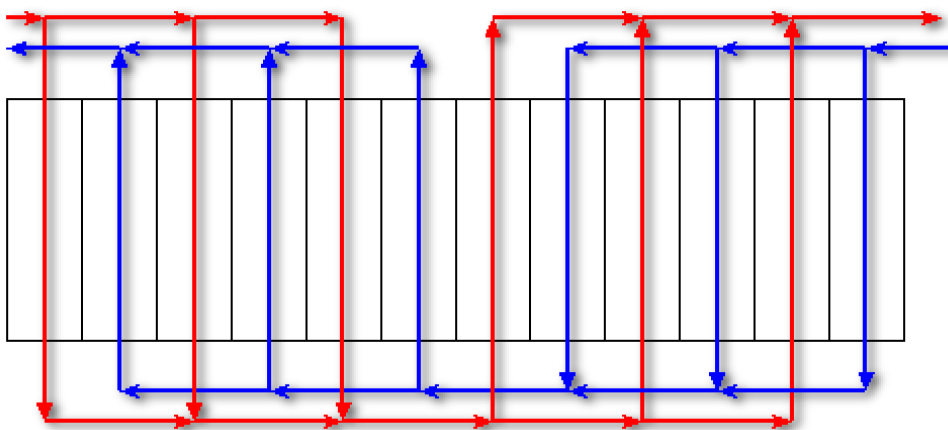


Figure 8: Plate heat exchanger, two-/two-pass arrangement (Andresen 2009)

3.7 Two-phase expanders

There are a few expander types that tolerate two-phase flow. For small scale (1-10 kW) applications scroll or rotary vane expanders may be used (Bao and Zhao 2013). For slightly larger systems, a reciprocating piston might be suitable. However, since the piston itself does not tolerate two-phase flow, it can only be used if a cyclone for phase separation is implemented upstream (Steffen, Löffler et al. 2013). For medium scale (50 – 250 kW) applications, like investigated in this study, screw expanders and the Variable Phase Turbine (VPT) are the most relevant expander types and are described below.

3.7.1 Screw expanders

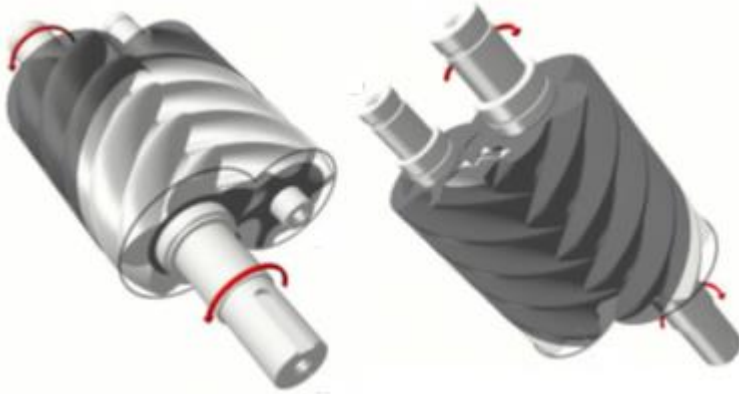


Figure 9: Schematic of a screw expander (Smith, Stosic et al. 2005)

A screw expander is a positive displacement expander that consists of a pair of meshing helical rotors in a casing. The volume trapped between the rotors and the casing changes as the rotors rotate. Whether the volume increases or decreases depends only on the direction of rotation. In an expander the volume will increase from the fluid is admitted at one end until it is expelled at the other. The power transfer between the fluid and the rotors are mainly due to the pressure on the rotors, and only to a small extent due to dynamic effects associated with fluid motion. This is why the presence of liquid in the vapor or gas being expanded or compressed has little effect on its mode of operation or efficiency (Smith, Stosic et al. 2005). The main requirements for efficient operation of the expander are; maximum flow area in the space formed between the lobes and the casing, minimum leakage, correct volume ratio of expansion and correct tip speed. For a more detailed description of the screw expander the reader is referred to (Smith, Stosic et al. 2005), which this paragraph is based on.

The use of two-phase screw expanders to improve the efficiency in geothermal power production was suggested in the early 1970s (Smith 1993). The Lysholm screw expander achieved maximum adiabatic efficiencies of only 53 % in small scale testing, and 68 % in a 1 MW machine. The screw expander did therefore not offer any improvement at this time compared to the methods already in use (flash expansion of the brine to intermediate pressures followed by separation of the dry steam for power generation and reinjection of the residual hot water).

In 1981 Smith conducted tests of a screw expander with Refrigerant 113 as working fluid in a closed cycle test rig (Smith 1993). He were able to obtain adiabatic efficiencies of over 70 % at 25 kW power output and concluded that adiabatic efficiencies of at least 77 % were likely in large-scale machines. Smith and Stosic have published many articles about their screw expander development and have summarized their almost 20 years of work in (Smith, Stosic et al. 2001). In one of their last publications, they state that low temperature heat sources can be utilized substantially cheaper with screw expanders than with standard turbines in the range of approximately 20-500 kW because they neither require a gearbox nor a lubrication system

Today screw compressors are used in a wide variety of applications, most commonly in air and refrigerant compression. These compressors can reach efficiencies of up to 90 % (Smith, Stosic et al. 2005). Their efficiencies as expanders are less well proven.

In (Öhman and Lundqvist 2013), Öhman and Lundqvist present their results from laboratory tests on a semi-hermetic Lysholm Turbine (screw expander) operating with R134a with superheated, saturated and wet inlet gas conditions. Efficiencies around 0.75 were measured with a peak of 0.92. However, the authors stress that it is notoriously difficult to get absolute levels of efficiencies derived from measurements in two-phase conditions. Their conclusions are that Lysholm Turbines are well suited for low temperature power generation and that further understanding of the performance during two-phase conditions is required.

3.7.2 Variable Phase Turbine

The VPT consists of a set of individual fixed nozzles and an axial impulse rotor. In the two-phase nozzles (Figure 10), the enthalpy is partly converted to two-phase kinetic energy in a near isentropic expansion. The liquid phase is broken up into small droplets by the expanding gas, and momentum is transferred from the gas to the droplets by pressure and shear forces.

The small size of the droplets leads to a close coupling of the gas and the liquid and efficient acceleration of both phases. The inlet to the nozzle can be liquid, two-phase, supercritical or vapor.

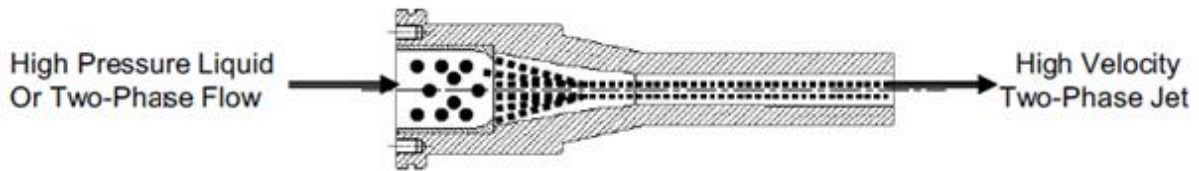


Figure 10: Schematic of two-phase VPT nozzle (Welch and Boyle 2009)

The kinetic energy of the two-phase jet is converted to shaft power in an axial impulse turbine (Figure 11). The arrangement of the Variable Phase Turbine is similar to a conventional axial impulse turbine. For a more detailed description of the VPT the reader is referred to (Welch and Boyle 2009), which this paragraph is based on.

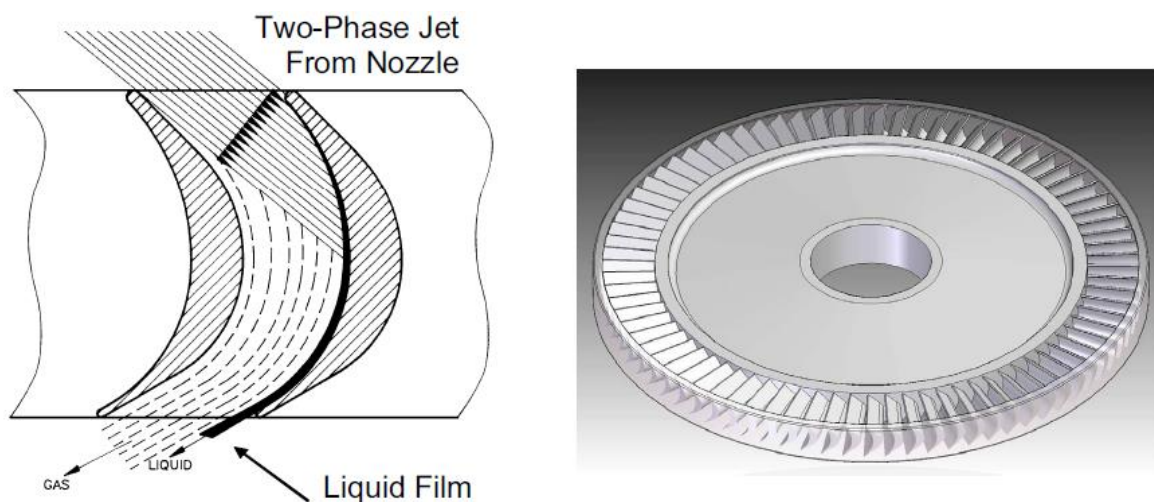


Figure 11: Schematic of flow path in two-phase VPT blades (left), and rotor (right) (Welch and Boyle 2009)

The two-phase nozzle efficiency is typically between 90 % and 97 %. It is strongly influenced by the surface tension of the working fluid and the vapor density at the condensing pressure. The rotor efficiency is typically between 78 % and 85 %, and is strongly influenced by the vapor quality at the nozzle exit. (Welch and Boyle 2009)

The VPT is used in a TFC demonstration project at Coso Geothermal, and is a promising type of two-phase expanders. According to Welch and Boyle in Energent Corporation, who produce VPTs, the isentropic efficiency of this expander is typically greater than 80 %. The VPT allows direct driving of the generator, which eliminates the need for a gearbox and lube

oil system. VPTs have been in use in refrigeration systems for several years (Welch and Boyle 2009), and has extensive commercial experience.

4 Literature review

In this chapter a review of some of the studies that have been published on the TFC and PEC are given.

4.1 Studies of the TFC and PEC

There are currently only a few published studies on the TFC, and most of them are theoretical considerations. The studies usually assume constant and equal expander efficiency for the ORC and TFC. The pressure losses are also neglected in the existing studies, and the required heat exchanger areas are usually not considered. There are even fewer studies on the PEC, and the same assumptions are used in these. The studies that are published on the cycles so far are however very promising for low temperature heat sources.

(Steffen, Löffler et al. 2013) studies a TFC with a variable expander efficiency. A detailed model of a piston engine expander is made, and used to calculate the expander efficiency. The TFC is then compared to an ORC. They find that the expander efficiency is 0.75 - 0.88 with water, 0.65 – 0.85 with ethanol, and 0.50 – 0.70 with isopentane as working fluid. The ORCs are assumed to have an expander efficiency of 0.85. For heat source temperatures up to 180 °C the TFC with water is found to have exergy efficiencies that are 35 - 70 % higher than for the best ORCs studied. The exergy efficiency is found to be up to 40 % higher for TFC using ethanol or cyclopentane as working fluid, even when supercritical ORCs are considered. At heat source temperatures above 220 °C the exergy efficiency is in the same order for the two cycles when supercritical ORCs are considered. When supercritical ORCs are not considered the TFC with water or ethanol outperforms the ORCs up to 260 °C.

In (Fischer 2011) an optimized TFC with water as working fluid is compared to the use of an optimized ORC with pure organic working fluids. Comparisons are made for five cases defined by the inlet temperature of the heat carrier and the cooling agent. Fischer assumes an isentropic expander efficiency of 0.85 for both ORC and TFC. The five cases and the main results are summarized in Table 1. The volume flow in to and out of the expander, \dot{V}_3 and \dot{V}_4 , and the exergy efficiency, ε , defined by the net power output over the incoming exergy flow of the heat carrier, are given.

Table 1: Fischer's results for the comparison between TFC and ORC for the five cases

Temperature pairs	(350°C, 62°C)		(280°C, 62°C)		(280°C, 15°C)		(220°C, 15°C)		(150°C, 15°C)	
Cycle	TFC	ORC	TFC	ORC	TFC	ORC	TFC	ORC	TFC	ORC
\dot{V}_3 [l/s]	7.00	51.0	10.4	121.0	6.24	113.7	9.53	74.8	22.4	201.3
\dot{V}_4 [l/s]	4993	1778	6540	1937	33546	4824	43550	1711	69896	997
ε	0.44	0.38	0.38	0.33	0.65	0.54	0.58	0.51	0.48	0.37

Fischer finds that the exergy efficiency is 14 – 29 % higher for TFC than ORC for a heat carrier inlet temperature of 350 to 150 °C. He also finds that the volume flow at the expander outlet is significantly higher for TFC than for ORC (2.8 to 70 times higher), because of the low vapor pressure for water at low temperatures. These large flow rates at the expander outlet may be difficult to handle in a real power plant. The volume flow at the expander outlet is important for the design of the expander and the sizing of the heat exchangers. The volume ratios over the expander are also higher for the TFC. For the ORC the volume ratios are between 5 and 42 for the five cases, while they are between 710 and 5375 for TFC. Fischer recommends the use of working fluids with higher vapor pressures, like cyclopentane, pentane, or butane to reduce the volume flows. Water may be used as the working fluid in systems with higher heat rejection temperatures (e.g. the upper stages of a power producing cascade).

In a follow up study (Lai and Fischer 2012), Lai and Fischer models the TFC using pure organic working fluids under the same conditions as was used in (Fischer 2011). The TFC with organic working fluids is compared to the TFC with water, the ORC and Clausius-Rankine cycles for the five cases.

Lai and Fischer finds that the exergy efficiency is highest or nearly highest for TFC with water in all the five cases. For the three highest temperature cases the volume flows at the expander outlet is tolerable for TFC with water as working fluid. For the two low temperature cases however the volume flows become extremely large. They conclude that of the working fluids tested, cyclopentane is the best working fluid for these two cases. It has exergy efficiencies of 95 % and 96 % of that of water, while the volume flows at the expander outlet are only 15 % of that of water. Cyclopentane also gives good results for the (280 °C, 62 °C) and (280 °C, 15 °C) cases, with exergy efficiencies of 93 % and 94 % of that of water while the volume flows at the expander outlet are only 33 % and 15 % of that of water. Other working fluids, like pentane and butane gave similar efficiency and volume flows.

The volume flows at the expander outlet is lowest for the ORC in all cases. In case (150 °C, 15 °C) the exergy efficiency of the ORC is 81 % of that of TFC with cyclopentane, but the volume flow at the expander outlet is only 10 % of that of the TFC.

Welch and Boyle in Energent Corporation conducted a study where the TFC, referred to as a Variable Phase Cycle (VPC) in the paper, is compared to an ORC for a geothermal system (Welch and Boyle 2009). Energent's Variable Phase Turbine (see section 3.7.2) is modeled as the two-phase expander in the study. Comparisons are made for inlet temperatures of 121 °C to 177 °C for the heat source, using R134a as working fluid for both TFC and ORC. They find that the TFC is able to produce more power than the ORC under almost all conditions, but especially at low heat source inlet temperatures.

Welch and Boyle estimates that a 1 MW TFC system for geothermal power production will cost \$1279/kW, whereas ORC systems in the same size range typically has a cost between \$2300 and \$2500/kW. The costs of the TFC is lower because of elimination of the gearbox, lube oil system and seals, and the use of simpler heat exchangers.

A 1 MW geothermal TFC demonstration project using the VPT is constructed at Coso Geothermal in California, with a scheduled startup in 2011 (Welch, Boyle et al. 2011). This system is designed for heat recovery from a 110 °C brine stream. The working fluid is R134a. At this time the system has been operated up to a power output of 795 kW, and the power generated agrees well with predictions (Boyle and Hays 2013). The system is illustrated in Figure 12.

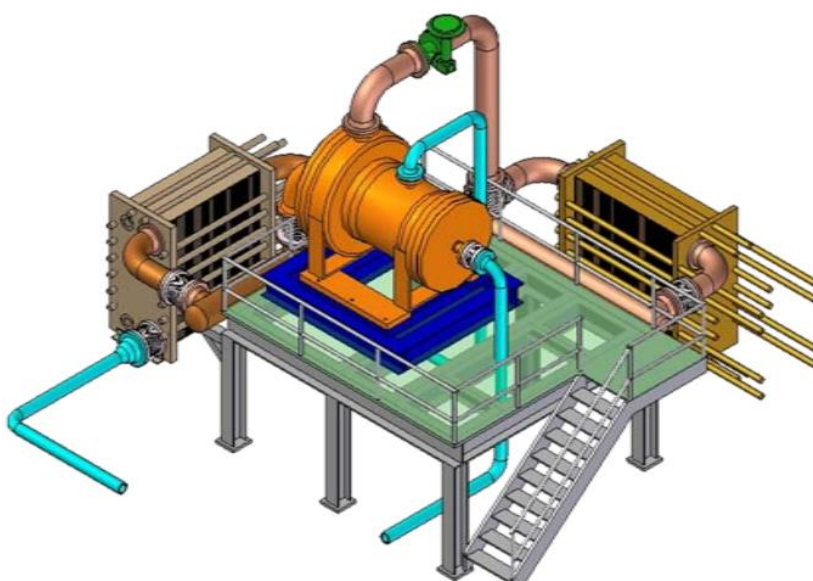


Figure 12: TFC geothermal power plant, 1 MW, (Welch, Boyle et al. 2010)

In (Zamfirescu and Dincer 2008), Zamfirescu and Dincer assess the performance of a TFC using an ammonia–water mixture as working fluid. The use of an ammonia–water mixture instead of pure water makes it possible to match the temperature profiles better in the condenser. The ammonia-water TFC is compared to four ORCs using different working fluids and a Kalina cycle. All cycles are subjected to the same conditions for the heat source, brine at 150 °C, and cooling agent, air from the environment. An expander efficiency of 0.70 is assumed for both ORC and TFC. Zamfirescu and Dincer’s results are summarized in Table 2. The parameters energy efficiency, η , exergy efficiency, ε , and heat extracted from the source, \dot{Q} , is included in the table.

Table 2: Zamfirescu and Dincer's results

Parameter	ORC cycles				Ammonia-water cycles	
	R141b	R123	R245fa	R21	Kalina	TFC
Working fluid	R141b	R123	R245fa	R21	Kalina	TFC
η [%]	10	9	9	9	3	8
ε [%]	15	19	20	21	14	43
\dot{Q} [kW]	132	179	189	198	373	477

Zamfirescu and Dincer finds that the exergy efficiency is 43 % for the TFC versus 21 % for the best of the other cycles. The TFC with ammonia-water is also compared to a TFC with pure water. The exergy efficiency is found to be 7 % higher for the one with ammonia-water because of the better temperature matching in the condenser.

In (Brown and Mines 1998), Brown and Mines performs a working fluid study for the TFC with 20 different working fluids, using two different inlet temperatures of the heat source (geothermal brine), which are set to 93 °C and 160 °C. The performance criteria for the working fluids are net power output, expansion ratio and critical temperature. No working fluid is in the top ten in all categories. In the same paper, there is a comparison of the cycle performance between ORC with isobutene and TFC with pentane, using brine at 160 °C as the heat source. They find that the TFC can produce 15 % more power than the ORC from the same amount of brine. On the other hand, the TFC requires a 86 % larger heater and a 17 % larger condenser than the ORC. By varying the two-phase expander efficiency, Brown and Mines finds that the TFC outperforms the ORC when the expander efficiencies are equal at 85 %. When the efficiency of the TFC expander is reduced to 76 %, equal performance is obtained.

In (Smith 1993), Smith compares the TFC and ORC using several different working fluids, and water at 100 °C to 200 °C as the heat source. He finds that the TFC output exceeds that

of the ORCs over the entire temperature range. The largest relative gains are found at low temperatures where the TFC exceeds the ORC power outputs in the order of 80 %.

(Lecompte, van den Broek et al. 2013) studies the use of a PEC compared to a pure TFC. R245fa is used as the working fluid in the study, and heat sources at 100 °C, 120 °C and 140 °C are investigated. Lecompte et al. finds that with a heat source of 140 °C the net power peaks when the working fluid is evaporated to a vapor quality of 0.23. The required pumping power is then reduced by 24 % compared to a pure TFC. The results are similar for the other temperatures, but shifted towards lower vapor qualities. It is concluded that the PEC can improve the net power output of the system, especially when the pump isentropic efficiency is low.

Several other more sophisticated cycles using two-phase expansion has been proposed.

(Smith, Stosic et al. 2004) suggested a cycle with two expansion stages of which one would be two-phase and one dry vapor, which requires a phase separation after the first expansion.

(Ho, Mao et al. 2012) investigated similar and even more advanced configurations with several expansion stages and reports efficiency improvements for low temperature applications compared to ORC. These are only theoretical considerations, but indicate that advanced cycle configurations can have a better performance than a standard TFC.

5 Methodology

In this chapter the methodology, software and equations that are used for simulating the ORC, TFC and PEC are described.

5.1 Software

To compare the three cycles they have been simulated using Microsoft Excel with Visual Basic for Applications (VBA). REFPROP 9 by (Lemmon, Huber et al. 2013) is used for the thermodynamic properties of the working fluids.

5.2 Cycle simulations

The main components of the three cycles are pump, heat recovery heat exchanger (HRHE), expander and condenser. The ORC also has a recuperator that can be included or excluded in the simulation. Table 3 gives an overview of the parameters used in the calculations. As seen in the table, the following parameters are optimized during the simulations: working fluid mass flow, pump outlet pressure, vapor quality at expander inlet (only PEC), condensation temperature, heat sink outlet temperature, superheat at expander inlet (only ORC) and recuperator capacity (only ORC). Heat source and sink specifications as well as component efficiencies are constant inputs that have to be chosen by the user. The only exceptions to this are the expander efficiencies for the TFC and PEC, which are calculated automatically. The heat transfer coefficients and pressure losses are calculated using the correlations and equations in chapter 6. Due to software limitations the pressure loss and heat transfer coefficient calculations are not done inside the cycle simulations. Instead, these calculations are done separately and the pressure losses and heat transfer coefficients are then specified as constants in the cycle simulation. Multiple iterations are done such that they are calculated at the right conditions for each case.

Table 3: Calculation parameters

	Parameter	Type
Heat source	Fluid Mass flow Inlet temperature Inlet pressure Outlet temperature Pressure loss Fan efficiency Fan work HTC	User input User input User input User input Calculated Calculated User input Calculated Calculated
Heat sink	Fluid Mass flow Inlet temperature Inlet pressure Outlet temperature Pressure loss Pump efficiency Motor efficiency Pump work	User input Calculated User input User input Optimized Calculated User input User input Calculated
Pump	Mass flow working fluid Isentropic efficiency Motor efficiency Inlet pressure Outlet pressure Work	Optimized User input User input Calculated Optimized Calculated
HRHE	Pressure losses HTC heater HTC evaporator (ORC and PEC) HTC superheater (ORC) Amount of superheat (ORC) Pinch point Area	Calculated Calculated Calculated Calculated Optimized Calculated Calculated
Expander	Isentropic efficiency (ORC) Nozzle efficiency (TFC and PEC) Rotor efficiency (TFC and PEC) Generator efficiency Inlet vapor quality (PEC) Minimum vapor fraction (ORC) Work	User input Calculated Calculated User input Optimized User input Calculated
Condenser	Condensation temperature Working fluid pressure loss Heat sink pressure loss HTC desuperheater HTC condenser Pinch point Area	Optimized Calculated Calculated Calculated Calculated Calculated Calculated
Cycle	Working fluid Heat loss to ambient Total heat exchanger area Efficiency Net power output	User input Neglected Calculated Calculated Maximized

The cycles are calculated based on enthalpy balances (see section 5.2.1– 5.2.3) with a number of constraints to avoid unfeasible solutions: The minimum pinch point temperatures in the heat exchangers and the minimum superheat throughout the ORC expander are specified. Both are calculated by dividing the component into several small sections and ensuring the limits in each section. In addition, the pump outlet pressure is limited to 95 % of the working fluid's critical pressure and the condensation pressure is kept above 1 bar to avoid a sub-atmospheric system. The total heat exchanger area is constrained during the case studies to compare the performances of the cycles at different system sizes. The cooling of the heat source is not limited although some practical limitations can occur.

5.2.1 Simulation of the ORC

A Th-diagram for an ORC with propane as working fluid and a heat source inlet temperature of 100 °C is shown in Figure 13, with the different state points numbered.

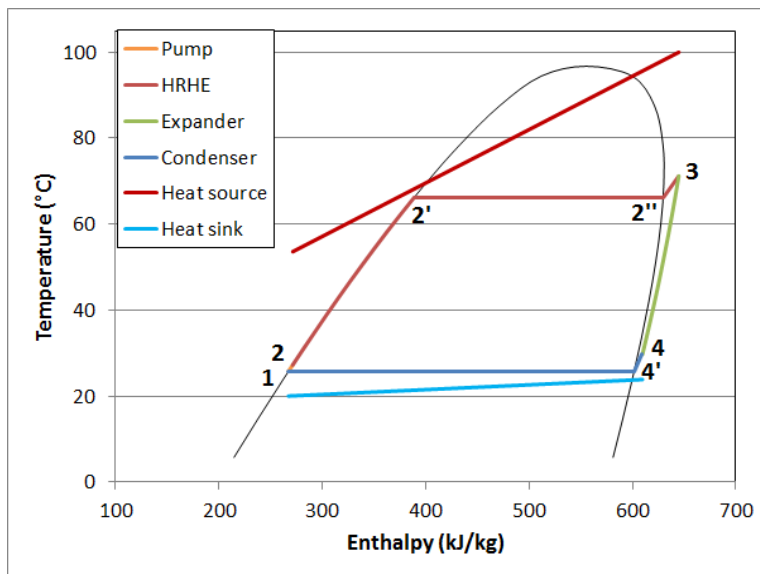


Figure 13: Th-diagram for ORC with propane as working fluid

In the following, T_i is referring to the temperature at state i , P_i to the pressure at state i etc.

The different state points in the cycle are calculated as following:

State 1, the pump inlet, is given by T_1 that is found in the optimization and P_1 that is determined such that state 1 is at the bubble point.

$$h_1 = h(T_1, \text{bubble point})$$

If a recuperator is included, state 2r, the inlet to the high-pressure side of the recuperator, is given by:

$$h_{2r} = h_1 + \frac{h(s_1, P_{2r}) - h_1}{\eta_{pump, wf}}$$

Where $\eta_{pump, wf}$ is the working fluid pump efficiency. P_{2r} and P_2 are found from P_2' , which is found in the optimization, and the pressure losses, ΔP , in the components as following:

$$P_2 = P_2' + \Delta P_{Preheat}$$

$$P_{2r} = P_2 + \Delta P_{Recuperator}$$

State 2, the inlet to the preheat part of the HRHE is then given by:

$$h_2 = h_{2r} + \frac{\dot{Q}_{Recuperator, optimum}}{\dot{m}}$$

Where $\dot{Q}_{Recuperator, optimum}$ is the heat recovery in the recuperator, found in the optimization, and \dot{m} is the mass flow of working fluid.

If the recuperator is not included, state 2 is equal to state 2r:

$$h_2 = h_{2r}$$

The inlet to the HRHE evaporator, state 2', is given by:

$$h_{2'} = h(P_{2'}, \text{bubble point})$$

The inlet to the HRHE superheater, state 2'', is given by:

$$h_{2''} = h(P_{2''}, \text{Dew point})$$

Where $P_{2''}$ is given by

$$P_{2''} = P_2' - \Delta P_{Evaporator}$$

State 3, the inlet to the expander, is given by:

$$h_3 = h(P_3, T_3)$$

T_3 is found in the optimization, and P_3 by:

$$P_3 = P_{2''} - \Delta P_{Superheater}$$

If a recuperator is included, State 4r, the inlet to the low-pressure side of the recuperator is given by:

$$h_{4r} = h_3 + (h(P_{4r}, s_3) - h_3) * \eta_{exp}$$

Where η_{exp} is the expander efficiency. P_{4r} is given by:

$$P_{4r} = P_4 + \Delta P_{Recuperator}$$

P_4 by:

$$P_4 = P_{4'} + \Delta P_{Desuperheater}$$

And $P_{4'}$ by:

$$P_{4'} = P_1 + \Delta P_{Condenser}$$

State 4, the inlet to the desuperheater, is then given by:

$$h_4 = h_{4r} + \frac{\dot{Q}_{Recuperator, optimum}}{\dot{m}}$$

Without a recuperator state 4 is equal to state 4r.

$$h_4 = h_{4r}$$

State 4', the inlet to the condenser is given by:

$$h_{4'} = h(P_{4'}, Dew\ point)$$

The required electric power for the working fluid pump from state 1 to 2 is calculated by:

$$\dot{W}_{Pump} = \dot{m} * \frac{h_2 - h_1}{\eta_{mo}}$$

Where η_{mo} is the motor efficiency.

The heat addition to the cycle, state 2 to 3, is divided into three stages, preheating, evaporating and superheating. The different stages has different heat transfer coefficients.

The heat addition for the three stages is given by the following equations:

$$\dot{Q}_{Preheat} = \dot{m} * (h_{2'} - h_2)$$

$$\dot{Q}_{Evaporater} = \dot{m} * (h_{2''} - h_{2'})$$

$$\dot{Q}_{Superheat} = \dot{m} * (h_3 - h_{2''})$$

The total heat addition to the cycle is then given by:

$$\dot{Q}_{Total\ in} = \dot{Q}_{Preheat} + \dot{Q}_{Evaporater} + \dot{Q}_{Superheat}$$

The electric power produced in the expander, state 3 to 4, is given by:

$$\dot{W}_{expander} = \dot{m} * (h_3 - h_4) * \eta_{mo}$$

The heat removal from the cycle, state 4 to 1, is divided into a desuperheating and a condensing part. The heat removal is given by:

$$\dot{Q}_{Desuperheat} = \dot{m} * (h_4 - h_{4'})$$

$$\dot{Q}_{Condenser} = \dot{m} * (h_{4'} - h_1)$$

The total heat removal from the cycle is then given by:

$$\dot{Q}_{Total\ out} = \dot{Q}_{Desuperheat} + \dot{Q}_{Condenser}$$

When the recuperator is included, some of the heat from the desuperheating is recovered and used in the preheating of the working fluid.

The required electric power for the heat sink pump is found by:

$$\dot{W}_{pump,heat\ sink} = \dot{V}_{heat\ sink} * \frac{\Delta P_{heat\ sink}}{\eta_{pump,hs} * \eta_{mo}}$$

Where $\dot{V}_{heat\ sink}$ is the volume flow of the heat sink medium and $\Delta P_{heat\ sink}$ is the pressure loss for the heat sink in the condenser.

The electric power needed for the heat source fan is calculated by:

$$\dot{W}_{fan,heat\ source} = \dot{V}_{air} * \frac{\Delta P_{air}}{\eta_{fan} * \eta_{mo}}$$

Where \dot{V}_{air} is the volume flow of the air, ΔP_{air} is the pressure loss on the air side of the heater and η_{fan} is the fan efficiency.

The net power production from the cycle is calculated by:

$$\dot{W}_{net} = \dot{W}_{expander} - \dot{W}_{pump} - \dot{W}_{pump,heat\ sink} - \dot{W}_{fan,heat\ source}$$

The necessary heat exchanger area is calculated by the LMTD-method. For each heat exchanger part the area is calculated as:

$$A = \frac{\dot{Q}}{h * LMTD}$$

Where \dot{Q} is the heat transfer, h the heat transfer coefficient and LMTD the Logarithmic Mean Temperature Difference, calculated as:

$$LMTD = \frac{\Delta T_1 - \Delta T_2}{\ln\left(\frac{\Delta T_1}{\Delta T_2}\right)}$$

Where ΔT_1 and ΔT_2 are the temperature differences between the heat source or sink and the working fluid at the inlet and the outlet of the heat exchanger. All the areas are summed to get the total heat exchanger area.

5.2.2 Simulation of the TFC

In the TFC the two-phase expander is modeled as a VPT with a variable nozzle and rotor efficiency calculated by:

$$\eta_{Nozzle} = 0.865 + 0.00175 * d_v$$

$$\eta_{rotor} = 0.575 + 0.325 * x$$

Where d_v is the vapor density at condensing pressure and x the vapor quality at the outlet of the nozzle.

The equations for the two-phase expander is based on information given in (Welch and Boyle 2009) and personal communication with Lance Hays (Hays 2014), one of the inventors of the VPT (Hays and Sahabian 2006). This model allows for a more realistic comparison between different working fluids, as the main influencing properties (vapor density and vapor quality) are taken into account. It should be noted that this is a simplified model that has not been validated.

A Th-diagram for a TFC using propane as working fluid and a heat source inlet temperature of 100 °C is shown in Figure 14.

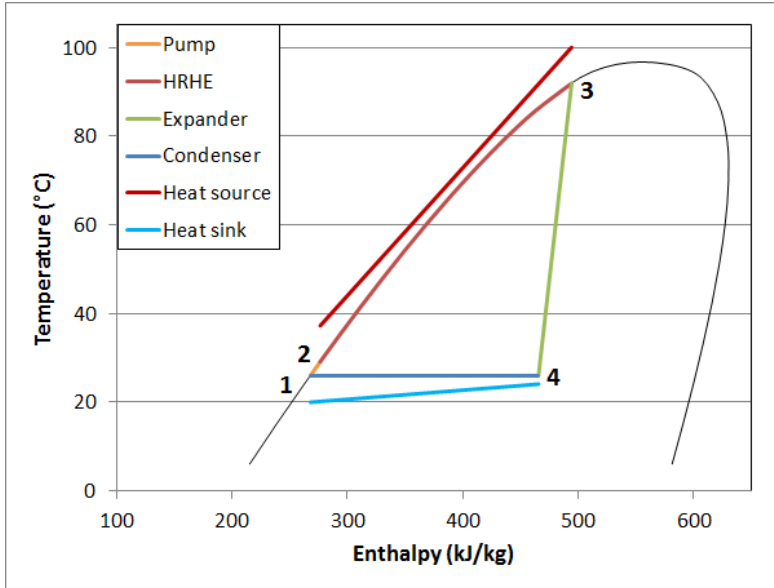


Figure 14: Th-diagram for a TFC with propane as working fluid

The different state points are calculated as following:

State 1, the pump inlet, is given by T_1 that is found in the optimization and P_1 that is determined such that state 1 is at the bubble point.

$$h_1 = h(T_1, \text{bubble point})$$

State 2, the inlet to the heater, is given by:

$$h_2 = h_1 + \frac{h(s_1, P_2) - h_1}{\eta_{\text{pump}, wf}}$$

Where P_2 is found by:

$$P_2 = P_3 + \Delta P_{HRHE}$$

P_3 is found in the optimization.

State 3, the inlet to the expander, is given by:

$$h_3 = h(P_3, \text{bubble point})$$

State 4, the inlet to the condenser (desuperheater if 4 is in the dry vapor region) is given by:

$$h_4 = h_3 + (h(s_3, P_4) - h_3) * \eta_{\text{exp}, nozzle}$$

Where $\eta_{\text{exp}, nozzle}$ is the expander nozzle efficiency. The rotor efficiency is not included in the calculation of h_4 because the rotor is a pure impulse turbine. P_4 is given by:

$$P_4 = P_1 + \Delta P_{Condenser} + \Delta P_{Desuperheater}$$

If 4 is in the dry vapor region, then state 4' is the inlet to the condenser, and is given by:

$$h_{4'} = h(P_4, Dew\ point)$$

The electric power required by the working fluid pump from state 1 to 2 is calculated by:

$$\dot{W}_{pump} = \dot{m} * \frac{h_2 - h_1}{\eta_{mo}}$$

The heat addition during the heating, state 2 to 3, is calculated by:

$$\dot{Q}_{heater} = \dot{m} * (h_3 - h_2)$$

The electric power produced in the two-phase expander, state 3 to 4, is calculated by:

$$\dot{W}_{Expander} = \dot{m} * (h_3 - h_4) * \eta_{mo} * \eta_{exp,rotor}$$

$\eta_{exp,rotor}$ is the rotor efficiency. The nozzle efficiency, $\eta_{exp,nozzle}$, is accounted for when state 4 is calculated.

The heat rejected in the condenser, state 4 to 1, is given by:

$$\dot{Q}_{Condenser} = \dot{m} * (h_4 - h_1)$$

The required electric power for the heat sink pump is found by:

$$\dot{W}_{pump,heat\ sink} = \dot{V}_{heat\ sink} * \frac{\Delta P_{heat\ sink}}{\eta_{pump,hs} * \eta_{mo}}$$

The electric power needed for the heat source fan is calculated by:

$$\dot{W}_{fan,heat\ source} = \dot{V}_{air} * \frac{\Delta P_{air}}{\eta_{fan} * \eta_{mo}}$$

The net power production from the cycle is calculated by:

$$\dot{W}_{net} = \dot{W}_{expander} - \dot{W}_{pump} - \dot{W}_{pump,heat\ sink} - \dot{W}_{fan,heat\ source}$$

The heat exchanger area is calculated the same way as for ORC.

5.2.3 Simulation of the PEC

In the PEC the two-phase expander is modeled as a VPT and the efficiency is calculated the same way as for the TFC.

A Th-diagram for a PEC using R245fa as working fluid and a heat source inlet temperature of 150 °C is shown in Figure 15.

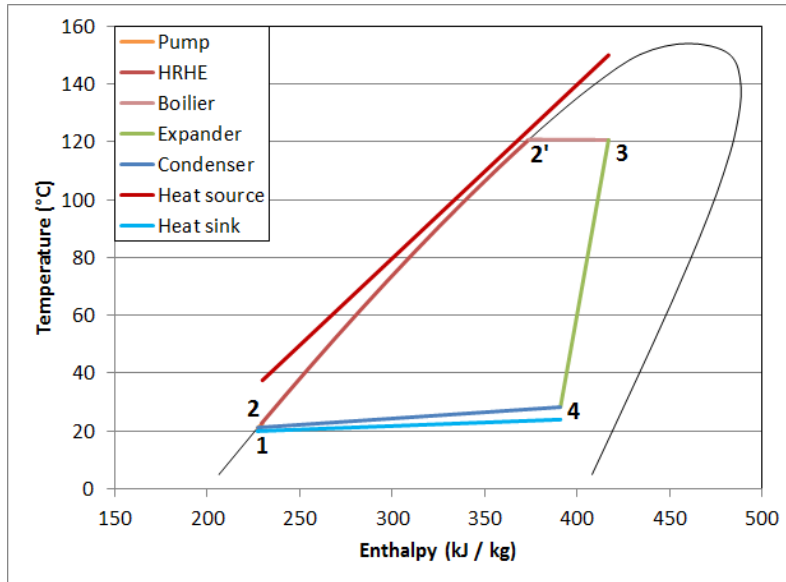


Figure 15: Th-diagram for PEC with R245fa as working fluid

The different state points are calculated as following:

State 1, the pump inlet, is given by T_1 that is found in the optimization and P_1 that is determined such that state 1 is at the bubble point.

$$h_1 = h(T_1, \text{bubble point})$$

State 2, the inlet to the heater, is given by:

$$h_2 = h_1 + \frac{h(s_1, P_2) - h_1}{\eta_{\text{pump}, \text{wf}}}$$

Where P_2 is found by:

$$P_2 = P_{2'} + \Delta P_{\text{preheat}}$$

State 2', the inlet to the evaporator, is found by:

$$h_{2'} = h(P_{2'}, \text{bubble point})$$

Where $P_{2'}$ is found in the optimization.

State 3, the inlet to the expander, is given by:

$$h_3 = h(P_3, x_3)$$

Where the vapor quality x_3 is found in the optimization and the pressure P_3 is given by:

$$P_3 = P_2' - \Delta P_{Evaporator}$$

State 4, the inlet to the condenser (desuperheater if 4 is in the dry vapor region) is given by:

$$h_4 = h_3 + (h(s_3, P_4) - h_3) * \eta_{exp, nozzle}$$

Where $\eta_{exp, nozzle}$ is the expander nozzle efficiency. P_4 is given by:

$$P_4 = P_1 + \Delta P_{Condenser} + \Delta P_{Desuperheater}$$

If 4 is in the dry vapor region, then state 4' is the inlet to the condenser, and is given by:

$$h_{4'} = h(P_4, Dew\ point)$$

The electric power required by the working fluid pump from state 1 to 2 is calculated by:

$$\dot{W}_{pump} = \dot{m} * \frac{h_2 - h_1}{\eta_{mo}}$$

The heat addition during the heating, state 2 to 3, is calculated by:

$$\dot{Q}_{Preheat} = \dot{m} * (h_{2'} - h_2)$$

$$\dot{Q}_{Evaporator} = \dot{m} * (h_3 - h_{2'})$$

The total heat input is given by:

$$\dot{Q}_{Total, in} = \dot{Q}_{Preheat} + \dot{Q}_{Evaporator}$$

The electric power produced in the two-phase expander, state 3 to 4, is calculated by:

$$\dot{W}_{Expander} = \dot{m} * (h_3 - h_4) * \eta_{exp, rotor} * \eta_{mo}$$

The heat rejected in the condenser, state 4 to 1, is given by:

$$\dot{Q}_{Condenser} = \dot{m} * (h_4 - h_1)$$

The required electric power for the heat sink pump is found by:

$$\dot{W}_{pump, heat\ sink} = \dot{V}_{heat\ sink} * \frac{\Delta P_{heat\ sink}}{\eta_{pump, hs} * \eta_{mo}}$$

The electric power needed for the heat source fan is calculated by:

$$\dot{W}_{fan,heat\ source} = \dot{V}_{air} * \frac{\Delta P_{air}}{\eta_{fan} * \eta_{mo}}$$

The net power production from the cycle is calculated by:

$$\dot{W}_{net} = \dot{W}_{expander} - \dot{W}_{pump} - \dot{W}_{pump,heat\ sink} - \dot{W}_{Fan,heat\ source}$$

The heat exchanger area is calculated in the same way as for ORC.

5.3 Macros

Several macros have been programmed in VBA to optimize the three cycles, and to do the simulations for several different working fluids at several different conditions.

The most important macros are the following:

Reset: Resets all values to reasonable starting values for optimization.

Optimize: Optimizes the cycle by maximizing net work output or efficiency. This is done by varying the “optimization variables” that can be seen in Table 3. To perform the optimization, the GRG nonlinear optimization method with forward derivatives from the Excel solver is applied. A high number of starting points are used to ensure that the global maximum is found with a high probability.

SaveResults: saves all results.

Several other macros have also been made to reduce manual work. The most important macros are given in Appendix E.

6 Heat exchanger models

In this chapter, the heat exchanger models are described. The correlations and equations used to calculate the heat transfer coefficients, pressure losses and geometry of the heat exchangers are given.

6.1 Heating process

In the heating process, a plate finned-tube heat exchanger with plain fins is used (see section 3.6.1). The working fluid on the tube side is heated by hot air that flows across the finned tubes on the outside.

The heater consists of a single-phase preheating section, a two-phase evaporating section (ORC and PEC) and a single-phase superheating section (ORC). The air side consists of one cooling section for all cycles.

6.1.1 Heat transfer coefficients and pressure losses

The overall heat transfer coefficient for the heater is found using the method from (Bell and Mueller 2001). The same equation is used for the preheating, evaporating and superheating part, but the working fluid heat transfer coefficient, h_{wf} , is different for each.

$$U_{heating} = \frac{1}{\frac{1}{h_{wf}} * \frac{A_o}{A_i} + R_{Wall} * \frac{A_o}{A_m} + R_{fin} + \frac{1}{h_{Air}}}$$

The finned-tube outside area per length is calculated as:

$$\frac{A_o}{L} = \frac{A_t}{L} + \frac{A_f}{L}$$

The tube area is found by:

$$\frac{A_t}{L} = \pi * D_o * (F_p - t) * \frac{1}{F_p}$$

Where D_o is the tube outside diameter, F_p the fin pitch and t the fin thickness. The fin area is found by:

$$\frac{A_f}{L} = 2 * \left(S_T * S_L - \frac{\pi * D_o^2}{4} \right) * \frac{1}{F_p}$$

S_T and S_L are the distances between the tubes in the transverse and longitudinal direction. The area in the middle of the tube wall is found by:

$$\frac{A_m}{L} = \pi * \frac{D_i + D_o}{2}$$

Where D_i is the tube inner diameter.

The tube inside wall area is found by:

$$\frac{A_i}{L} = \pi * D_i$$

The wall resistance is calculated as:

$$R_{Wall} = \frac{t_w}{k}$$

Where t_w is the wall thickness and k the conductivity.

The fin resistance is calculated by the method described in (Bell and Mueller 2001):

$$R_{fin} = \left[\frac{1 - \Phi}{\frac{A_t}{A_f} + \Phi} \right] * \frac{1}{h_{Air}}$$

Where Φ is the fin efficiency, given by:

$$\Phi = \frac{1}{1 + \frac{m^2}{3} * \sqrt{\frac{D_{fin}}{D_o}}}$$

D_{fin} is calculated as:

$$D_{fin} = \frac{S_L + S_T}{2}$$

And m as:

$$m = H_f * \sqrt{\frac{2}{\frac{1}{h_{Air}} * k * t}}$$

Where H_f is the fin height.

The heat transfer coefficients and friction factors are calculated as following in the heater:

Single phase (working fluid): The heat transfer coefficient and friction factor for the single phase sections (preheating and superheating) are calculated from the (Gnielinski 1976) correlation.

The Nusselt number is calculated by:

$$Nu = \frac{\left(\frac{f}{8}\right) * (Re - 1000) * Pr}{1 + 12.7 \sqrt{\left(\frac{f}{8}\right) * (Pr^{\frac{2}{3}} - 1)} * \left[1 + \left(\frac{D_i}{L}\right)^{\frac{2}{3}}\right] * K}$$

Where Re is the Reynolds number, Pr the Prandtl number and K is given by:

$$K = \left(\frac{Pr}{Pr_w}\right)^{0.11}$$

K is assumed to be 1 in this model.

The friction factor, f , is calculated by the equation given by G. K. Filonenko:

$$f = (1.82 * \text{Log}(Re) - 1.64)^{-2}$$

The pressure loss is calculated as:

$$\Delta P = f * \frac{L}{D} * \frac{G^2}{2 * \rho}$$

Where G is the mass flux and ρ is the density.

Two-phase: In the evaporating section for the ORC and PEC the heat transfer coefficient is found from the (Liu and Winterton 1991) correlation. In this correlation the contribution from the convective and nucleate boiling heat transfer mechanisms are combined as following:

$$h_{TP}^2 = (F * h_L)^2 + (S * h_{Pool})^2$$

$F * h_L$ is the forced convection contribution, where h_L is the liquid-only heat transfer coefficient calculated from the Dittus-Boelter equation:

$$h_L = 0.023 * \frac{k_l}{D_i} * Re_L^{0.8} * Pr_l^{0.4}$$

F is the forced convective heat transfer enhancement factor, and is calculated by:

$$F = [1 + x * Pr_l * \left(\frac{\rho_l}{\rho_g} - 1\right)]^{0.35}$$

$S * h_{pool}$ is the nucleate boiling contribution. h_{pool} is calculated from Cooper's pool boiling correlation (the wall roughness has been set to 1.0×10^{-6} m):

$$h_{pool} = 55 * P_r^{0.12} * q^{\frac{2}{3}} * (-\log(P_r))^{-0.55} * M^{-0.5}$$

Where q is the heat flux, P_r the reduced pressure and M the molecular weight.

S is the suppression factor, calculated by:

$$S = (1 + 0.055 * F^{0.1} * Re_L^{0.16})^{-1}$$

The pressure loss is calculated by the correlation method of (Friedel 1979), which uses a two-phase multiplier.

$$\Delta P_{frict} = \Delta P_L * \Phi_{fr}^2$$

ΔP_L is calculated for the liquid-phase flow as:

$$\Delta P_L = 4 * f_L * \frac{L}{D_i} * \dot{m}_{total}^2 * \frac{1}{2 * \rho_l}$$

The liquid friction factor and Reynolds number are obtained from:

$$f_L = \frac{0.079}{Re^{0.25}}$$

$$Re = \frac{\dot{m}_{total} * D_i}{\mu}$$

Where μ is the viscosity. The two-phase multiplier, Φ_{fr}^2 , is calculated by:

$$\Phi_{fr}^2 = E + \frac{3.24 * F * H}{Fr_H^{0.045} * We_L^{0.035}}$$

The dimensionless factors Fr_H , E , F and H are found by:

$$Fr_H = \frac{\dot{m}_{total}^2}{g * D_i * \rho_H^2}$$

Where g is the gravitational acceleration.

$$E = (1 - x)^2 + x^2 * \frac{\rho_L * f_G}{\rho_G * f_L}$$

Where f_G is found the same way as f_L only using the Reynolds number for the gas.

$$F = x^{0.78} * (1 - x)^{0.224}$$

$$H = \left(\frac{\rho_L}{\rho_G}\right)^{0.91} * \left(\frac{\mu_G}{\mu_L}\right)^{0.19} * \left(1 - \frac{\mu_G}{\mu_L}\right)^{0.7}$$

The liquid Weber number is defined as:

$$We_L = \frac{\dot{m}_{total}^2 * d_i}{\sigma * \rho_H}$$

Where σ is the surface tension and the homogeneous density, ρ_H , is calculated as:

$$\rho_H = \left(\frac{x}{\rho_G} + \frac{1 - x}{\rho_L}\right)^{-1}$$

Other pressure losses: The pressure losses in the header and tube entrance is estimated using the method from (Bell and Mueller 2001).

$$\Delta P_{ent} = 3 * \frac{G^2}{2 * \rho}$$

The pressure losses in the bends are calculated using the method from (White 2009). The method is for single-phase flow, but in this model it is also used to estimate the pressure losses for the bends where there are two-phase flow. The pressure loss in each bend is calculated by:

$$\Delta P_b = K * \frac{1}{2} * \frac{G^2}{\rho}$$

where

$$K = 0.388 * \alpha * \left(\frac{R}{D_i}\right)^{0.84} * Re^{-0.17},$$

$$\alpha = 0.95 + 4.42 * \left(\frac{R}{D_i}\right)^{-1.96}$$

and

$$R = \frac{S_L}{2}$$

The total pressure loss over all the bends is estimated as the average bend pressure loss times the number of bends:

$$\Delta P_{bends} = \Delta P_{b,ave} * (N_L - 1)$$

N_L is the number of tubes in the longitudinal direction (one tube folded back and forth).

Air side: The heat transfer coefficient and the friction factor is calculated from the (Gray and Webb 1986) correlations as following:

$$j = 0.14 * Re^{-0.328} * \left(\frac{S_T}{S_L}\right)^{-0.502} * \left(\frac{F_P}{D}\right)^{0.0312}$$

Where j is the Colburn j -factor defined by:

$$j = \frac{Nu}{Re * Pr^{\frac{1}{3}}}$$

The pressure loss is found by:

$$\Delta P = \Delta P_t + \Delta P_f$$

Where ΔP_f and ΔP_t are calculated as:

$$\Delta P_f = f_f * \frac{A_f}{A_c} * \frac{G_c^2}{2 * \rho}$$

$$\Delta P_t = f_t * \frac{A_t}{A_{c,t}} * \frac{G_c^2}{2 * \rho}$$

Where

$$G_c = G_{max} = \rho_{air} * V_{max}$$

and

$$V_{max} = \frac{S_T}{S_T - D_o} * V_{face}$$

Where V_{face} is the face velocity.

The minimum flow area A_c is found by:

$$A_c = (F_p - t) * S_T$$

The minimum flow area for bare tubes $A_{c,t}$ is found by:

$$A_{c,t} = F_p * S_T$$

The Zukauskas correlation is used to find the bare tube bank friction factor f_t , which is tabulated in Figure 7.14, in (Incropera, DeWitt et al. 2007). The friction factor associated with the fins, f_f is found by:

$$f_f = 0.508 * Re^{-0.521} * \left(\frac{S_T}{D}\right)^{1.318}$$

6.1.2 Heater geometry

The heat exchanger geometry is calculated as following:

The front area is calculated by:

$$A_{front} = \frac{\dot{V}_{air}}{v_{face}}$$

Where the volume flow, \dot{V}_{air} is found by:

$$\dot{V}_{air} = \frac{\dot{m}_{air}}{\rho_{air}}$$

The height of the heat exchanger, H , is found by:

$$H = N_T * S_T$$

N_T is the number of pipes, and S_T the distance between the pipes in the transverse direction.

N_T is calculated as:

$$N_T = \frac{4 * \frac{\dot{m}_{wf}}{G}}{\pi * D_i^2}$$

\dot{m}_{wf} is found in the cycle optimization and G is specified.

The width is found by:

$$W = \frac{A_{front}}{H}$$

And the depth by:

$$L_D = \frac{L}{W} * S_L$$

L is the required length of each pipe.

$$L = \frac{A_{HRHE}}{\left(\frac{A_o}{L}\right) * N_T}$$

A_{HRHE} is found in the optimization.

The number of pipes in the longitudinal direction is found by:

$$N_L = \frac{L}{W}$$

The tube inside diameter, D_i , is found such that $H/W = 2$ (unless it is outside a specified minimum and maximum diameter):

$$D_i = \frac{4 * \frac{\dot{m}_{wf}}{G} * S_T}{\pi * \sqrt{2} * A_{front}}$$

The outside diameter is found by:

$$D_o = D_i + 2 * t_w$$

Where t_w is the wall thickness.

The distance between the pipes for the longitudinal and transverse direction is found by:

$$S_L = 2 * D_o$$

and

$$S_T = 1.7 * D_o$$

The geometry calculation procedure is iterative.

6.2 Condensing process

The condenser is modelled as a plate heat exchanger (described in section 3.6.2).

The condenser is divided into two sections for all of the cycles, a desuperheating section, and a condensing section. The water side is one single-phase heating section.

6.2.1 Heat transfer coefficients and pressure losses

The overall heat transfer coefficients for the desuperheater and condenser are calculated as:

$$U_{desup} = \frac{1}{\frac{1}{h_{wf,vap}} + R_{wall} + \frac{1}{h_{water}}}$$

and

$$U_{cond} = \frac{1}{\frac{1}{h_{wf,TP}} + R_{wall} + \frac{1}{h_{water}}}$$

The wall resistance is calculated as:

$$R_{Wall} = \frac{t_w}{k}$$

The heat transfer coefficients and friction factors are calculated as following in the desuperheater and condenser.

Single-phase: The (Martin 1996) correlations are used to calculate the heat transfer coefficients and pressure losses for the desuperheating on the working fluid side and the heating on the heat sink side. It is a semi-theoretical correlation for single phase flow in chevron type heat exchangers. Chevron angle, φ , and heat transfer area enhancement ratio, Φ , due to corrugations are used as special parameters in the correlations.

For a given chevron angle, the friction factor is calculated as a combination of the 0° and 90° angle friction factors, f_0 and f_1 :

$$\frac{1}{\sqrt{f}} = \frac{\cos \varphi}{\sqrt{b * \tan \varphi + c * \sin \varphi + \frac{f_0}{\cos \varphi}}} + \frac{1 - \cos \varphi}{\sqrt{f_1}}$$

Where b and c are constants.

f_0 is found by:

$$f_0 = \frac{B_0}{Re}, \text{ Re} < 2000 \text{ (laminar)}$$

$$f_0 = (1.8 * \text{Log}(Re) - 1.5)^{-2}, \text{ Re} > 2000 \text{ (turbulent)}$$

The constant B_0 depends on the shape of the cross-section.

f_1 is approximated as:

$$f_1 \approx a * f_{1,0}$$

Where a is a constant and $f_{1,0}$ is found by:

$$f_{1,0} = \frac{B_1}{Re} + C_1, \text{ Re} < 2000 \text{ (laminar)}$$

$$f_{1,0} = \frac{K_1}{Re^n}, \text{ Re} > 2000 \text{ (turbulent)}$$

B_1, C_1, K_1 and n are constants.

The pressure loss is calculated by:

$$\Delta P = f * \frac{L}{D_h} * \frac{G^2}{2 * \rho}$$

The Nusselt number is calculated as:

$$Nu = 0.122 * Pr^{\frac{1}{3}} * \left(\frac{\mu}{\mu_w}\right)^{\frac{1}{6}} * [f * Re^2 * \sin 2\varphi]^{0.374}$$

$\left(\frac{\mu}{\mu_w}\right)^{\frac{1}{6}}$ is assumed to be 1 in this model.

Two-phase: The (Han, Lee et al. 2003) correlations are used to find the heat transfer coefficient and friction factor for the condensation of the working fluid. It uses corrugation pitch and chevron angle as parameters.

The Nusselt number is calculated as:

$$Nu = Ge_1 * Re_{Eq}^{Ge_2} * Pr^{\frac{1}{3}}$$

Where Re_{Eq} is the equivalent Reynolds number found by:

$$Re_{Eq} = \frac{Ge_{Eq} * D_h}{\mu}$$

And Ge_{Eq} is the equivalent mass flux:

$$Ge_{Eq} = G * [1 - x + x * \left(\frac{\rho_l}{\rho_g}\right)^{0.5}]$$

Ge_1 and Ge_2 are functions of the heat exchanger geometry:

$$Ge_1 = 11.22 * \left(\frac{F_p}{D_h}\right)^{-2.83} * \varphi^{-4.5}$$

$$Ge_2 = 0.35 * \left(\frac{F_p}{D_h}\right)^{0.23} * \varphi^{1.48}$$

The friction factor is calculated as:

$$f = Ge_3 * Re_{Eq}^{Ge_4}$$

where

$$Ge_3 = 3521.1 * \left(\frac{F_p}{D_h}\right)^{4.17} * \varphi^{-7.75}$$

$$Ge_4 = -1.024 * \left(\frac{F_p}{D_h}\right)^{0.0925} * \varphi^{-1.3}$$

The pressure loss is calculated as:

$$\Delta P_f = f * \frac{L}{D_h} * \frac{G_{Eq}^2}{\rho_l}$$

Other pressure losses: The pressure losses for the inlet and outlet ports are calculated as (Han, Lee et al. 2003):

$$\Delta P_{ports} = \frac{1.4 * G_p^2}{2 * \rho_m}$$

Where

$$G_p = \frac{4 * \dot{m}_{Eq}}{\pi * D_p^2}$$

D_p is the port diameter and

$$\frac{1}{\rho_m} = \frac{x}{\rho_g} + \frac{(1-x)}{\rho_l}$$

The equivalent mass flow rate is defined as:

$$\dot{m}_{Eq} = \dot{m} * \left[1 - x + x * \left(\frac{\rho_l}{\rho_g}\right)^{0.5} \right]$$

The acceleration pressure loss is calculated as (Han, Lee et al. 2003):

$$\Delta P_a = -\left[\left(\frac{G_{Eq}^2 * x}{\rho_{fg}} \right)_{in} - \left(\frac{G_{Eq}^2 * x}{\rho_{fg}} \right)_{out} \right]$$

6.2.2 Condenser geometry

The condenser geometry (see Figure 16) is calculated as following:

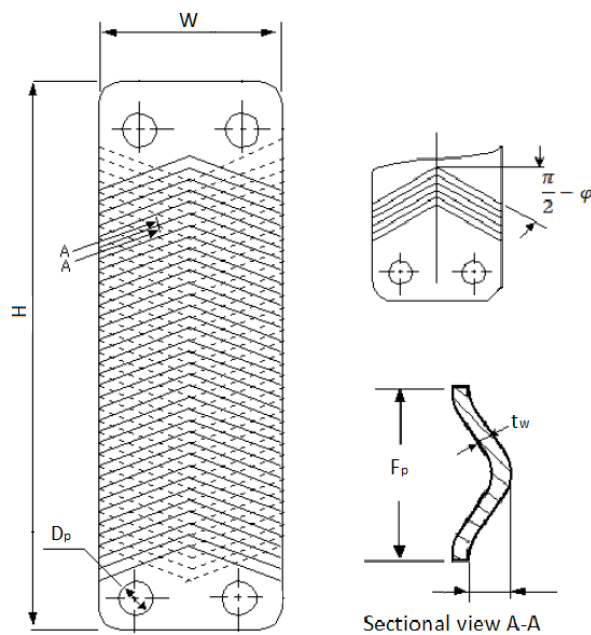


Figure 16: Condenser geometry

W and H are specified and the depth, L_D , is calculated as:

$$L_D = (N_{PC,wf} * N_{pass,wf} + N_{PC,air} * N_{pass,air}) * b + (N_{PC,wf} * N_{pass,wf} + N_{PC,air} * N_{pass,air} + 1) * t_w$$

Where b is the channel spacing and t_w the plate thickness. N_{PC} is the number of channels for each pass, and N_{pass} is the number of passes. N_{PC} and N_{pass} are calculated as following for both the desuperheater and the condenser:

$$N_{PC} = \frac{\dot{m}_{wf}}{G * b * W}$$

$$N_{Pass} = \frac{A_{desup\ or\ cond}}{2 * H * W * \Phi * N_{PC}}$$

The mass flow rate and required area in the desuperheater, A_{desup} , and condenser, A_{cond} , are found in the optimization.

The enhancement factor, Φ , can be estimated by (Martin 1996):

$$\Phi \approx \frac{1}{6} * (1 + \sqrt{1 + X^2} + 4 * \sqrt{1 + \frac{X^2}{2}})$$

where

$$X = \frac{\pi * b}{F_p}$$

The pitch is found by:

$$F_p = 2 * b$$

The hydraulic diameter is calculated as:

$$D_h = \frac{2 * b}{\Phi}$$

For the heat sink side N_{PC} and N_{pass} are calculated as:

$$N_{PC} = \frac{\dot{m}_{heat\ sink}}{G * b * W}$$

$$N_{Pass} = \frac{A_{desup} + A_{cond}}{2 * H * W * \Phi * N_{PC}}$$

The geometry calculation procedure is iterative.

7 Case Studies

In this chapter, the simulated cases and working fluid selection are described.

7.1 Case definition

In this study, three different cases have been simulated. An overview is given in Table 4. Most of the specifications and boundary conditions for the ORC, TFC and PEC are the same, so they are given in the same table, Table 5.

Table 4: Overview of the three cases

	heat source:	heat sink:
Case I	1 kg/s air at 100 °C	water at 20 °C
Case II	1 kg/s air at 150 °C	water at 20 °C
Case III	1 kg/s air at 200 °C	water at 20 °C

All cycles are simulated using R123, R134a, R245fa, R1234ze(E), butane (R600), pentane (R601), isopentane (R601a) and propane (R290) as working fluid, and a heat source of 10 kg/s air at 100 °C for Case I, 150 °C for Case II and 200 °C for Case III. Water at 20 °C is used as the heat sink for all cases. The cycles are optimized for maximum net power production. The maximum total heat exchanger area is set to 1000, 1500, 2000, 2500, 3000, 3500 and 4000 m². This maximum area includes all sections: heater, evaporator, superheater, desuperheater and condenser.

Table 5: Input data for the ORC, TFC and PEC simulations

	Parameter	Value
Cycle	Working Fluid	R123, R134a, R245fa, R1234ze, butane, pentane, isopentane and propane
	Total area restriction	1000, 1500, 2000, 2500, 3000, 3500 and 4000 m ²
Heat source	Fluid	Air
	Mass flow	10 kg/s
	Inlet temperature	100, 150 and 200 °C
	Inlet pressure	0.3 MPa
	Fan efficiency	0.92
Pressure loss	Calculated in heat exchanger simulation	
Heat sink	Fluid	Water
	Inlet temperature	20 °C
	Inlet pressure	0.3 MPa
	Pump efficiency	0.70
	Motor efficiency	0.95
	Pressure loss	Calculated in heat exchanger simulation

Pump	Isentropic efficiency Motor efficiency	0.70 0.95
HRHE	HTC heater HTC evaporator (ORC and PEC) HTC superheater (ORC) Minimum pinch temperature Pressure losses	Calculated in heat exchanger simulation Calculated in heat exchanger simulation Calculated in heat exchanger simulation 1 °C Calculated in heat exchanger simulation
Expander	Isentropic efficiency (ORC) Isentropic efficiency, nozzle (TFC and PEC) Isentropic efficiency, rotor (TFC and PEC)	0.80 $0.865 + 0.00175 * \text{vapor density}$ $0.575 + 0.325 * \text{vapor quality}$
Condenser	HTC condenser HTC desuperheater Pressure losses	Calculated in heat exchanger simulation Calculated in heat exchanger simulation Calculated in heat exchanger simulation

The heat transfer coefficients and pressure losses are calculated in the heat exchanger model.

The input and output parameters for the model are given in Table 6.

Table 6: Input and output data for the heater and condenser calculations

	Parameter	Value
Heater	Working fluid	R123, R134a, R245fa, R1234ze, butane, pentane, isopentane, and propane
	Working fluid side	Temperature From Cycle calculation Pressure From Cycle calculation Heat flux From Cycle calculation Mass flow From Cycle calculation Mass flux (ORC) 300 kg/m ² s Mass flux (TFC) 350 kg/m ² s Mass flux (PEC) 300 kg/m ² s Inner diameter Calculated (range 0.009 – 0.025 m)
Heat source side	Heat source fluid	Air
	Temperature, in 100, 150 and 200 °C Pressure, in 0.3 MPa Mass flow 10 kg/s Face velocity, air 2.2 m/s	
	Outer diameter	Calculated
	Wall thickness	1.0 mm
	Fin thickness	0.13 mm
	Fin pitch	2.3 mm
	Distance between tubes, transverse	Calculated
	Distance between tubes, longitudinal	Calculated
	Wall and fin material	Copper
	Wall conductivity	401 W/mK
	Pipe length	Calculated
	Number of pipes, transverse	Calculated
	Number of pipes, longitudinal	Calculated
	Overall HTC, preheater	Output
	Overall HTC, evaporator	Output
	Overall HTC, superheater	Output
	Pressure loss, preheater	Output
	Pressure loss, evaporator	Output
	Pressure loss, superheater	Output
	Pressure loss, air side	Output

Condenser	Working fluid	R123, R134a, R245fa, R1234ze, butane, pentane, isopentane, and propane
Working fluid side	Temperature	From Cycle calculation
	Pressure	From Cycle calculation
Heat sink side	Mass flow	From Cycle calculation
	Mass flux (ORC, TFC, PEC)	50 kg/m ² s
	Constants a, b, c	Standard set: 3.8, 0.18, 0.36
	Constants, K1, n, B ₀ , B ₁ , C ₁	38.7, 0.289, 64, 589.6, 3.82
	Heat sink fluid	Water
	Temperature, in	20 °C
	Pressure, in	0.3 Mpa
	Mass flow	From Cycle calculation
	Mass flux	250 kg/m ² s
	Height	1.8 m
	Width	1.0 m
	Mean channel spacing	6.0 mm
	Hydraulic diameter	8.14 mm
	Corrugation pitch	12.0 mm
	Wall thickness	0.4 mm
	Wall and fin material	Copper
	Wall conductivity	401 W/mK
Corrugation angle	35°	
Number of passes	Calculated	
Number of channels per pass.	Calculated	
Enhancement factor	Calculated	
Overall HTC, desuperheater	Output	
Overall HTC, condenser	Output	
Pressure loss, desuperheater	Output	
Pressure loss, condenser	Output	
Pressure loss, heat sink	Output	

7.2 Working fluid selection

Several working fluid studies can be found in the literature. In most cases these studies present a comparison of the thermodynamic performance for a set of candidate working fluids (Quoilin, Van Den Broek et al. 2013). However, other aspects like environmental impact and safety level of the fluids should also be considered, as mentioned in section 3.5.

In this study, we have considered the environmental parameters Ozone Depleting Potential (ODP) (relative to R-11), and Global Warming potential (GWP) (relative to CO₂). The safety parameter we have used indicate if the working fluid is toxic and/or flammable (ASHRAE Standard 34). The leading letters A and B signify “lower” and “higher” toxicity, based on occupational exposure limits. The numbers 1, 2 and 3 indicate “no flame propagation”, “lower flammability”, and “higher flammability” respectively. Group 2 is subdivided, based on burning velocity, with 2L implying those more difficult to ignite (Calm and Hourahan 2011).

The standard fluids used in low temperature ORC plants today are R134a and R245fa (Quoilin, Van Den Broek et al. 2013) and are therefore chosen as reference. R123 is chosen as it is suitable for low temperature applications (Li, Wang et al. 2013). R1234ze(E) was chosen as it is a promising refrigerant for the future (Zyhowski and Brown 2011). To compare the performance of these refrigerants to natural working fluids, three hydrocarbons with different critical temperatures were chosen. One of the biggest disadvantages of hydrocarbons is their high flammability which can be reduced by mixing them with CO₂ (Garg, Kumar et al. 2013). However, only pure fluids are investigated in this study.

The selected fluids are listed with their critical temperature, GWP and safety class in Table 7. The ODP is not listed as it is negligible for all selected fluids. A more extensive table of working fluid properties are given in Appendix B.

Table 7: Properties of selected working fluids (Calm and Hourahan 2011, Fukuda, Kondou et al. 2014)

Fluid	T_{crit} (°C)	GWP	Safety class
R134a	101.1	1300	A1
R245fa	154.0	1030	B1
R123	183.7	77	B1
R1234ze(E)	109.4	6	A2L
Butane	152.0	20	A3
Pentane	196.6	20	A3
Isopentane	187.2	20	A3
Propane	96.7	20	A3

8 Results

In this chapter, the results from the case studies are presented. The net power production for the five best working fluids for the ORC, TFC and PEC are shown in Figure 17, Figure 18 and Figure 19 for Case I, Case II and Case III respectively. The power production for ORC, TFC and PEC using the same working fluid are shown next to each other. The maximum heat exchanger area limits are shown as different colors in the bar graphs.

Selected result details for the two best working fluids for each cycle with maximum area are given in Table 8, Table 9 and Table 10 for Case I, Case II and Case III. The results for all the different working fluids are given in Appendix A.

8.1 Case I, heat source: 10 kg/s air at 100 °C

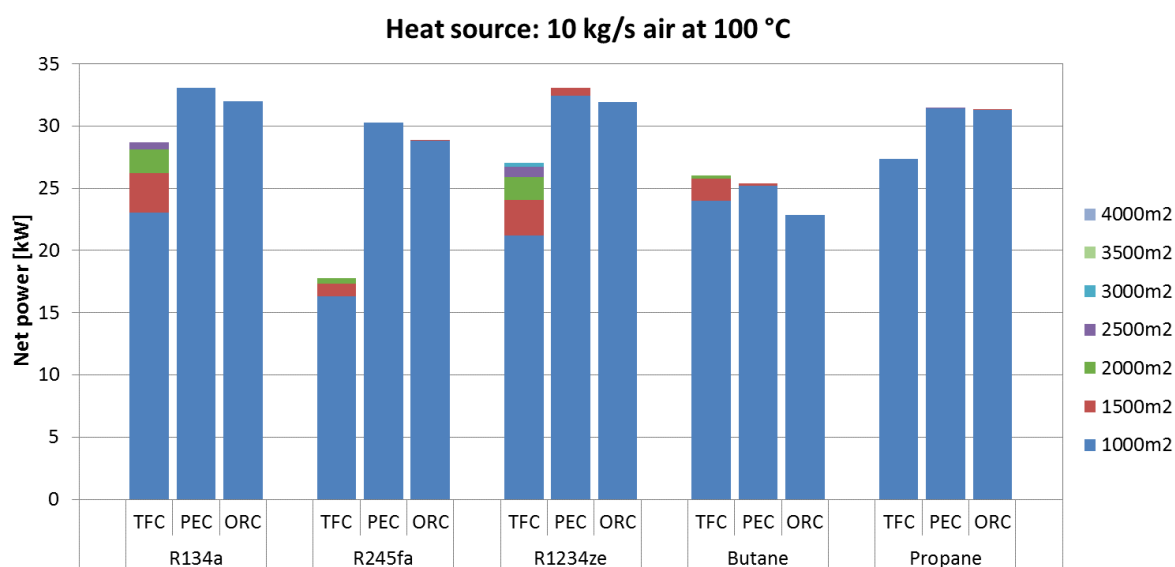


Figure 17: Case I, Net power for TFC, PEC and ORC for the five best working fluids

The ORC and PEC outperforms the TFC. The best PEC, with R134a, has a power production that is 15 % higher than for the best TFC, with R134a, and 3 % higher than for the best ORC, with R134a. The vapor quality at the expander inlet is 1.00 for the PEC, which makes it an ORC without superheating. The best TFC requires a 178 % larger heater, a 32 % larger condenser and a 106 % higher working fluid mass flow rate than the best PEC. However, the second best TFC, with propane, has a similar area requirement and mass flow of working fluid as the best PEC. The volume flow at the expander outlet is 30 % higher for the best TFC compared to the PEC and ORC.

The TFC with butane has a slightly higher power production than the PEC with butane. This is possible because the mass flux in the heater is set to 350 kg/m²s for the TFC while it is set to 300 kg/m²s for the PEC. This is done to limit the pressure loss in the evaporator for the PEC.

The total expander efficiency ranges from 0.59 to 0.71 for the TFC and 0.59 to 0.82 for the PEC. The expander efficiency is slightly better for the best PECs compared to the ORC because the variable two-phase efficiency is at its optimum for these cases.

Table 8: Case I, Performance parameters and details for the two best ORCs, TFCs and PECs

Case I, 100 °C		ORC		TFC		PEC	
		R134a	R1234ze	R134a	Propane	R134a	R1234ze
Working fluid		R134a	R1234ze	R134a	Propane	R134a	R1234ze
Net power	kW	32.0	31.9	28.7	27.4	33.1	33.1
Total area	m ²	1000	1000	2500	1000	1000	1305
Working fluid mass flow	kg/s	2.5	2.6	5.3	2.6	2.6	2.8
Volume flow expander outlet	m ³ /s	0.09	0.11	0.11	0.09	0.08	0.12
Pump outlet pressure	MPa	1.9	1.4	3.6	4.0	1.9	1.4
Heat source outlet temperature	°C	51	51	36	39	50	48
Vapor quality	-	-	-	-	-	1.00	0.97
Expander (nozzle)	-	-	-	0.92	0.90	0.92	0.91
Expander (rotor)	-	-	-	0.77	0.78	0.89	0.90
Superheat expander inlet	°C	2	1	-	-	-	-
Heat input	kW	497	492	646	618	407	488
Area		0.0	0.0	0.0	0.0	0.0	0.0
Heater	m ²	800	789	2246	805	807	1091
Condenser	m ²	200	211	255	195	193	213
Power production/consumption							
Expander	kW	40.7	39.8	58.1	58.3	41.8	42.3
Working fluid pump	kW	4.2	3.4	20.6	25.8	4.2	3.6
Fan power	kW	4.0	3.8	7.9	4.5	3.9	5.0
Heat sink pump	kW	0.6	0.6	0.8	0.7	0.5	0.6
Pressure losses							
HRHE	kPa	1.3	1.3	4.0	8.8	1.3	1.6
Evaporator	kPa	7.1	8.2	-	-	6.9	8.8
Superheater	kPa	0.0	0.0	-	-	-	-
Desuperheater	kPa	0.7	2.1	0.0	0.0	0.0	0.0
Condenser	kPa	1.0	1.3	2.7	0.8	1.0	1.6
Heat sink	kPa	3.2	3.3	3.6	3.2	3.2	3.4
Heat source	kPa	1.0	1.0	2.0	1.1	1.0	1.2
Heat transfer coefficients							
Preheating	W/m ² K	40	38	38	82	40	35
Evaporating	W/m ² K	82	81	-	-	82	80
Superheating	W/m ² K	47	47	-	-	-	-
Desuperheating	W/m ² K	333	323	333	555	333	320
Condensing	W/m ² K	1649	1600	1650	1812	1649	1599

8.2 Case II, heat source: 10 kg/s air at 150 °C

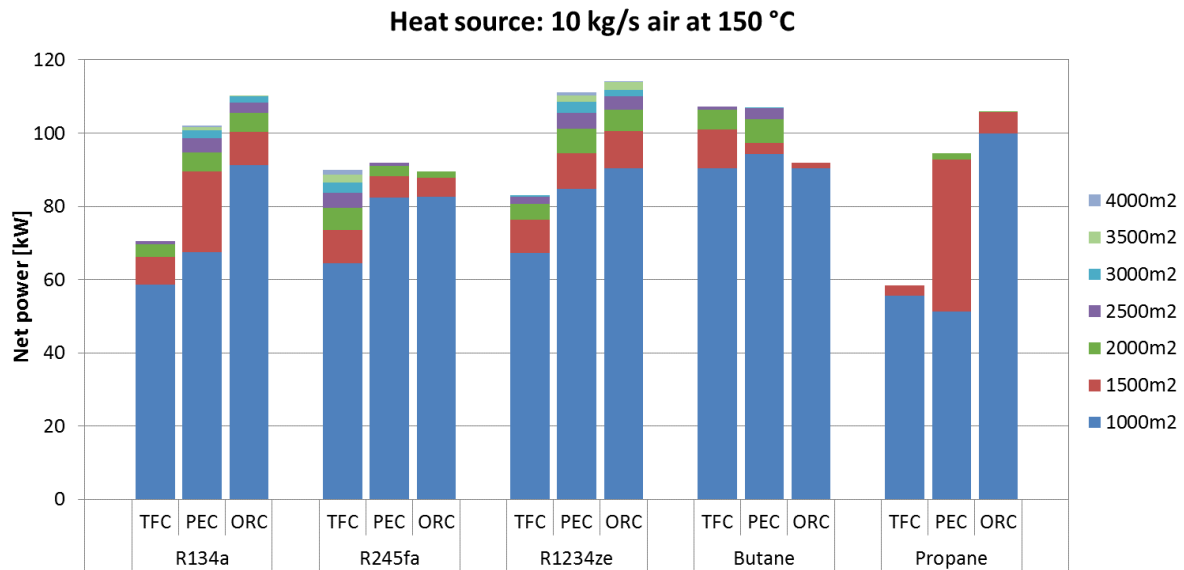


Figure 18: Case II, Net power for TFC, PEC and ORC for the five best working fluids

The ORC has the highest power production. The best ORC, with R1234ze, has a power production that is 3 % higher than for the best PEC, with R1234ze and 6 % higher than for the best TFC, with butane. The PEC has a vapor quality of 1.00 at the expander inlet, which makes it an ORC. The best TFC requires 36 % less heater area and 20 % less condenser area compared to the best ORC, due to higher heat transfer coefficients. The working fluid mass flow is lower for the best TFC while the volume flow at the expander outlet is 87 % higher than for the ORC and PEC.

The total expander efficiency ranges from 0.67 to 0.74 for the TFC and 0.70 to 0.81 for the PEC.

Table 9: Case II, Performance parameters and details for the two best ORCs, TFCs and PECs

Case II, 150 °C		ORC		TFC		PEC	
		R1234ze	R134a	Butane	R245fa	R1234ze	Butane
Working fluid							
Net power	kW	114.1	110.1	107.3	90.0	111.1	107.1
Total area	m ²	3784	3000	2500	4000	4003	2998
Working fluid mass flow	kg/s	5.8	5.3	3.4	5.9	6.3	3.3
Volume flow expander outlet	m ³ /s	0.25	0.19	0.47	0.48	0.25	0.47
Pump outlet pressure	MPa	3.5	3.9	3.2	3.0	3.3	3.1
Heat source outlet temperature	°C	34	37	33	40	32	34
Vapor quality	-	-	-	-	-	1.00	0.06
Expander (nozzle)	-	-	-	0.87	0.88	0.91	0.87
Expander (rotor)	-	-	-	0.84	0.84	0.89	0.84
Superheat expander inlet	°C	4	13	-	-	-	-
Heat input	kW	1180	1150	1183	1114	1141	1094

Area							
Heater	m ²	3266	2551	2086	3812	3525	2578
Condenser	m ²	519	449	414	188	479	420
Power production/consumption							
Expander	kW	148.8	142.1	145.5	122.0	146.4	144.8
Working fluid pump	kW	23.5	22.2	27.6	20.3	24.0	26.5
Fan power	kW	8.6	7.9	9.5	11.2	9.3	10.1
Heat sink pump	kW	2.5	2.0	1.1	0.5	2.1	1.1
Pressure losses							
HRHE	kPa	2.5	2.3	13.8	4.9	2.5	9.7
Evaporator	kPa	0.4	0.5	-	-	0.5	0.0
Superheater	kPa	0.1	0.6	-	-	-	-
Desuperheater	kPa	2.2	2.2	0.0	0.0	0.0	0.0
Condenser	kPa	5.8	2.9	15.7	48.2	6.6	16.0
Heat sink	kPa	6.9	6.0	5.0	4.9	6.7	5.3
Heat source	kPa	2.1	1.9	2.3	2.6	2.2	2.4
Heat transfer coefficients							
Preheating	W/m ² K	31	35	61	27	27	52
Evaporating	W/m ² K	61	67	-	-	57	69
Superheating	W/m ² K	43	39	-	-	-	-
Desuperheating	W/m ² K	324	336	522	338	320	521
Condensing	W/m ² K	1600	1649	2042	1902	1600	2040

8.3 Case III, heat source: 10 kg/s air at 200 °C

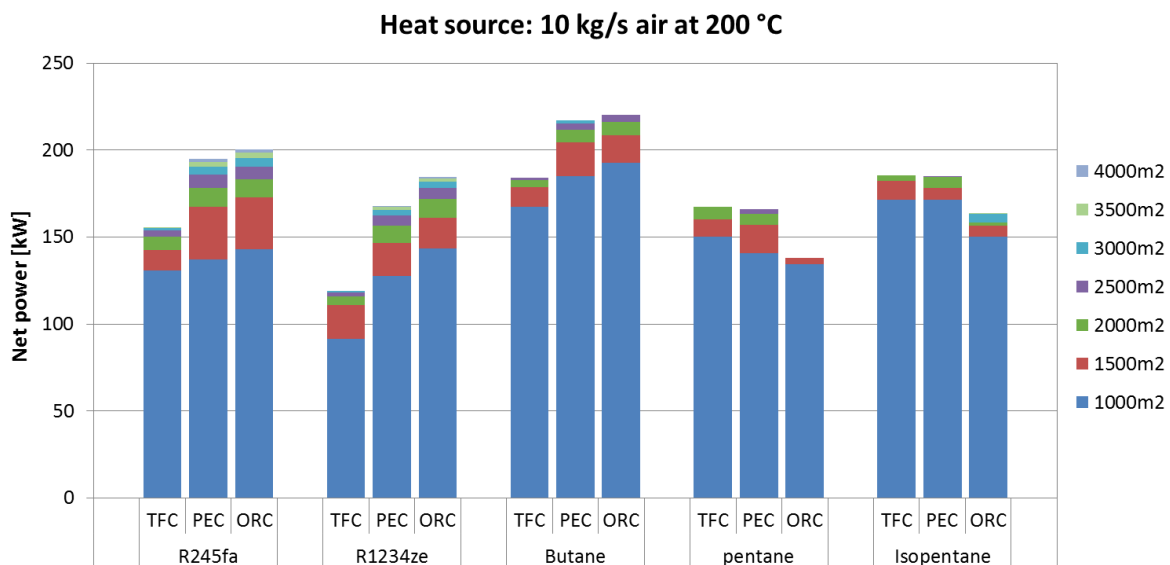


Figure 19: Case III, Net power for TFC, PEC and ORC for the five best working fluids

The ORC with butane has a power production that is 19 % higher than for the best TFC, with isopentane and 1 % higher than the best PEC, with butane. The best PEC has a vapor quality of 1.00 at the expander inlet and is an ORC. The required heater area are about the same for the best ORC and TFC, but the ORC requires 599 % more condenser area. The mass flow of

working fluid is similar for the ORC and TFC, while the volume flow at the expander outlet is 38 % higher for the TFC.

The total expander efficiency ranges from 0.70 to 0.78 for the TFC and 0.77 to 0.81 for the PEC.

Table 10: Case III, Performance parameters and details for the two best ORCs, TFCs and PECs

Case III, 200 °C		ORC		TFC		PEC	
Working fluid		Butane	R245fa	Isopentane	Butane	Butane	R245fa
Net power	kW	220.4	200.6	185.6	183.9	217.2	194.8
Total area	m ²	2502	4000	2000	2501	3001	4000
Working fluid mass flow	kg/s	3.4	6.3	3.6	4.6	3.7	6.8
Volume flow expander outlet	m ³ /s	0.61	0.67	0.84	0.66	0.63	0.66
Pump outlet pressure	MPa	3.6	3.5	3.2	3.6	3.6	3.5
Heat source outlet temperature	°C	33	36	40	25	28	33
Vapor quality	-	-	-	-	-	1.00	1.00
Expander (nozzle)	-	-	-	0.87	0.87	0.87	0.88
Expander (rotor)	-	-	-	0.90	0.86	0.90	0.90
Superheat expander inlet	°C	3	3	-	-	-	-
Heat input	kW	1696	1662	1622	1772	1680	1629
Area							
Heater	m ²	2011	3758	1930	2015	2428	3758
Condenser	m ²	491	242	70	486	573	243
Power production/consumption							
Expander	kW	261.8	235.3	222.6	234.5	261.8	231.4
Working fluid pump	kW	31.6	24.8	28.8	42.4	34.1	26.6
Fan power	kW	7.8	9.4	8.0	6.9	9.0	9.5
Heat sink pump	kW	1.9	0.5	0.2	1.3	1.5	0.5
Pressure losses							
HRHE	kPa	7.3	2.7	11.4	8.1	8.1	2.6
Evaporator	kPa	0.8	0.2	-	-	0.6	0.2
Superheater	kPa	0.1	0.1	-	-	-	-
Desuperheater	kPa	12.8	3.6	5.7	0.0	9.6	1.9
Condenser	kPa	16.8	53.9	44.9	28.3	19.2	59.7
Heat sink	kPa	6.6	3.9	3.0	6.1	6.4	3.8
Heat source	kPa	1.8	2.1	1.8	1.6	2.1	2.2
Heat transfer coefficients							
Preheating	W/m ² K	59	27	63	58	56	27
Evaporating	W/m ² K	103	61	-	-	100	62
Superheating	W/m ² K	74	44	-	-	-	-
Desuperheating	W/m ² K	543	347	530	525	533	343
Condensing	W/m ² K	2040	1890	2138	2042	2040	1889

8.4 Discussion

For the 100 °C case, the TFC has the lowest power production but requires significantly larger heat exchanger areas, higher mass flow of working fluid and volume flow at the expander outlet, which indicates a larger system. As seen in Table 8, both the heat input and

power produced in the expander are highest for the TFC, but the required working fluid pump power and heat source fan power are also much higher for the TFC, resulting in the lowest net power production. The reason for the high pump power is that the working fluid mass flow is much higher than for the two other cycles, and that it needs to be pumped to a higher pressure. The fan power is higher because the higher heater area requirement leads to higher pressure losses in the heater (the front area of the heater is the same for all cycles).

When comparing the average values for mass flow of working fluid, volume flow rate at the expander outlet and total heat exchanger area requirement over all the different working fluids, shown in Table 11, the TFC is estimated to have a significantly larger total system size than the ORC and PEC for Case I.

Table 11: Average values over all working fluids for system size estimation for Case I, II and III

Case	Cycle	Working fluid mass flow [kg/s]	Expander outlet volume flow [m ³ /s]	Total heat exchanger area [m ²]
I, 100 °C	ORC	1.6	0.16	837
	TFC	4.4	0.21	1688
	PEC	2.7	0.23	1059
II, 150 °C	ORC	3.3	0.36	1935
	TFC	5.9	0.40	2875
	PEC	4.3	0.42	2688
III, 150 °C	ORC	4.6	0.54	3076
	TFC	7.7	0.56	2688
	PEC	6.0	0.56	3250

The TFC has the lowest power production for the 150 °C case as well. The total area requirement is lower for the best TFC compared to the best ORC and PEC. When comparing the average values over all the different working fluids (see Table 11), the TFC still has a significantly larger estimated total system size than the ORC, however not as much as for Case I. The estimated system size for the PEC is between the ORC and the TFC.

The TFC has the lowest power production for Case III also. The total area requirement is lower for the best TFC compared to the ORC and PEC. When comparing the average values over all the working fluids (see Table 11), the TFC requires a significantly larger mass flow of working fluid, a slightly higher volume flow at the expander outlet, and less total heat exchanger area compared to the ORC. This is also the case for the PEC, and both cycles are estimated to have a larger total system size than the ORC.

The calculated expander efficiency for the TFC is lower than the assumed 0.80 for the ORC expander for all cases. The efficiency increases with increasing heat source temperature and has a maximum of 0.78 for isopentane in the 200 °C case.

The pressure losses in the evaporator are significantly higher for the natural working fluids butane, pentane and isopentane compared to the standard refrigerants. Despite this, these working fluids are among the best for the 150 °C and 200 °C cases. The parameters are within the range where the Friedel correlation used to calculate the pressure loss is recommended for all the fluids (Thome 2004).

The top three PECs are pure or very close to pure ORCs or TFCs for all the cases (vapor quality 1.0 or 0.0 at expander inlet). Previous studies have found that the advantage of the PEC is highest for systems with low heat source temperatures and low working fluid pump efficiency. To investigate this, Case I and II have been simulated with a working fluid pump efficiency of 0.50. This leads to the PECs performing better compared to the TFCs. The best PECs that does not end up as pure ORCs or TFCs in the optimization are however still outperformed by the ORCs. This is as expected since reducing the pump efficiency gives the PEC an advantage over the TFC, but not over the ORC (due to the reduced mass flow of working fluid for the PEC compared to the TFC).

The results from this study deviates from the results found in my project thesis (Trædal 2013) where the pressure losses were neglected and heat transfer coefficients assumed constant and equal for all working fluids. In that study the TFC was found to have a higher power production than the ORC for the 100 °C case, and the difference in net power production between the TFC and ORC was found to be insignificant for the 150 °C and 200 °C cases. The system size was estimated to be larger for the TFC, especially at lower heat source temperatures. Now that the pressure losses and heat transfer coefficients are included, as well as a better two-phase expander efficiency model, the TFC can no longer outperform the ORC. The reason is that the increase in pressure losses and associated increase in pump power outweighs the increase in heat input and higher expander power output obtained by increasing the heater area in the TFC. The heat transfer coefficient for the TFC heater was also overestimated in the previous study. The new heat exchanger models have shown that the heat transfer coefficients are lower than earlier predicted, and that there are big differences between the different working fluids used.

This study deviates even more from other published studies on the TFC (see chapter 4) by being less promising. This is mainly due to the variable two-phase expander efficiency used here, and that none of the other studies considers pressure losses in the system or calculation of heat transfer coefficients for each working fluid.

To improve this model the mass flux of working fluid should be optimized in the cycle simulations to get the optimal tradeoff between the heat transfer coefficients and pressure losses. To do this the calculations need to be done in another software.

The use of working fluid mixtures and more complex cycle configurations (see chapter 4) could also be investigated.

9 Conclusions

The calculation tool for the TFC and ORC from my project thesis (Trædal 2013) has been further developed and improved, and a calculation tool for the PEC has been made.

Heat exchanger models for the heater and condenser have been included in the model as described in chapter 6. The heater is modeled as a plate finned-tube heat exchanger, and the condenser as a plate heat exchanger. The pressure losses and heat transfer coefficients are calculated with appropriate correlations. This improves the accuracy of the results for the cycle simulations and gives better heat exchanger area estimates.

The two-phase expander has been modeled as a VPT. The nozzle and rotor efficiencies are calculated separately in the model, and takes the main influencing properties into account (see section 5.2.2). The nozzle efficiency depends on the vapor density of the working fluid at condensing pressure and the rotor efficiency on the vapor quality at the nozzle exit.

Several working fluids have been evaluated for the three cycles. They were selected as described in section 7.2.

Based on the simulations from the new model the following conclusions can be made:

- The TFC has the lowest power production in all cases, and the total system size is estimated to be larger for the TFC compared to the other cycles, especially at the lower heat source temperature cases.
- The top three PECs are close to pure ORCs or TFCs for all cases, and do not show an advantage over the ORC for the cases studied here.
- The TFC system is estimated to have a lower cost than the ORC due to the elimination of the evaporator, separator drum, gear box, lube oil system and the fact that simpler heat exchangers can be used (see chapter 4). The TFC can therefore be suitable in systems with a heat source in the 100 °C to 150 °C range, where the power production for the TFC and ORC is similar, when system size is not a critical factor.
- The PEC is not recommended for systems similar to the cases investigated in this study. The power production is similar to that of an ORC, but the system is more complex. The PEC also does not have the cost advantages of the TFC, as it requires an evaporator, and might need a gear box and lube oil system.

- The calculated expander efficiency for the TFC is lower than the assumed 0.80 for the ORC expander for all cases. The efficiency increases with increasing heat source temperature.
- The results are much less promising for the TFC than the results from my project thesis (Trædal 2013) and the other published studies on the TFC (see chapter 4) now that the pressure losses, heat transfer coefficients for each working fluid and better two-phase expander model are included.
- The natural working fluids with low environmental impact can match standard refrigerants in terms of performance despite having significantly higher pressure losses in the evaporator. However, the flammability of the investigated hydrocarbons is a disadvantage that needs to be kept in mind.

10 References

Andresen, T. (2009). Mathematical modeling of CO₂ based heat pumping systems. Faculty of Engineering Science and Technology

Department of Energy and Process Engineering, Norwegian University of Science and Technology. **Philosophiae Doctor**.

Bao, J. and L. Zhao (2013). "A review of working fluid and expander selections for organic Rankine cycle." Renewable and Sustainable Energy Reviews **24**: 325-342.

Bell, K. J. and A. C. Mueller (2001). Wolverine Engineering Data Book II, Wolverine Tube, Inc.

Boyle, P. and L. Hays (2013). "Variable Phase Cycle." Journal of the Gas Turbine Society of Japan **41**(6): 461-466.

Brown, B. W. and G. L. Mines (1998). "Flowsheet Simulation of the Trilateral Cycle." The Geothermal Resources Council **22**: 373-378.

Calm, J. M. and G. C. Hourahan (2011). Physical, Safety, and Environmental Data for Current and Alternative Refrigerants. 23rd International Congress of Refrigeration. Prague, Czech Republic.

Chan, C. W., et al. (2013). "A review of chemical heat pumps, thermodynamic cycles and thermal energy storage technologies for low grade heat utilization." Applied Thermal Engineering **50**(1): 1257-1273.

Fischer, J. (2011). "Comparison of trilateral cycles and organic Rankine cycles." Energy **36**(10): 6208-6219.

Friedel, L. (1979). Improved friction pressure drop correlations for horizontal and vertical two phase pipe flow. European Two Phase Flow Group Meeting.

Fukuda, S., et al. (2014). "Low GWP refrigerants R1234ze(E) and R1234ze(Z) for high temperature heat pumps." International Journal of Refrigeration **40**: 161-173.

Garg, P., et al. (2013). "Evaluation of carbon dioxide blends with isopentane and propane as working fluids for organic Rankine cycles." Applied Thermal Engineering **52**(2): 439-448.

Gnielinski, V. (1976). "New equations for heat and mass transfer in turbulent pipe and channel flow." International Chemical Engineering **16**(2): 359-368.

Gray, D. L. and R. L. Webb (1986). Heat Transfer and Friction Correlations for Plate Finned-Tube Heat Exchangers having Plain Fins. International Heat Transfer Conference.

Han, D. H., et al. (2003). "The Characteristics of Condensation in Brazed Plate Heat Exchangers with Different Chevron Angles." Journal of the Korean Physical Society **43**(1): 66 -73.

Hays, L. (2014). "Personal communication."

Hays, L. and D. Sahabian (2006). Variable Phase Turbine. U. S. Patent. USA, Energent Corporation.

Ho, T., et al. (2012). "Comparison of the Organic Flash Cycle (OFC) to other advanced vapor cycles for intermediate and high temperature waste heat reclamation and solar thermal energy." Energy **42**(1): 213-223.

Ho, T., et al. (2012). "Increased power production through enhancements to the Organic Flash Cycle (OFC)." Energy **45**(1): 686-695.

Incropera, F. P., et al. (2007). Fundamentals of heat and mass transfer, Wiley.

Kaka, S. and H. Liu (2002). Heat Exchangers: Selection, Rating and Thermal Design, CRC Press.

Lai, N. A. and J. Fischer (2012). "Efficiencies of power flash cycles." Energy **44**(1): 1017-1027.

Lecompte, S., et al. (2013). Thermodynamic analysis of the partially evaporating trilateral cycle. 2nd International Seminar on ORC Power Systems, Proceedings.

Lemmon, E. W., et al. (2013). NIST Standard Reference Database 23: Reference Fluid Thermodynamic and Transport Properties-REFPROP, Version 9.1. S. R. D. P. National Institute of Standards and Technology.

Li, M., et al. (2013). "Construction and preliminary test of a low-temperature regenerative Organic Rankine Cycle (ORC) using R123." Renewable Energy **57**(0): 216-222.

Liu, Z. and R. H. S. Winterton (1991). "A general correlation for saturated and subcooled flow boiling in tubes and annuli, based on a nucleate pool boiling equation." International Journal of Heat and Mass Transfer **34**(11): 2759–2766.

Martin, H. (1996). "A theoretical approach to predict the performance of chevron-type plate heat exchangers." Chemical Engineering and Processing **35**: 301 - 310.

Öhman, H. and P. Lundqvist (2013). "Experimental investigation of a Lysholm Turbine operating with superheated, saturated and 2-phase inlet conditions." Applied Thermal Engineering **50**(1): 1211-1218.

Quoilin, S., et al. (2013). "Techno-economic survey of Organic Rankine Cycle (ORC) systems." Renewable and Sustainable Energy Reviews **22**: 168 - 186.

Smith, I. K. (1993). "Development of the Trilateral Flash Cycle System: Part 1: Fundamental Considerations." Proceedings of the Institution of Mechanical Engineers, Part A: Journal of Power and Energy **207**.

Smith, I. K., et al. (2001). "Power Recovery from Low Cost Two-Phase Expanders." Geothermal Resources Council Transactions **25**: 601-605.

Smith, I. K., et al. (2004). "An Improved System for Power Recovery from Higher Enthalpy Liquid Dominated Fields." Geothermal Resources Council Transactions **28**: 561-565.

Smith, I. K., et al. (2005). "Screw Expanders Increase Output and Decrease the Cost of Geothermal Binary Power Plant Systems." Geothermal Resource Council Transactions **29**: 787-794.

Steffen, M., et al. (2013). "Efficiency of a new Triangle Cycle with flash evaporation in a piston engine." Energy **57**: 295 - 307.

Thome, J. R. (2004). Engineering Data Book III, Wolverine Tube, Inc.

Trædal, S. (2013). Analysis of the Trilateral Flash Cycle from surplus heat. Department of Energy and Process Engineering, Norwegian University of Science and Technology. **Project thesis**.

Welch, P. and P. Boyle (2009). "New Turbines to Enable Efficient Geothermal Power Plants." Geothermal Resource Council Transactions **33**: 765-772.

Welch, P., et al. (2011). "Construction and Startup of Low Temperature Geothermal Power Plants." Geothermal Resource Council Transactions **35**: 1351-1356.

White, F. M. (2009). Fluid mechanics, McGraw-Hill.

Zamfirescu, C. and I. Dincer (2008). "Thermodynamic analysis of a novel ammonia–water trilateral Rankine cycle." Thermochimica Acta **477**(1 - 2): 7 - 15.

Zyhowski, G. and A. Brown (2011). Low Global Warming Fluids for Replacement of HFC-245fa and HFC-134a in ORC Applications. First International Seminar on ORC Power Systems. Delft, The Netherlands.

11 Appendix A: Results for all working fluids

ORC, Case I, 100 °C									
Working fluid		Propane	Iso-pentane	Pentane	Butane	R1234ze	R245fa	R134a	R123
Net power	kW	31.3	6.4	1.9	22.8	31.9	28.8	32.0	20.7
Total area	m ²	905	701	393	1000	1000	989	1000	705
Working fluid mass flow	kg/s	1.4	0.6	0.3	1.0	2.6	2.1	2.5	2.0
Pump outlet pressure	MPa	2.3	0.5	0.5	0.8	1.4	0.5	1.9	0.4
Condensation temperature	°C	22	27	29	22	22	21	22	27
Heat source outlet temperature	°C	49	78	88	59	51	53	51	61
Heat sink outlet temperature	°C	21	27	36	21	21	22	21	30
Superheat expander inlet	°C	2	1	1	1	1	1	2	1
Volume flow expander inlet	m ³ /s	0.03	0.08	0.06	0.06	0.03	0.08	0.03	0.10
Volume flow expander outlet	m ³ /s	0.07	0.16	0.09	0.17	0.11	0.27	0.09	0.28
Heat input	kW	521	222	122	412	492	477	497	395
Heat sink mass flow	kg/s	115	7	2	91	108	51	109	9
Heat rejection	kW	479	211	118	380	451	440	456	367
Area									
Preheater	m ²	319	107	56	183	427	413	428	312
Evaporator	m ²	396	559	324	675	360	341	368	315
Superheater	m ²	3	0	0	1	2	1	4	1
Desuperheater	m ²	4	5	3	9	17	16	7	15
Condenser	m ²	183	28	9	133	195	218	193	62
Power production/consumption									
Expander	kW	42.6	10.4	3.9	29.9	39.8	34.3	40.7	24.9
Working fluid pump	kW	6.3	0.6	0.3	1.6	3.4	1.0	4.2	0.6
Heat source fan	kW	4.4	3.2	1.6	5.1	3.8	4.1	4.0	3.5
Heat sink pump	kW	0.6	0.1	0.0	0.4	0.6	0.4	0.6	0.1
Pressure losses									
HRHE	kPa	4.2	3.1	2.9	3.2	1.3	1.6	1.3	1.2
Evaporator	kPa	26.7	261.6	285.6	152.3	8.2	25.9	7.1	33.0
Superheater	kPa	0.1	0.0	0.0	0.2	0.0	0.1	0.0	0.1
Desuperheater	kPa	1.2	21.5	20.9	11.9	2.1	7.0	0.7	7.7
Condenser	kPa	0.4	0.9	1.0	1.8	1.3	9.8	1.0	10.7
Heat sink	kPa	3.2	5.4	7.2	2.6	3.3	5.2	3.2	9.1
Heat source	kPa	1.1	0.8	0.4	1.3	1.0	1.0	1.0	0.9
Heat Transfer coefficients									
Preheating	W/m ² K	71	59	60	63	38	34	40	31
Evaporating	W/m ² K	90	23	22	40	81	102	82	102
Superheating	W/m ² K	78	70	69	72	47	49	47	41
Desuperheating	W/m ² K	555	510	516	529	323	334	333	249
Condensing	W/m ² K	1814	2158	2218	2038	1600	1911	1649	1758

TFC, Case I, 100 °C									
Working fluid		Propane	Iso-pentane	Pentane	Butane	R1234ze	R245fa	R134a	R123
Net power	kW	27.4	13.9	8.5	26.0	27.1	17.8	28.7	7.9
Total area	m ²	1000	1000	1000	2000	3000	2000	2500	1000
Expander (nozzle)	-	0.90	0.87	0.87	0.87	0.91	0.88	0.92	0.88
Expander (rotor)	-	0.78	0.70	0.68	0.73	0.77	0.72	0.77	0.68
Working fluid mass flow	kg/s	2.6	3.3	3.2	3.5	5.6	5.8	5.3	5.8
Pump outlet pressure	MPa	4.0	0.6	0.5	1.4	2.8	1.1	3.6	0.6
Condensation temperature	°C	22	27	36	21	22	21	22	27
Heat sink outlet temperature	°C	21	26	31	22	21	24	21	27
Heat source outlet temperature	°C	39	46	52	32	36	43	36	61
Volume flow expander inlet	m ³ /s	0.01	0.01	0.01	0.01	0.01	0.01	0.01	0.00
Volume flow expander outlet	m ³ /s	0.09	0.32	0.28	0.29	0.14	0.26	0.11	0.20
Heat input	kW	618	546	485	685	643	579	646	391
Heat sink mass flow	kg/s	134	20	10	85	136	35	139	13
Heat rejection	kW	558	513	461	626	582	538	582	370
Area									
Heater	m ²	805	974	986	1768	2719	1892	2246	977
Desuperheater	m ²	0	0	0	0	0	0	0	0
Condenser	m ²	195	26	14	232	281	108	255	23
Power production/consumption									
Expander	kW	58.3	23.1	16.8	45.5	53.8	30.2	58.1	14.7
Working fluid pump	kW	25.8	4.6	3.7	11.3	17.6	6.4	20.6	3.4
Heat source fan	kW	4.5	4.5	4.6	7.7	8.2	5.7	7.9	3.3
Heat sink pump	kW	0.7	0.1	0.0	0.5	0.9	0.2	0.8	0.0
Pressure losses									
HRHE	kPa	8.8	6.0	6.3	9.7	3.7	2.5	4.0	1.5
Desuperheater	kPa	0.0	0.0	0.0	0.0	0.0	0.0	0.0	0.0
Condenser	kPa	0.8	39.5	39.6	17.4	5.3	44.7	2.7	46.8
Heat sink	kPa	3.2	1.6	1.8	3.8	4.1	3.8	3.6	2.3
Heat source	kPa	1.1	1.1	1.1	2.0	2.1	1.4	2.0	0.8
Heat transfer coefficients									
Heating	W/m ² K	82	51	52	53	29	23	38	22
Desuperheating	W/m ² K	555	516	524	522	320	338	333	254
Condensing	W/m ² K	1812	2123	2168	2040	1600	1900	1650	1724

PEC, Case I, 100 °C									
Working fluid		Propane	Iso-pentane	Pentane	Butane	R1234ze	R245fa	R134a	R123
Net power	kW	31.4	19.3	8.3	25.4	33.1	30.3	33.1	22.1
Total area	m ²	916	1000	1000	1504	1305	1000	1000	747
Expander (nozzle)	-	0.90	0.87	0.87	0.87	0.91	0.88	0.92	0.88
Expander (rotor)	-	0.89	0.72	0.68	0.73	0.90	0.90	0.89	0.90
Working fluid mass flow	kg/s	1.4	3.3	3.1	3.5	2.8	2.2	2.6	2.2
Pump outlet pressure	MPa	2.3	0.7	0.5	1.5	1.4	0.5	1.9	0.4
Condensation temperature	°C	22	27	36	22	22	21	22	27
Vapor quality		1.0	0.0	0.0	0.0	1.0	0.9	1.0	1.0
Heat sink outlet temperature	°C	21	24	31	21	21	22	21	30
Heat source outlet temperature	°C	48	44	54	33	48	53	50	60
Volume flow expander inlet	m ³ /s	0.03	0.01	0.01	0.01	0.04	0.08	0.03	0.11
Volume flow expander outlet	m ³ /s	0.07	0.41	0.26	0.30	0.12	0.28	0.08	0.31
Heat input	kW	631	547	721	526	488	524	407	0
Heat sink mass flow	kg/s	115	32	9	148	114	60	108	9
Heat rejection	kW	479	528	442	618	477	437	453	375
Area									
Preheater	m ²	331	1392	986	1534	637	454	439	351
Evaporator	m ²	401	-423	0	-261	454	349	368	330
Desuperheater	m ²								0
Condenser	m ²	184	32	14	231	213	197	193	67
Power production/consumption									
Expander	kW	43.0	30.3	15.8	46.9	42.3	35.8	41.8	26.2
Working fluid pump	kW	6.5	5.4	3.5	12.6	3.6	1.1	4.2	0.6
Heat source fan	kW	4.6	5.5	4.0	8.1	5.0	4.1	3.9	3.4
Heat sink pump	kW	0.6	0.1	0.0	0.7	0.6	0.3	0.5	0.1
Pressure losses									
HRHE	kPa	4.3	3.3	3.8	3.3	1.6	1.6	1.3	1.1
Evaporator	kPa	27.5	52.0	0.0	240.1	8.8	22.5	6.9	29.1
Desuperheater	kPa	0.0	0.0	0.0	0.0	0.0	0.0	0.0	0.0
Condenser	kPa	0.4	17.6	39.3	2.3	1.6	10.5	1.0	12.4
Heat sink	kPa	3.1	1.3	2.1	3.1	3.4	3.5	3.2	6.4
Heat source	kPa	1.1	1.3	1.0	2.0	1.2	1.0	1.0	0.8
Heat transfer coefficient									
Heating	W/m ² K	71	56	44	63	35	33	40	29
Evaporating	W/m ² K	89	23	15	30	80	100	82	99
Desuperheating	W/m ² K	554	516	521	521	320	329	333	244
Condensing	W/m ² K	1814	2134	2174	2045	1599	1906	1649	1750

ORC, Case II, 150 °C

Working fluid		Propane	Iso-pentane	Pentane	Butane	R1234ze	R245fa	R134a	R123
Net power	kW	105.9	69.1	56.1	91.9	114.1	89.5	110.1	70.4
Total area	m ²	1692	1000	1000	1501	3784	2000	3000	1500
Working fluid mass flow	kg/s	2.8	1.8	1.6	2.0	5.8	3.8	5.3	3.8
Pump outlet pressure	MPa	4.0	0.7	0.7	1.5	3.5	1.2	3.9	0.7
Condensation temperature	°C	22	27	36	21	22	21	22	27
Heat source outlet temperature	°C	36	71	80	59	34	59	37	71
Heat sink outlet temperature	°C	21	23	26	21	21	22	21	26
Superheat expander inlet	°C	15	1	1	1	4	1	13	1
Volume flow expander inlet	m ³ /s	0.03	0.10	0.10	0.05	0.02	0.06	0.02	0.09
Volume flow expander outlet	m ³ /s	0.16	0.53	0.49	0.36	0.25	0.46	0.19	0.48
Heat input	kW	1159	802	712	918	1180	924	1150	798
Heat sink mass flow	kg/s	214	51	25	147	227	79	213	28
Heat rejection	kW	1026	719	643	807	1036	816	1012	713
Area									
Preheater	m ²	1089	383	336	622	2967	1307	2169	963
Evaporator	m ²	134	569	639	558	232	469	230	477
Superheater	m ²	83	1	1	1	67	2	152	2
Desuperheater	m ²	27	9	6	21	40	21	40	12
Condenser	m ²	359	37	18	299	479	201	410	46
Power production/consumption									
Expander	kW	142.1	77.5	63.8	106.1	148.8	100.9	142.1	78.3
Working fluid pump	kW	27.7	2.9	2.3	6.7	23.5	4.6	22.2	2.6
Heat source fan	kW	5.9	5.3	5.4	6.3	8.6	6.3	7.9	5.2
Heat sink pump	kW	2.6	0.1	0.1	1.1	2.5	0.5	2.0	0.1
Pressure losses									
HRHE	kPa	6.1	3.7	3.7	5.2	2.5	2.0	2.3	1.4
Evaporator	kPa	1.4	72.8	102.7	35.7	0.4	6.8	0.5	9.9
Superheater	kPa	0.9	0.1	0.2	0.1	0.1	0.0	0.6	0.0
Desuperheater	kPa	4.0	11.6	9.3	14.4	2.2	5.1	2.2	3.1
Condenser	kPa	1.1	14.2	11.5	6.4	5.8	23.9	2.9	30.6
Heat sink	kPa	7.5	1.3	1.3	4.7	6.9	3.7	6.0	2.6
Heat source	kPa	1.4	1.2	1.2	1.5	2.1	1.5	1.9	1.2
Heat Transfer coefficients									
Preheating	W/m ² K	69	59	60	62	31	26	35	22
Evaporating	W/m ² K	113	50	44	68	61	73	67	70
Superheating	W/m ² K	75	75	74	76	43	40	39	33
Desuperheating	W/m ² K	563	526	530	537	324	340	336	255
Condensing	W/m ² K	1814	2123	2158	2040	1600	1904	1649	1729

TFC, Case II, 150 °C									
Working fluid		Propane	Iso-pentane	Pentane	Butane	R1234ze	R245fa	R134a	R123
Net power	kW	58.5	75.1	59.0	107.3	82.9	90.0	70.6	48.9
Total area	m ²	1500	3000	2500	2500	3000	4000	2501	4000
Expander (nozzle)	-	0.90	0.87	0.87	0.87	0.91	0.88	0.92	0.88
Expander (rotor)	-	0.78	0.82	0.79	0.84	0.81	0.84	0.79	0.77
Working fluid mass flow	kg/s	5.1	3.6	3.5	3.4	8.8	5.9	9.3	7.9
Pump outlet pressure	MPa	4.0	1.7	1.4	3.2	3.5	3.0	3.9	1.8
Condensation temperature	°C	22	27	36	21	21	21	22	27
Heat sink outlet temperature	°C	21	30	32	22	21	24	21	32
Heat source outlet temperature	°C	29	39	48	33	27	40	28	51
Volume flow expander inlet	m ³ /s	0.02	0.01	0.01	0.01	0.01	0.01	0.01	0.01
Volume flow expander outlet	m ³ /s	0.17	0.63	0.57	0.47	0.27	0.48	0.21	0.41
Heat input	kW	1222	1122	1030	1183	1249	1114	1234	1007
Heat sink mass flow	kg/s	203	24	18	135	194	59	194	18
Heat rejection	kW	1104	996	927	1016	1107	971	1104	914
Area									
Heater	m ²	1097	2943	2472	2086	2428	3812	2013	3948
Desuperheater	m ²	0	0	0	0	0	0	0	0
Condenser	m ²	403	57	28	414	572	188	488	52
Power production/consumption									
Expander	kW	114.9	102.9	82.1	145.5	127.2	122.0	117.2	74.1
Working fluid pump	kW	50.9	15.2	12.5	27.6	35.7	20.3	39.2	14.9
Heat source fan	kW	3.6	12.4	10.5	9.5	6.5	11.2	5.3	10.2
Heat sink pump	kW	1.9	0.1	0.1	1.1	2.2	0.5	2.0	0.1
Pressure losses									
HRHE	kPa	4.1	15.5	13.6	13.8	2.3	4.9	1.8	3.3
Desuperheater	kPa	0.0	0.0	0.0	0.0	0.0	0.0	0.0	0.0
Condenser	kPa	2.9	45.9	46.0	15.7	13.0	48.2	9.9	87.1
Heat sink	kPa	6.0	3.9	1.9	5.0	7.1	4.9	6.6	3.4
Heat source	kPa	0.9	2.9	2.5	2.3	1.6	2.6	1.3	2.4
Heat transfer coefficients									
Heating	W/m ² K	56	51	52	61	34	27	33	19
Desuperheating	W/m ² K	556	521	526	522	321	338	333	259
Condensing	W/m ² K	1814	2154	2168	2042	1601	1902	1650	1710

PEC, Case II, 150 °C									
Working fluid		Propane	Iso-pentane	Pentane	Butane	R1234ze	R245fa	R134a	R123
Net power	kW	94.6	74.6	69.6	107.1	111.1	91.8	102.0	70.3
Total area	m ²	2000	3001	1500	2998	4003	2501	4000	1502
Expander (nozzle)	-	0.90	0.87	0.87	0.87	0.91	0.88	0.92	0.88
Expander (rotor)	-	0.87	0.82	0.80	0.84	0.89	0.90	0.87	0.90
Working fluid mass flow	kg/s	3.4	3.6	3.4	3.3	6.3	4.2	6.5	4.0
Pump outlet pressure	MPa	3.7	1.7	1.6	3.1	3.3	1.3	3.6	0.8
Condensation temperature	°C	22	27	36	21	22	21	22	27
Vapor quality		1.0	0.0	0.0	0.1	1.0	0.9	1.0	0.9
Heat sink outlet temperature	°C	21	28	27	22	21	23	21	25
Heat source outlet temperature	°C	31	41	53	34	32	56	30	71
Volume flow expander inlet	m ³ /s	0.03	0.01	0.01	0.01	0.02	0.05	0.02	0.08
Volume flow expander outlet	m ³ /s	0.16	0.62	0.70	0.47	0.25	0.47	0.20	0.48
Heat input	kW	1128	1048	1196	1094	1141	898	1167	526
Heat sink mass flow	kg/s	207	30	31	129	199	68	209	33
Heat rejection	kW	1067	980	871	1013	1034	833	1058	708
Area									
Preheater	m ²	1460	2950	1723	2526	3268	1789	3285	1007
Evaporator	m ²	151	0	-251	53	256	493	264	449
Desuperheater	m ²								0
Condenser	m ²	389	51	28	420	479	218	451	46
Power production/consumption									
Expander	kW	133.7	100.5	90.8	144.8	146.4	105.5	138.3	78.1
Working fluid pump	kW	30.8	14.8	13.0	26.5	24.0	5.8	24.7	2.9
Heat source fan	kW	6.2	11.0	8.2	10.1	9.3	7.5	9.4	4.9
Heat sink pump	kW	2.1	0.1	0.0	1.1	2.1	0.4	2.3	0.1
Pressure losses									
HRHE	kPa	5.7	9.3	5.0	9.7	2.5	2.3	2.4	1.3
Evaporator	kPa	1.4	0.0	125.5	0.0	0.5	5.1	0.5	7.5
Desuperheater	kPa	0.0	0.0	0.0	0.0	0.0	0.0	0.0	0.0
Condenser	kPa	1.5	45.4	15.3	16.0	6.6	28.9	4.9	33.9
Heat sink	kPa	6.5	2.3	1.0	5.3	6.7	3.8	6.8	1.6
Heat source	kPa	1.5	2.6	1.9	2.4	2.2	1.7	2.3	1.1
Heat transfer coefficient									
Heating	W/m ² K	55	43	60	52	27	24	26	21
Evaporating	W/m ² K	99	31	36	69	57	67	57	67
Desuperheating	W/m ² K	555	518	521	521	320	334	333	249
Condensing	W/m ² K	1814	2131	2158	2040	1600	1902	1649	1720

ORC, Case III, 200 °C

Working fluid		Propane	Iso-pentane	Pentane	Butane	R1234ze	R245fa	R134a	R123
Net power	kW	170.4	163.2	138.2	220.4	184.4	200.6	180.6	146.4
Total area	m ²	2000	3102	1500	2502	4000	4000	4000	3500
Working fluid mass flow	kg/s	3.2	2.9	2.5	3.4	6.8	6.3	6.2	5.7
Pump outlet pressure	MPa	4.0	1.4	1.3	3.6	3.5	3.5	3.9	1.6
Condensation temperature	°C	22	27	36	21	22	21	22	27
Heat source outlet temperature	°C	31	55	74	33	29	36	31	71
Heat sink outlet temperature	°C	22	35	27	22	22	24	22	28
Superheat expander inlet	°C	51	1	1	3	34	3	51	1
Volume flow expander inlet	m ³ /s	0.05	0.07	0.07	0.03	0.04	0.02	0.04	0.06
Volume flow expander outlet	m ³ /s	0.22	0.86	0.73	0.61	0.35	0.67	0.28	0.64
Heat input	kW	1712	1477	1286	1696	1732	1662	1722	1312
Heat sink mass flow	kg/s	214	20	39	184	218	87	228	32
Heat rejection	kW	1506	1280	1124	1433	1509	1423	1502	1138
Area									
Preheater	m ²	1256	2064	932	1878	2978	3534	2909	2754
Evaporator	m ²	107	850	529	108	156	180	183	664
Superheater	m ²	190	2	1	24	244	44	353	4
Desuperheater	m ²	45	38	11	33	78	28	73	18
Condenser	m ²	402	148	26	458	544	214	482	60
Power production/consumption									
Expander	kW	212.1	185.3	152.5	261.8	223.7	235.3	219.0	164.9
Working fluid pump	kW	32.5	9.9	7.5	31.6	27.4	24.8	26.3	9.6
Heat source fan	kW	6.1	12.1	6.7	7.8	8.5	9.4	8.7	8.7
Heat sink pump	kW	3.1	0.2	0.1	1.9	3.4	0.5	3.5	0.1
Pressure losses									
HRHE	kPa	5.4	9.4	5.4	7.3	2.2	2.7	2.2	2.0
Evaporator	kPa	0.8	27.0	25.7	0.8	0.2	0.2	0.2	3.1
Superheater	kPa	2.3	0.1	0.0	0.1	0.5	0.1	0.8	0.0
Desuperheater	kPa	6.4	13.2	9.5	12.8	4.1	3.6	3.5	2.5
Condenser	kPa	1.4	21.1	26.7	16.8	7.9	53.9	4.7	57.7
Heat sink	kPa	9.2	5.2	1.3	6.6	9.7	3.9	9.6	2.4
Heat source	kPa	1.4	2.6	1.4	1.8	2.0	2.1	2.0	1.9
Heat Transfer coefficients									
Preheating	W/m ² K	64	50	53	59	31	27	30	17
Evaporating	W/m ² K	107	50	59	103	64	61	64	48
Superheating	W/m ² K	66	67	70	74	38	44	37	28
Desuperheating	W/m ² K	595	565	548	543	342	347	350	262
Condensing	W/m ² K	1815	2169	2148	2040	1601	1890	1651	1710

TFC, Case III, 200 °C									
Working fluid		Propane	Iso-pentane	Pentane	Butane	R1234ze	R245fa	R134a	R123
Net power	kW	84.1	185.6	167.5	183.9	119.0	155.4	101.5	145.8
Total area	m ²	2000	2000	2000	2501	3000	3502	2500	4000
Expander (nozzle)	-	0.90	0.87	0.87	0.87	0.91	0.88	0.92	0.88
Expander (rotor)	-	0.78	0.90	0.90	0.86	0.81	0.86	0.79	0.86
Working fluid mass flow	kg/s	7.3	3.6	3.3	4.6	12.4	8.5	13.2	8.5
Pump outlet pressure	MPa	4.0	3.2	3.0	3.6	3.5	3.5	3.9	3.5
Condensation temperature	°C	22	27	36	21	21	21	22	27
Heat sink outlet temperature	°C	21	26	27	23	22	27	22	30
Heat source outlet temperature	°C	27	40	52	25	26	27	28	43
Volume flow expander inlet	m ³ /s	0.02	0.01	0.01	0.01	0.02	0.01	0.02	0.01
Volume flow expander outlet	m ³ /s	0.25	0.84	0.83	0.66	0.37	0.63	0.29	0.62
Heat input	kW	1753	1622	1505	1772	1768	1756	1748	1595
Heat sink mass flow	kg/s	254	51	41	132	193	54	214	33
Heat rejection	kW	1585	1287	1246	1509	1572	1531	1566	1381
Area									
Heater	m ²	1431	1930	1963	2015	2083	3258	1782	3931
Desuperheater	m ²	0	9	3	0	0	0	0	0
Condenser	m ²	569	61	34	486	917	243	718	69
Power production/consumption									
Expander	kW	164.3	222.6	201.6	234.5	177.4	197.6	164.4	187.2
Working fluid pump	kW	73.0	28.8	25.5	42.4	50.4	33.3	55.5	31.4
Heat source fan	kW	3.7	8.0	8.6	6.9	5.3	8.3	4.6	9.8
Heat sink pump	kW	3.5	0.2	0.1	1.3	2.8	0.5	2.8	0.1
Pressure losses									
HRHE	kPa	3.3	11.4	13.6	8.1	1.6	3.0	1.3	3.3
Desuperheater	kPa	0.0	5.7	2.1	0.0	0.0	0.0	0.0	0.0
Condenser	kPa	5.9	44.9	40.3	28.3	25.5	81.9	19.5	96.5
Heat sink	kPa	8.6	3.0	1.5	6.1	9.0	6.0	8.2	2.7
Heat source	kPa	0.9	1.8	1.9	1.6	1.2	1.9	1.1	2.2
Heat transfer coefficients									
Heating	W/m ² K	47	63	63	58	34	30	33	25
Desuperheating	W/m ² K	556	530	529	525	321	344	334	261
Condensing	W/m ² K	1814	2138	2153	2042	1602	1893	1650	1697

PEC, Case III, 200 °C									
Working fluid		Propane	Iso-pentane	Pentane	Butane	R1234ze	R245fa	R134a	R123
Net power	kW	139.4	185.1	166.1	217.2	167.8	194.8	152.3	156.5
Total area	m ²	2500	2500	2500	3001	4000	4000	3500	4000
Expander (nozzle)	-	0.90	0.87	0.87	0.87	0.91	0.88	0.92	0.88
Expander (rotor)	-	0.87	0.90	0.90	0.90	0.90	0.90	0.87	0.88
Working fluid mass flow	kg/s	4.9	3.6	3.4	3.7	9.1	6.8	9.2	7.3
Pump outlet pressure	MPa	3.6	3.2	3.0	3.6	3.1	3.5	3.4	3.5
Condensation temperature	°C	22	27	36	21	22	21	22	27
Vapor quality		1.0	0.0	0.0	1.0	1.0	1.0	1.0	0.4
Heat sink outlet temperature	°C	21	29	28	22	22	24	21	27
Heat source outlet temperature	°C	27	39	51	28	27	33	28	56
Volume flow expander inlet	m ³ /s	0.05	0.01	0.01	0.02	0.04	0.02	0.04	0.01
Volume flow expander outlet	m ³ /s	0.24	0.85	0.82	0.63	0.37	0.66	0.28	0.62
Heat input	kW	1678	1514	1404	1680	1712	1629	1687	1318
Heat sink mass flow	kg/s	258	37	39	144	237	81	245	45
Heat rejection	kW	1550	1382	1290	1451	1523	1436	1527	1248
Area									
Preheater	m ²	1831	2422	2463	2333	3086	3611	2689	3787
Evaporator	m ²	123	0	0	95	159	146	165	151
Desuperheater	m ²		10	2	30		18		
Condenser	m ²	546	68	34	543	755	224	646	62
Power production/consumption									
Expander	kW	192.1	223.1	201.2	261.8	212.0	231.4	197.0	193.2
Working fluid pump	kW	43.1	28.9	25.6	34.1	32.5	26.6	33.9	26.7
Heat source fan	kW	5.8	9.0	9.5	9.0	8.3	9.5	7.3	10.0
Heat sink pump	kW	3.8	0.1	0.1	1.5	3.5	0.5	3.5	0.1
Pressure losses									
HRHE	kPa	4.0	8.1	9.3	8.1	1.9	2.6	1.6	2.4
Evaporator	kPa	0.6	0.0	0.0	0.6	0.2	0.2	0.2	0.1
Desuperheater	kPa	0.0	4.6	1.3	9.6	0.0	1.9	0.0	0.0
Condenser	kPa	2.8	46.5	43.2	19.2	13.7	59.7	9.6	78.9
Heat sink	kPa	9.3	2.3	1.2	6.4	9.2	3.8	9.0	1.7
Heat source	kPa	1.3	2.0	2.1	2.1	1.9	2.2	1.7	2.2
Heat transfer coefficient									
Heating	W/m ² K	43	52	51	56	25	27	26	23
Evaporating	W/m ² K	84	93	84	100	59	62	60	55
Desuperheating	W/m ² K	556	527	526	533	321	343	334	256
Condensing	W/m ² K	1813	2126	2140	2040	1600	1889	1649	1691

12 Appendix B: Working fluid properties

Some of the fluid properties for the eight working fluids used in the study are given in the table below for comparison. The properties are found from REFPROP 9 and (Calm and Hourahan 2011, Fukuda, Kondou et al. 2014).

Fluid List									
	Vapour density [kg/m ³]	Conductivity [mW/m-K]	Viscosity [μPa-s]	Surface tension (liquid) [mN/m]	Surface tension (vapor) [mN/m]	Toxicity	Flammability	GWP	Tcrit [°C]
Temp [°C]	25	50	50	0.95 * Tcrit	25				
R134a	32	70	142	0.27	8	1	1	1300	101
R245fa	9	80	300	0.38	14	2	1	950	154
R123	6	70	316	0.45	15	2	1	120	184
R1234ze	26	66	148	0.31	9	1	2	6	109
Butane	6	95	125	0.34	12	1	3	20	152
Pentane	2	102	177	0.45	15	1	3	2	197
Isopentane	3	99	171	0.46	14	1	3	11	187
Propane	21	83	74	0.23	7	1	3	20	97

13 Appendix C: Scientific paper submitted to Energy

Comparison of ORC and TFC for power production from low temperature waste heat sources

Daniel Rohde¹, Stian Trædal², Brede Hagen¹, Trond Andresen¹, Trygve M. Eikevik²

¹ SINTEF Energy Research, Postboks 4761 Sluppen, 7465 Trondheim, Norway

² The Norwegian University of Science and Technology (NTNU),
Kolbjørn Hejes vei 1B, 7034 Trondheim, Norway

Abstract

In this paper, the Organic Rankine Cycle (ORC) and the Trilateral Flash Cycle (TFC) are compared for power production from low temperature heat sources. Both cycles are simulated with air as heat source at 10 kg/s and temperatures of 100, 150 and 200 °C and heat rejection to water at 20 °C. All cases are simulated for seven different working fluids: R134a, R245fa, R123, R1234ze(E), butane, isopentane and propane. The cycles are optimized for maximum net power production with a variable efficiency for the TFC's two-phase expander.

The results show 10% higher power outputs for the best TFC compared to the best ORC for the 100 °C case. However, the required heat exchanger area and expander outlet volume flow rate are significantly higher for the TFC, indicating a larger and more expensive system. At 150 °C and 200 °C, the power outputs are very similar for both cycles and the difference in system size decreases.

Natural working fluids with low environmental impact show similar performance compared to standard refrigerants. Isopentane showed the best performance when used in a TFC system but does not outperform the ORC.

Keywords: ORC; TFC; Power production; Low temperature; Waste heat

1. Introduction

The world's energy demand is rising and the emission of greenhouse gases such as CO₂ is increasing as an effect. It is therefore necessary to search for alternate energy sources and improve existing methods for power production. In this study, we look at the possibility of improving power production from low temperature waste heat sources by using the Trilateral Flash Cycle (TFC) instead of the Organic Rankine Cycle (ORC).

The ORC is a well-established technology for power production from low to medium temperature heat sources. Its applications range from waste heat recovery to solar and geothermal power plants (Quoilin, Broek et al. 2013). A known drawback of the ORC from a thermodynamic point of view is the suboptimal temperature matching in the heat recovery heat exchanger (HRHE), see Figure 1. This is a result of the constant evaporation temperature of the working fluid and leads to exergy losses (Galanis, Cayer et al. 2009).

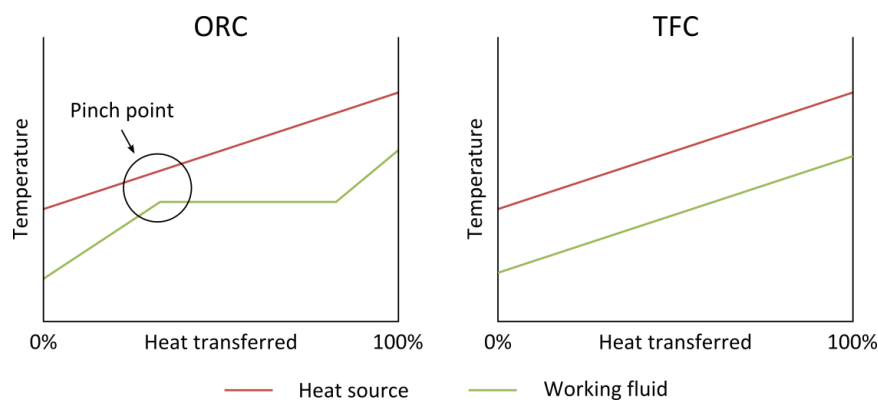


Figure 1: Variation in stream temperature during heat addition process for ORC (left) and TFC (right)

To improve the temperature matching, the use of zeotropic working fluid mixtures or supercritical pressures has been suggested to absorb the heat source at a gliding and thus better temperature profile. However, the best temperature match can be obtained when both fluids are in liquid phase so that the temperature difference in the heat exchanger is almost constant (DiPippo 2007; Ho, Mao et al. 2012). This is the case for the TFC, which can be seen in Figure 2.

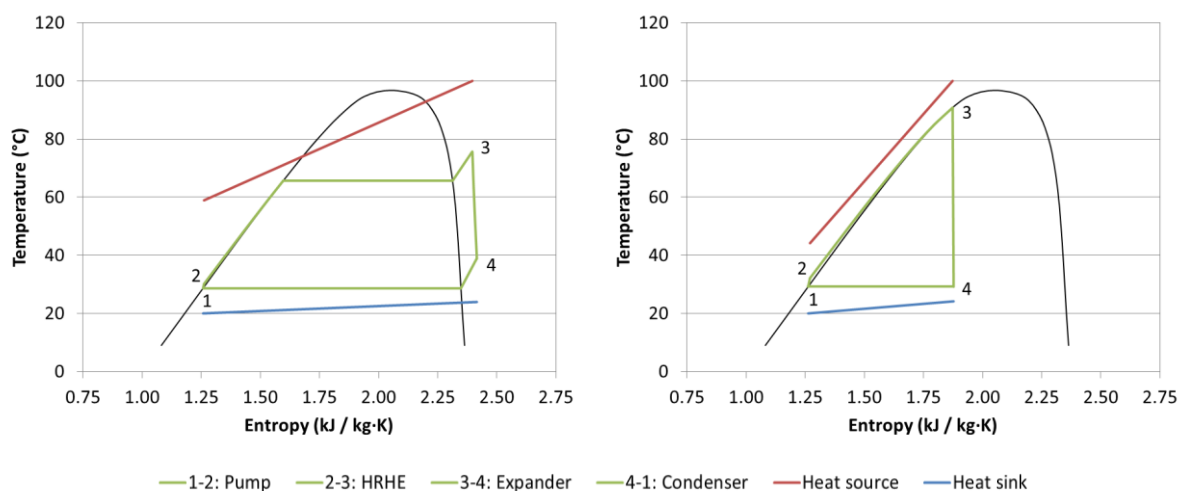


Figure 2: T,s-diagrams of ORC (left) and TFC (right) with propane as working fluid

The main components of both ORC and TFC are pump, HRHE, expander and condenser. However, the expansion process is entirely different: While an ORC has its expansion in the superheated vapor region, a TFC expands into the two-phase region. Turbines and expanders commonly used in ORCs do not tolerate liquids or even liquid droplets, so this two-phase expansion requires specially designed expanders which are described below.

1.1. Expander technology

The technically most challenging component of the TFC is the two-phase expander, as the expansion into the two-phase area includes flash evaporation of the working fluid (giving the TFC its name). This leads to much higher volume ratios between inlet and outlet than for dry vapor expanders and also makes the flow characteristics harder to predict and optimize. An efficient expansion process is vital for the TFC though if it is to outperform an ORC with a high efficiency dry vapor turbine.

There are a few expander types that tolerate two-phase flow. For small-scale (1-10 kW) applications, scroll or rotary vane expanders can be used (Bao and Zhao 2013). For slightly larger systems, a reciprocating piston might be suitable. However, since the piston itself does not tolerate two-phase flow, it can only be used as expander in a TFC when a cyclone for phase separation is implemented upstream (Steffen, Löffler et al. 2013). For medium-scale (50-250 kW) systems as investigated in this paper, screw expanders and the Variable Phase Turbine (VPT) are the most relevant expander types and are described below.

A screw expander is a positive displacement expander that consists of a pair of meshing helical rotors in a casing. The volume trapped between the rotors and the casing changes as the rotors rotate. Whether the volume increases or decreases depends only on the direction of rotation which is why the same machine can be used as compressor and expander. The energy transfer between the fluid and the rotor depends mainly on the pressure on the rotors and only to a small extent on the dynamic effects of fluid motion. This is why the presence of liquid in the expander has little effect on its mode of operation or efficiency (Smith, Stosic et al. 1994; Smith, Stosic et al. 2005).

The VPT consists of a set of individual fixed nozzles and an axial impulse rotor. In the nozzles, the working fluid's enthalpy is partly converted to kinetic energy in a near isentropic expansion. The liquid phase is broken up into small droplets by the expanding gas, and momentum is transferred from the gas to the droplets by pressure and shear forces. The small size of the droplets leads to a close coupling of the gas and the liquid and efficient acceleration of both phases. The inlet to the nozzle can be liquid, two-phase, supercritical or vapor. The kinetic energy of the two-phase jets is converted to shaft power in an axial impulse turbine that allows direct driving of the generator, so no gearbox and lube oil systems are needed (Welch and Boyle 2009).

1.2. Literature study

Currently, only a few studies on the TFC can be found. The TFC was originally developed for geothermal applications and was investigated as far back as 1989 (Hu, Wang et al. 1989). The first publications describing the TFC in detail are from Smith and indicate great potential for geothermal applications (Smith 1993; Smith, Stosic et al. 1995). Smith and Stosic focused on the implementation of screw expanders and pointed out cost-advantages of TFC systems with screw expanders compared to commonly used ORC systems with dry vapor turbines. They state that low temperature heat sources

can be utilized substantially cheaper in the range of approximately 20-500 kW because screw expanders neither require a gearbox nor a lubrication system (Smith, Stosic et al. 2007). However, no report of a commercial application could be found.

Recently, Öhman and Lundqvist tested a screw expander with R134a as working fluid and power outputs around 30 kW (Öhman and Lundqvist 2013). The expander was tested with superheated, saturated and mixed inlet state, and efficiencies around 0.75 were measured with a peak of 0.92. However, the authors stress that it is notoriously difficult to get absolute levels of efficiencies derived from measurements in two-phase conditions.

Brown and Mines performed a fluid study for the TFC with 20 working fluids and analyzed two different inlet temperatures of the heat source (geothermal brine), which were set to 93°C and 160°C. The performance criteria for the working fluid were net power output, expansion ratio and critical temperature. No working fluid was in the top 10 in all categories. They then compared the cycle performance of an ORC with isobutane to a TFC with n-pentane as working fluids and find that the TFC can give higher power output when the expander efficiencies are equal. However, it requires a larger heat exchanger area. They mention that the two-phase expansion would very likely be less efficient and show that it needs to be at least 0.76 to match the performance of the ORC (Brown and Mines 1998).

Energent Corporation has successfully used their Variable Phase Turbine (VPT) in refrigeration systems for 10 years with power outputs up to 20 kW. Due to good test results from a TFC testrig, a 1 MW TFC power plant with R134a as working fluid has been built at Coso Geothermal in California which is designed for power production from a 113 °C brine stream (Welch, Boyle et al. 2010). The system has been operated up to 795 kW (Boyle and Hays 2013) and several other installations from 1.5 kW to 1.5 MW are reported in (Welch and Boyle 2009). A 500 kW geothermal plant is now planned with an advanced VPT, which is hermetically sealed with turbine and generator submerged in the working fluid R134a (Welch, Boyle et al. 2011).

Zamfirescu and Dincer analyzed a TFC with a mixture of ammonia and water as working fluid for a geothermal heat source with 150 °C. They found that it outperforms the ORC, but mention possible difficulties with material selection due to the corrosiveness of the ammonia–water solution (Zamfirescu and Dincer 2008).

Fischer (Fischer 2011) analyzed heat source temperatures from 150 °C to 350 °C with water as working fluid for the TFC. He found that the exergy efficiency (net power output divided by incoming exergy flow of the heat source) was 14 – 29 % higher for the TFC than the ORC. However, water had been reported to be unsuitable by Smith (Smith 1993) and Fischer comes to the same conclusion, mainly due to very high volume flows. In a follow-up study, Lai and Fischer analyzed more working fluids (all pure organic substances) with exergy efficiency as optimization target (Lai and Fischer 2012). Cyclopentane is stated as most promising for low temperatures, although other working fluids like pentane and butane gave similar efficiency and volume flow. The volume flows at the expander outlet were found to be higher for the TFCs compared to the ORCs, indicating larger systems for the TFCs. Working fluid mixtures are mentioned as promising but were not investigated. An expander efficiency of 0.85 was used for both ORC and TFC in these studies.

More sophisticated cycles using two phase expanders have also been analyzed. Smith suggested a cycle with two expansion stages of which one would be two-phase and one dry vapor, which requires

a phase-separation after the first expansion (Smith, Stosic et al. 2004). Ho investigated similar and even more advanced configurations with several expansion stages and reports efficiency improvements for low temperature applications compared to ORC (Ho, Mao et al. 2012). Lecompte studied the use of a partially evaporating cycle to combine the advantages of TFC and ORC and reports improvements over a pure TFC, especially when assuming low pump efficiencies (due to the reduced mass flow in a partially evaporating cycle) (Lecompte, van den Broek et al. 2013). While these are only theoretical considerations, they indicate that advanced cycle configurations can have a better performance than a standard TFC.

2. Calculations

To compare the TFC to the ORC, both cycles have been simulated in Microsoft Excel. Visual Basic for Applications (VBA) was used to automatize the calculations, REFPROP 9 by the National Institute of Standards and Technology (NIST) was used for the thermodynamic properties of the working fluids (Lemmon, Huber et al. 2013) and the Excel solver was used as optimization engine.

2.1. Cycle simulation

Table 1 gives an overview over all parameters that were used during the calculations. It can be seen that the following variables were optimized during the simulations: Working fluids mass flow, pump outlet pressure, condensation temperature, heat sink outlet temperature, superheat at expander inlet (only ORC) and recuperator capacity (only ORC). Heat source and sink specifications as well as pressure drops, overall heat transfer coefficients and component efficiencies are constant inputs which have to be chosen by the user. The only exception to this is the expander efficiency for the TFC which is calculated automatically.

Table 1: Calculation parameter types

	Parameter	Type
Heat source	Fluid	User input
	Mass flow	User input
	Inlet temperature	User input
	Inlet pressure	User input
	Outlet temperature	Calculated
Heat sink	Fluid	User input
	Mass flow	Calculated
	Inlet temperature	User input
	Inlet pressure	User input
	Outlet temperature	Optimized
	Pump efficiency	User input
	Motor efficiency	User input
Pump work	Calculated	

Pump	Mass flow working fluid	Optimized
	Isentropic efficiency	User input
	Motor efficiency	User input
	Inlet pressure	Calculated
	Outlet pressure	Optimized
	Work	Calculated
HRHE	Pressure drops	User input
	U heater	User input
	U evaporator (ORC)	User input
	U superheater (ORC)	User input
	Amount of superheat (ORC)	Optimized
	Pinch point	Calculated
	Area	Calculated
Expander	Isentropic efficiency (ORC)	User input
	Nozzle efficiency (TFC)	Calculated
	Rotor efficiency (TFC)	Calculated
	Generator efficiency	User input
	Minimum vapor fraction (ORC)	User input
	Work	Calculated
Condenser	Condensation temperature	Optimized
	Working fluid pressure drop	User input
	Heat sink pressure drop	User input
	U desuperheater	User input
	U condenser	User input
	Pinch point	Calculated
	Area	Calculated
Cycle	Working fluid	User input
	Heat loss to ambient	Neglected
	Total heat exchanger area	Calculated
	Efficiency	Calculated
	Net power output	Maximized

The cycle is calculated based on enthalpy balances with a number of constraints to avoid unfeasible solutions: The minimum pinch point temperatures in the heat exchangers and the minimum superheat throughout the ORC expander were set to 1 °C. Both were calculated by dividing the component into several small sections and ensuring the limits in each section. This is necessary because the phase envelope of the working fluid is not taken into account if only inlet and outlet states are considered. Also, the pump outlet pressure was limited to 95% of the working fluid's critical pressure and the condensation pressure was kept above 1 bar to avoid a sub-atmospheric system. The total heat exchanger area was constrained during the case studies to compare the performances of the cycles at different system sizes. The cooling of the heat source is not limited although some practical limitations can occur, e.g. in aluminum production plants (Børgund 2009).

The optimization target for the excel solver is the net power output which is set to be maximized. Using the net power output instead of cycle efficiency is recommended for waste heat sources, as explained in (Quoilin, Declaye et al. 2011). It is defined as

$$P_{\text{net}} = P_{\text{expander}} \cdot \eta_{\text{generator}} - \frac{P_{\text{pumps}}}{\eta_{\text{motor}}} \quad (1)$$

with P_{pumps} being the sum of working fluid pump power and heat sink pump power. To perform the optimization, the Excel solver is used with the GRG Nonlinear solving method with forward derivatives. This kind of optimization problem can have many local maximums and the starting values of the optimization variables determine which local maximum is found. As there is no way for the solver to recognize the global maximum or to know how many local maximums exist, it cannot find the global maximum with absolute certainty. Thus, a high number of starting points was chosen to ensure that the global maximum is found with high probability.

To calculate the heat exchanger area, the well-known log mean temperature difference (LMTD) is used. Although the assumptions made in this method are not fully fulfilled in all of our cases, it gives a good approximation. The heat transfer coefficients for the heat exchangers are defined per section, see Table 1. The heat recovery heat exchanger (HRHE) is divided into a heating, boiling, and superheating part. The condenser is divided into a desuperheating and a condensing part. The area for each section is calculated individually with the following formula:

$$A = \frac{\dot{Q}}{U \cdot \Delta T_{\text{lm}}} \quad (2)$$

Here \dot{Q} is the heat flow in the heat exchanger section in, U is the heat transfer coefficient and ΔT_{lm} is the LMTD.

All component efficiencies are assumed constant except for the expander efficiency in the TFC. The two-phase expander is modeled as a VPT which is explained in Section 1.1. The nozzle and rotor efficiencies are calculated separately. The nozzle efficiency is calculated as

$$\eta_{\text{nozzle}} = 0.865 + 0.00175 \cdot d_{4,\text{vapor}} \quad (3)$$

where $d_{4,\text{vapor}}$ is the vapor density (in kg/m^3) of the working fluid at condensing pressure. The rotor efficiency is calculated as

$$\eta_{\text{rotor}} = 0.575 + 0.325 \cdot q_4 \quad (4)$$

where q_4 is the vapor quality (dimensionless) of the working fluid at nozzle exit. These relationships are based on values given in (Hays 2010) and (Welch and Boyle 2009) and personal communication with Lance Hays, author of (Hays 2010). They allow a more realistic comparison between different working fluids, as the main influencing properties (vapor density and vapor fraction) are taken into account. However, these relationships are simplified and not validated and should therefore not be taken as accurate.

2.2. Case studies

Most of the specifications and boundary conditions for the ORC and TFC are the same as shown in Table 1. To define a case, all user input values have to be chosen which is explained below.

Case definition

Three fictive waste heat sources were chosen as case studies. Air was selected as heat source fluid with a mass flow of 10 kg/s and the temperatures were set to 100, 150 and 200 °C for Case I, Case II and Case III, respectively. Water at 20 °C was chosen as heat sink and kept constant for all cases.

To show how the power output changes with system size, the maximum total heat exchanger area was constrained during the calculations. All cases were calculated with five different limitations: 500, 1000, 1500, 2000 and 2500 m². The maximum total heat exchanger area includes all calculated sections: Heater, evaporator, superheater, desuperheater and condenser.

The heat transfer coefficients are assumed constant for each part in the HRHE and condenser. They were set according to values presented in (Ho 2012) where an order of magnitude approximation was used to define convective heat transfer coefficients for different stream combinations which were comparable to other published values.

All pressure drops were neglected, except for the heat sink side of the condenser. Here, the pressure drop is needed to calculate the heat sink pump power which influences the optimization target (net power output) and 100 kPa was chosen as value. As systems with lower absolute pressure usually suffer more from pressure drops than systems with higher absolute pressure, neglecting all other pressure drops introduces an error in favor of the low pressure systems.

All pump efficiencies were set to 0.7, the ORC expander efficiency was set to 0.8 and all motor and generator efficiencies were set to 0.9. All user input values are shown in Table 2, except for the working fluids which are explained separately and shown in Table 3.

Table 2: User input values for case studies

	Parameter	Value
Heat source	Fluid	Air
	Mass flow	10 kg/s
	Inlet temperature	100, 150, 200 °C
	Inlet pressure	0.3 MPa
Heat sink	Fluid	Water
	Inlet temperature	20 °C
	Inlet pressure	0.3 MPa
	Pump efficiency	0.70
	Motor efficiency	0.90
Pump	Isentropic efficiency	0.70
	Motor efficiency	0.90

HRHE	Pressure drops	Neglected
	U heater	90 W/(m ² ·K)
	U evaporator (ORC)	100 W/(m ² ·K)
	U superheater (ORC)	50 W/(m ² ·K)
Expander	Isentropic efficiency (ORC)	0.80
	Generator efficiency	0.90
	Minimum vapor fraction (ORC)	100%
Condenser	Working fluid pressure drop	Neglected
	Heat sink pressure drop	100 kPa
	U desuperheater	90 W/(m ² ·K)
	U condenser	900 W/(m ² ·K)

Working fluid selection

Many working fluid studies can be found in the literature, mostly presenting comparisons of thermodynamic performance. However, other aspects like safety (toxicity, flammability, etc.) and environmental impact (global warming potential (GWP) and ozone depletion potential (ODP)) should also be considered.

The standard fluids used in low temperature ORC plants today are R134a and R245fa (Quoilin, Broek et al. 2013) and are therefore chosen as reference. R123 was chosen as it is suitable for low temperature applications (Li, Wang et al. 2013). R1234ze(E) was chosen as it is a promising refrigerant for the future (Zyhowski and Brown 2011). To compare the performance of these refrigerants to natural working fluids, three hydrocarbons with different critical temperatures were chosen. One of the biggest disadvantages of hydrocarbons is their high flammability which can be reduced by mixing them with CO₂ (Garg, Kumar et al. 2013). However, in this paper only pure fluids are investigated.

All selected fluids are listed in Table 3 with their critical temperatures, GWP and safety class (according to ASHRAE Standard 34). The ODP is not listed as it is negligible for all selected fluids.

Table 3: Properties of selected working fluids (Calm and Hourahan 2011; Fukuda, Kondou et al. 2014)

Fluid	T _{crit} (°C)	GWP	Safety class
R134a	101.1	1300	A1
R245fa	154.0	1030	B1
R123	183.7	77	B1
R1234ze(E)	109.4	6	A2L
Butane	152.0	20	A3
Isopentane	187.2	20	A3
Propane	96.7	20	A3

3. Results and discussion

The results for all cases and working fluids are presented below. The values for net power production for each working fluid are shown in Figure 3, Figure 4 and Figure 5 for Case I, II and III, respectively.

The net power is shown in a separate column for each working fluid and cycle. The columns are divided into colored sections, representing the different constraint values for total heat exchanger area. Naturally, more power requires more heat exchanger area. However, when the pinch point limitation (1 °C) is reached in both heat exchangers, no area can be added anymore and increasing the maximum allowed area thus has no effect on the results anymore.

Adding a recuperator generally increases the power cycle efficiency and is thus favorable from a thermodynamic point of view. However, it adds cost and complexity to the system, so it should only be included if it is economically reasonable. Some cases in our calculations showed an available temperature difference for recuperation of 60 °C. However, when a recuperator was added, this difference decreased as the area for the recuperator was no longer available for the other heat exchangers due to the constrained total heat exchanger area. Thus, the net power output only increased slightly for some cases but not significantly enough to be included in the results.

3.1. Results for Case I (heat source inlet temperature: 100 °C)

The calculated net power output for Case I is very similar for all fluids: Around 30 kW can be produced when the heat source inlet temperature is 100 °C.

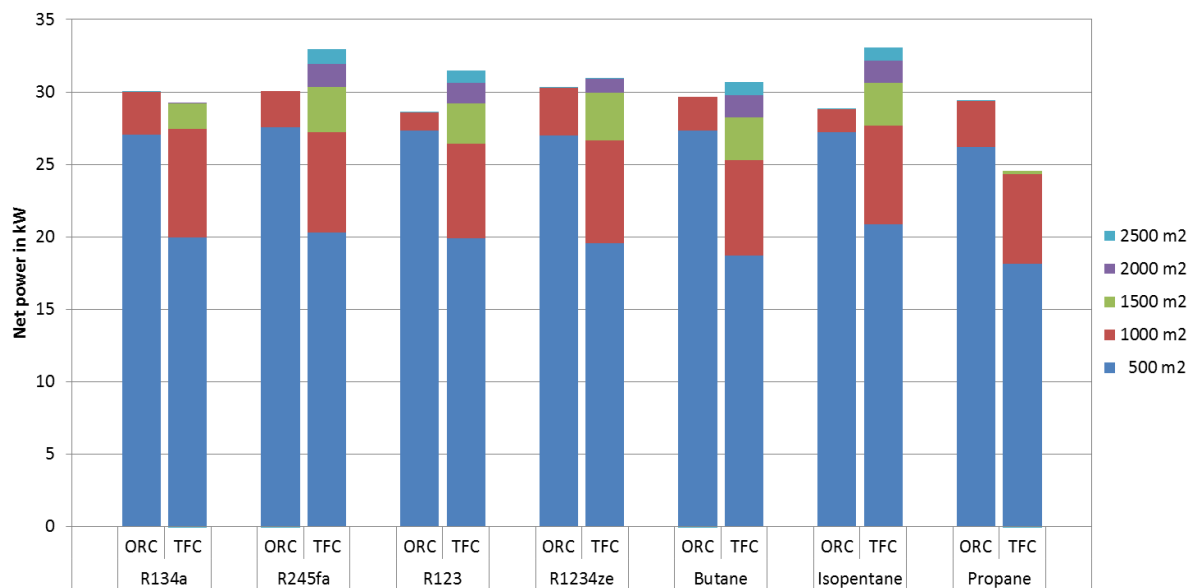


Figure 3: Net power for ORC and TFC for Case I (heat source inlet temperature: 100 °C)

The total expander efficiencies for the TFCs range from 0.617 to 0.705. Detailed results for the different systems with maximum heat exchanger area are shown in Table 4.

Table 4: Case I – selected result details (ORCs and TFCs with highest net power highlighted)

Fluid	Cycle	Net power output	Total heat exchanger area	Heat source outlet	Pump outlet pressure	Mass flow working fluid	Expander volume flow (out)
		kW	m ²	°C	bar	kg/s	m ³ /s
R134a	ORC	30.0	822	53.1	1.93	2.3	0.08
	TFC	29.2	1494	33.7	3.51	5.9	0.11
R245fa	ORC	30.0	747	54.6	0.53	2.1	0.26
	TFC	32.9	2500	30.9	1.20	6.9	0.39
R123	ORC	28.6	652	57.2	0.33	2.2	0.37
	TFC	31.5	2500	32.1	0.74	9.2	0.58
R1234ze(E)	ORC	30.3	826	52.1	1.48	2.6	0.10
	TFC	30.9	1980	31.5	2.75	6.4	0.14
Butane	ORC	29.7	745	54.7	0.71	1.1	0.19
	TFC	30.7	2500	31.4	1.46	3.6	0.28
Isopentane	ORC	28.8	686	56.2	0.31	1.1	0.39
	TFC	33.1	2500	32.1	0.68	4.0	0.61
Propane	ORC	29.4	837	53.2	2.39	1.2	0.06
	TFC	24.5	1093	38.3	3.99	2.7	0.08

3.2. Results for Case II (heat source inlet temperature: 150 °C)

Unlike for Case I, big differences can be seen for Case II: The net power ranges from 50 to 110 kW for a heat source inlet temperature of 150 °C.

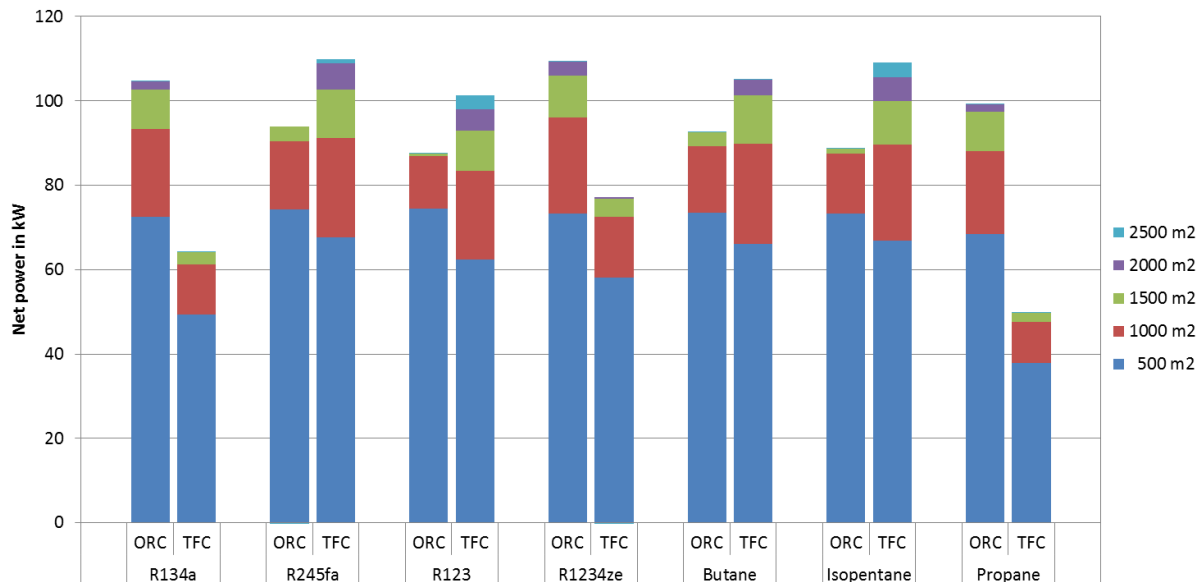


Figure 4: Net power for ORC and TFC for Case II (heat source inlet temperature: 150 °C)

The total expander efficiencies for the TFCs range from 0.693 to 0.740. Detailed results for the different systems with maximum heat exchanger area are shown in Table 5.

Table 5: Case II – selected result details (ORCs and TFCs with highest net power highlighted)

Fluid	Cycle	Net power output	Total heat exchanger area	Heat source outlet	Pump outlet pressure	Mass flow working fluid	Expander volume flow (out)
		kW	m ²	°C	bar	kg/s	m ³ /s
R134a	ORC	104.6	1731	37.1	3.86	5.4	0.18
	TFC	64.2	1520	29.1	3.86	9.6	0.19
R245fa	ORC	93.9	1346	58.0	1.13	3.9	0.50
	TFC	109.8	2273	33.2	2.93	6.6	0.62
R123	ORC	87.4	1069	65.1	0.66	4.1	0.69
	TFC	101.2	2500	36.1	1.93	8.8	0.92
R1234ze(E)	ORC	109.3	1814	36.2	3.45	5.8	0.23
	TFC	77.2	1680	28.8	3.45	9.0	0.25
Butane	ORC	92.6	1328	58.8	1.38	2.0	0.36
	TFC	105.0	1957	35.4	3.17	3.4	0.45
Isopentane	ORC	88.7	1168	61.9	0.62	2.0	0.74
	TFC	109.0	2500	36.2	1.73	3.7	0.96
Propane	ORC	99.2	1699	38.3	4.04	2.7	0.15
	TFC	49.7	1449	29.8	4.04	5.3	0.16

3.3. Results for Case III (heat source inlet temperature: 200 °C)

As expected, the differences in performance are even bigger for Case III: Power outputs from 70 to 225 kW are calculated for a heat source inlet temperature of 200 °C.

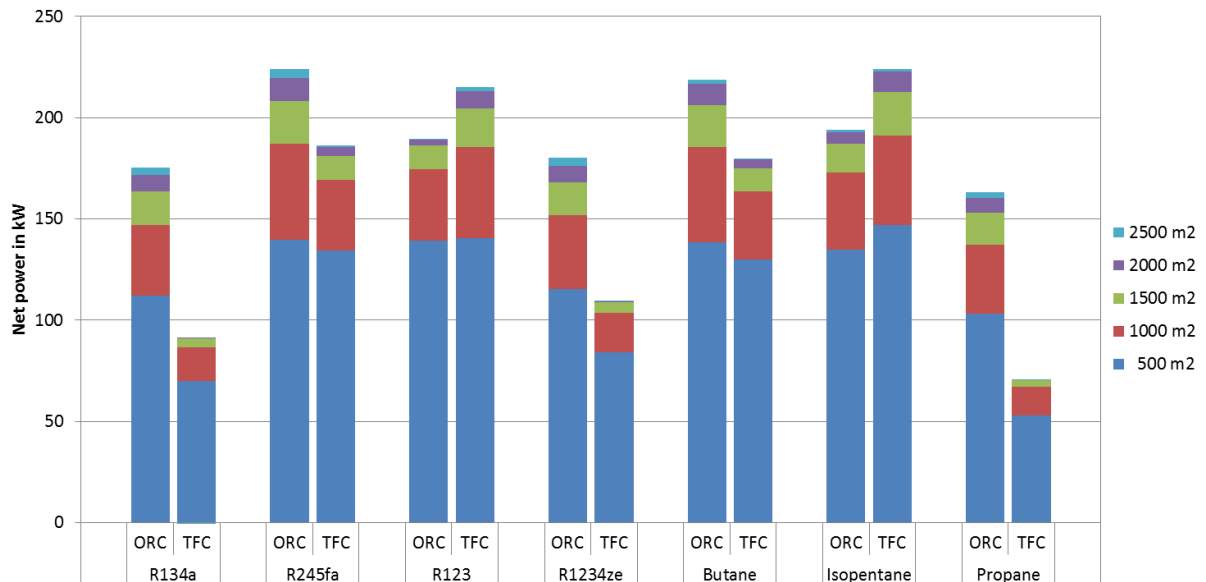


Figure 5: Net power for ORC and TFC for Case III (heat source inlet temperature: 200 °C)

The total expander efficiencies for the TFCs range from 0.703 to 0.783. Detailed results for the different systems with maximum heat exchanger area are shown in Table 6.

Table 6: Case III – selected result details (ORCs and TFCs with highest net power highlighted)

Fluid	Cycle	Net power output	Total heat exchanger area	Heat source outlet	Pump outlet pressure	Mass flow working fluid	Expander volume flow (out)
		kW	m ²	°C	bar	kg/s	m ³ /s
R134a	ORC	175.4	2472	30.5	3.86	6.4	0.26
	TFC	91.0	1520	29.3	3.86	13.7	0.27
R245fa	ORC	224.2	2373	34.8	3.47	6.5	0.86
	TFC	186.4	2216	28.2	3.47	8.7	0.90
R123	ORC	189.1	1829	60.7	1.40	6.3	1.09
	TFC	215.1	2212	34.7	3.48	9.0	1.27
R1234ze(E)	ORC	180.2	2500	30.7	3.45	6.6	0.33
	TFC	109.3	1589	29.0	3.45	12.8	0.35
Butane	ORC	218.9	2186	36.3	3.61	3.4	0.62
	TFC	179.8	2157	28.7	3.61	4.6	0.66
Isopentane	ORC	193.9	2242	52.3	1.30	3.0	1.17
	TFC	224.1	2276	35.4	3.07	3.8	1.31
Propane	ORC	163.4	2417	30.7	4.04	3.3	0.22
	TFC	70.6	1493	30.0	4.04	7.5	0.23

3.4. Discussion

The results presented in the previous sections show that the calculated expander efficiency for the TFC was always less than the assumed 0.8 for the ORC. This was expected as explained in Section 1.1. The efficiency increases with increasing heat source temperature and reaches a maximum of 0.783. The expander outlet volume flows are generally higher for the TFC, indicating a larger system.

The heat source utilization is much higher for the TFC for Case I, which leads to lower heat source outlet temperatures. However, this advantage comes at the cost of a higher total heat exchanger area which again leads to a larger and more expensive system. This difference between ORC and TFC decreases as the heat source temperature increases and the heat source outlet temperatures and total heat exchanger areas are similar for both cycles for Case III.

The two effects explained above lead to a 10% higher maximum net power output for the TFC for Case I. For Case II and Case III, the net power outputs are very similar. However, the total system size is believed to be higher for the TFC for all cases.

The investigated refrigerants are well-suited for power production and are commonly used in ORC systems. It can be seen that the critical temperature is an important parameter for the working fluid choice in a TFC. A high difference between heat source inlet temperature and critical temperature of the working fluid leads to poor temperature matching and thus low performance, see R134a, R1234ze(E) and propane for Case II and Case III.

The natural working fluids showed similar performance to the refrigerants, especially the TFC systems with isopentane. This might be an environmentally friendly alternative to the standard systems used

today. However, the differences were rather small and replacing R134a with R1234ze(E) in existing systems also seemed reasonable.

The presented results deviate from the results of many other studies like (Zamfirescu and Dincer 2008), (Fischer 2011), (Lai and Fischer 2012), or (Chan, Ling-Chin et al. 2013) by being less promising for the TFC. This is mainly due to the variable expander efficiency that was used for the two-phase expander in the TFC. All of the above mentioned studies assumed a constant (and rather optimistic) efficiency. An even more detailed and, most importantly, verified calculation method for the expander efficiency of both ORC and TFC is required for a more realistic comparison.

Future work will involve the implementation of correlations for the heat transfer coefficients and pressure drops in both heat exchangers. The use of working fluid mixtures and more complex cycle configurations like the Smith cycle (Smith, Stosic et al. 2005), a partially evaporating cycle (Lecompte, van den Broek et al. 2013) or a dual stage cycle (Choi and Kim 2013) might be promising and could also be investigated.

4. Conclusions

The following can be concluded from the performed calculations:

- For a heat source inlet temperature of 100 °C, up to 10% more power can be produced with a TFC. At 150 and 200 °C, the difference between the best ORC and TFC is insignificant.
- The system size is estimated to be larger for the TFC. Both the heat exchanger area and the expander outlet volume flow are generally higher for the TFC systems.
- This study thus shows less promising results for the TFC than other studies, mainly due to the lower expander efficiency.
- Natural working fluids with low environmental impact can match standard refrigerants in terms of performance, especially isopentane used in a TFC. However, the flammability of the investigated hydrocarbons is a disadvantage that needs to be kept in mind.

References

- Bao, J. and L. Zhao (2013). "A review of working fluid and expander selections for organic Rankine cycle." Renewable and Sustainable Energy Reviews **24**(0): 325-342.
- Boyle, P. and L. Hays (2013). "Variable Phase Cycle." Journal of the Gas Turbine Society of Japan **41**(6): 461-466.
- Brown, B. W. and G. L. Mines (1998). "Flowsheet Simulation of the Trilateral Cycle." Geothermal Resources Council Transactions **22**: 373-377.
- Børgund, M. A. (2009). Power Production from Low-Temperature Aluminium Electrolysis Cell Off-Gases Master's Thesis, Norwegian University of Science and Technology.
- Calm, J. M. and G. C. Hourahan (2011). Physical, Safety, and Environmental Data for Current and Alternative Refrigerants. 23rd International Congress of Refrigeration. Prague, Czech Republic.
- Chan, C. W., J. Ling-Chin, et al. (2013). "A review of chemical heat pumps, thermodynamic cycles and thermal energy storage technologies for low grade heat utilisation." Applied Thermal Engineering **50**(1): 1257-1273.
- Choi, B. C. and Y. M. Kim (2013). "Thermodynamic analysis of a dual loop heat recovery system with trilateral cycle applied to exhaust gases of internal combustion engine for propulsion of the 6800 TEU container ship." Energy **58**(0): 404-416.
- DiPippo, R. (2007). "Ideal thermal efficiency for geothermal binary plants." Geothermics **36**(3): 276-285.
- Fischer, J. (2011). "Comparison of trilateral cycles and organic Rankine cycles." Energy **36**(10): 6208-6219.
- Fukuda, S., C. Kondou, et al. (2014). "Low GWP refrigerants R1234ze(E) and R1234ze(Z) for high temperature heat pumps." International Journal of Refrigeration **40**(0): 161-173.
- Galanis, N., E. Cayer, et al. (2009). "Electricity Generation from Low Temperature Sources." Journal of Applied Fluid Mechanics **2**: 55-67.
- Garg, P., P. Kumar, et al. (2013). "Evaluation of carbon dioxide blends with isopentane and propane as working fluids for organic Rankine cycles." Applied Thermal Engineering **52**(2): 439-448.
- Hays, L. (2010). Demonstration of a Variable Phase Turbine Power System for Low Temperature Geothermal Resources. Geothermal Technologies Program 2010, U.S. Department of Energy.
- Ho, T. (2012). Advanced Organic Vapor Cycles for Improving Thermal Conversion Efficiency in Renewable Energy Systems PhD Thesis, University of California, Berkeley.
- Ho, T., S. S. Mao, et al. (2012). "Comparison of the Organic Flash Cycle (OFC) to other advanced vapor cycles for intermediate and high temperature waste heat reclamation and solar thermal energy." Energy **42**(1): 213-223.
- Ho, T., S. S. Mao, et al. (2012). "Increased power production through enhancements to the Organic Flash Cycle (OFC)." Energy **45**(1): 686-695.
- Hu, L., Z. Wang, et al. (1989). An organic total flow system for geothermal energy and waste heat conversion. 24th Intersociety Energy Conversion Engineering Conference, Washington, DC, USA.
- Lai, N. A. and J. Fischer (2012). "Efficiencies of power flash cycles." Energy **44**(1): 1017-1027.
- Lecompte, S., M. van den Broek, et al. (2013). Thermodynamic analysis of the partially evaporating trilateral cycle. ASME ORC 2013 - 2nd International Seminar on ORC Power Systems, Rotterdam, The Netherlands.
- Lemmon, E. W., M. L. Huber, et al. (2013). NIST Standard Reference Database 23: Reference Fluid Thermodynamic and Transport Properties-REFPROP, Version 9.1, National Institute of Standards and Technology, Standard Reference Data Program.
- Li, M., J. Wang, et al. (2013). "Construction and preliminary test of a low-temperature regenerative Organic Rankine Cycle (ORC) using R123." Renewable Energy **57**(0): 216-222.
- Quoilin, S., M. V. D. Broek, et al. (2013). "Techno-economic survey of Organic Rankine Cycle (ORC) systems." Renewable and Sustainable Energy Reviews **22**(0): 168-186.

- Quoilin, S., S. Declaye, et al. (2011). "Thermo-economic optimization of waste heat recovery Organic Rankine Cycles." Applied Thermal Engineering **31**(14–15): 2885-2893.
- Smith, I. K. (1993). "Development of the Trilateral Flash Cycle System: Part 1: Fundamental Considerations." Proceedings of the Institution of Mechanical Engineers, Part A: Journal of Power and Energy **207**: 179-194.
- Smith, I. K., N. Stosic, et al. (1994). Lysholm Machines as Two-Phase Expanders. International Compressor Engineering Conference, Purdue University, Indiana, USA.
- Smith, I. K., N. Stosic, et al. (1995). Trilateral Flash Cycle System: A High Efficiency Power Plant for Liquid Resources. World Geothermal Congress, Florence, Italy.
- Smith, I. K., N. Stosic, et al. (2004). "An Improved System for Power Recovery from Higher Enthalpy Liquid Dominated Fields." Geothermal Resources Council Transactions **28**: 561-565.
- Smith, I. K., N. Stosic, et al. (2005). "Screw Expanders Increase Output and Decrease the Cost of Geothermal Binary Power Plant Systems." Geothermal Resources Council Transactions **29**: 787-794.
- Smith, I. K., N. Stosic, et al. (2007). "Cost Effective Small Scale ORC Systems for Power Recovery from Low Enthalpy Geothermal Resources." Geothermal Resources Council Transactions **31**: 529-534.
- Steffen, M., M. Löffler, et al. (2013). "Efficiency of a new Triangle Cycle with flash evaporation in a piston engine." Energy **57**(0): 295-307.
- Welch, P. and P. Boyle (2009). "New Turbines to Enable Efficient Geothermal Power Plants." Geothermal Resources Council Transactions **33**: 765-772.
- Welch, P. and P. Boyle (2009). New Turbines to Enable Efficient Geothermal Power Plants. Geothermal Resources Council Annual Meeting. Reno, Nevada, USA.
- Welch, P., P. Boyle, et al. (2011). "Construction and Startup of Low Temperature Geothermal Power Plants." Geothermal Resources Council Transactions **35**: 1351-1356.
- Welch, P., P. Boyle, et al. (2010). "Performance of New Turbines for Geothermal Power Plants." Geothermal Resources Council Transactions **34**: 1091-1096.
- Zamfirescu, C. and I. Dincer (2008). "Thermodynamic analysis of a novel ammonia–water trilateral Rankine cycle." Thermochimica Acta **477**(1-2): 7-15.
- Zyhowski, G. and A. Brown (2011). Low Global Warming Fluids for Replacement of HFC-245fa and HFC-134a in ORC Applications. First International Seminar on ORC Power Systems. Delft, The Netherlands.
- Öhman, H. and P. Lundqvist (2013). "Experimental investigation of a Lysholm Turbine operating with superheated, saturated and 2-phase inlet conditions." Applied Thermal Engineering **50**(1): 1211-1218.

14 Appendix D: Scientific paper submitted to the Gustav Lorentzen conference

ANALYSIS OF THE TRILATERAL FLASH CYCLE AND THE PARTIALLY EVAPORATING CYCLE FOR POWER PRODUCTION FROM LOW TEMPERATURE HEAT SOURCES

S. TRÆDAL^(a), D. ROHDE^(b), T. M. EIKEVIK^(a)

(a) The Norwegian University of Science and Technology (NTNU), Kolbjørn Hejes vei 1B, Trondheim, 7034, Norway

Fax (+47) 73 59 35 80, trygve.m.eikevik@ntnu.no

(b) SINTEF Energy Research, Postboks 4761 Sluppen, Trondheim, 7465, Norway
daniel.rohde@sintef.no

Abstract The Trilateral Flash Cycle (TFC) and the Partially Evaporating Cycle (PEC) have been analyzed and compared to the Organic Rankine Cycle (ORC). Three cases have been investigated. Case I uses air at 100 °C, Case II air at 150 °C and Case III air at 200 °C as the heat source. Water at 20 °C is used as the heat sink for all cases. The cycles are optimized for maximum net power production with eight different working fluids, R123, R134a, R245fa, R1234ze, butane, pentane, isopentane and propane. Detailed heat exchanger models to calculate the pressure drops and heat transfer coefficients are included in the model.

The results show that the TFC has the lowest power production for all cases, and the total system size is estimated to be larger for the TFC compared to the other cycles. The PEC doesn't show any advantage over the ORC for the cases analyzed here.

Keywords Power generation, low temperature heat sources, Organic Rankine Cycle, Trilateral Flash Cycle, Partially Evaporating Cycle, working fluids

1. INTRODUCTION

Several studies have found the Trilateral Flash Cycle (TFC) very promising for power production from low temperature heat sources, like discussed in our previous paper [...]. However, none of these studies includes pressure losses in the system and calculation of heat transfer coefficients for each working fluid. In addition, the required heat exchanger areas are usually not considered and most of the studies assume constant and equal expander efficiency for the TFC and the ORC. The PEC is found to be promising for low temperature heat sources when the working fluid pump efficiency is low [1].

In our previous paper on the TFC [...], the cycle was compared to the ORC for three cases defined by different heat source inlet temperatures. Air with a mass flow of 10 kg/s and temperatures of 100, 150 and 200 °C were used as the heat source for Case I, II and III respectively. Water at 20 °C where used as the heat sink for all cases. The cycles were simulated with seven different working fluids, R123, R134a, R245fa, R1234ze, butane, isopentane and propane. The pressure losses were neglected, and the heat transfer coefficients where assumed to be the same for all working fluids. A variable two-phase expander efficiency was used. The TFC was then found to have a higher net power production than the ORC for the 100 °C case, and the difference was found to be insignificant for the 150 °C and 200 °C cases. The system size was estimated to be larger for the TFC, especially at lower heat source temperatures.

In this study, a detailed heat exchanger model is included to calculate the pressure losses and heat transfer coefficients. The cases investigated are the same as in our previous study.

This paper begins with a description of the TFC and PEC. A model description then follows before the results and conclusions are presented.

2. DESCRIPTION OF THE TFC AND PEC

The main components of the ORC, TFC and PEC are pump, heat recovery heat exchanger (HRHE), expander and condenser. The TFCs main difference from the ORC is that the heating process ends at the boiling point of the working fluid, i.e. there is no evaporation and superheating. Power is produced in a two-phase expander after the heating process. A temperature-entropy diagram for an ORC (left) and a TFC (right) with propane as working fluid is shown in Figure 1 below.

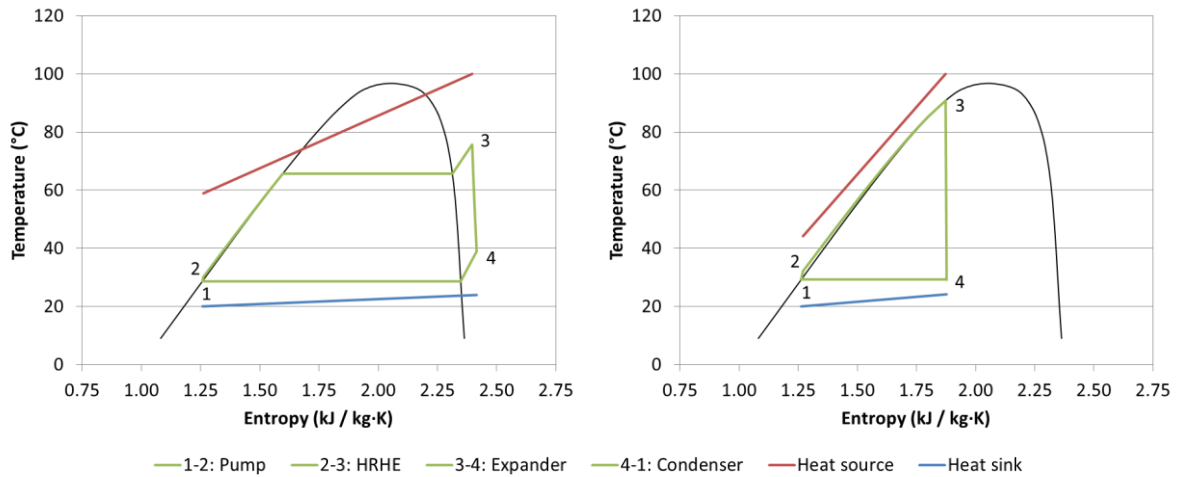


Figure 1: Temperature-entropy diagrams of ORC (left) and TFC (right) with propane as working fluid

The fact that there is no evaporation and superheating in the TFC leads to the possibility of a better temperature match between the working fluid and the heat source in the heat recovery heat exchanger. This is illustrated in the temperature vs. heat transferred diagrams in Figure 2.

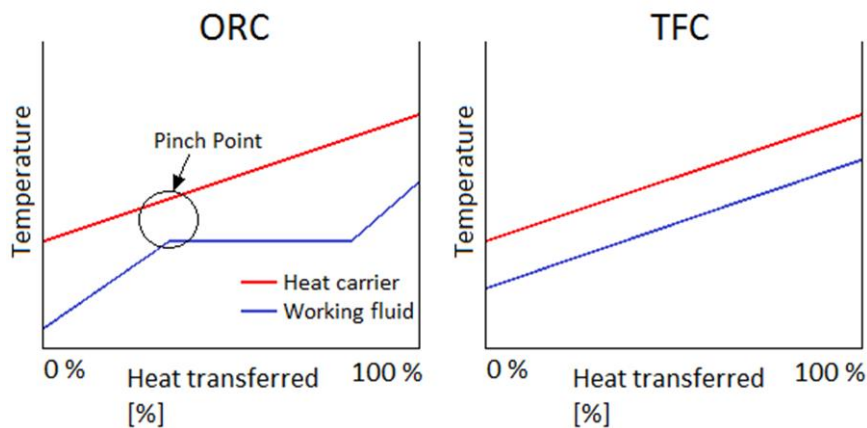


Figure 2: Variation in stream temperature during heat addition for ORC (left) and TFC (right)

As seen in Figure 2, there is a suboptimal temperature matching in the heat recovery heat exchanger for the ORC. This is a result of the constant evaporation temperature of the working fluid and leads to exergy losses. In the TFC both fluids are liquid during the heating process, such that the temperature difference in the heat exchanger is nearly constant.

The cost pr. kWh for TFC systems have been estimated to be lower than for ORC systems due to the elimination of the evaporator, separator drum, gear box, lube oil system and the fact that simpler heat exchangers can be used [2].

In the PEC the working fluid is allowed to be partially evaporated in the heating process. This is done in an attempt to combine the advantages of the TFC and ORC.

The two-phase expansion is the technically most challenging part of the TFC and PEC. For medium scale (50 – 250 kW) applications, like investigated in this study, screw expanders and the Variable Phase Turbine (VPT) are the most relevant expander types. These are described in [3] and [4], respectively.

3. MODEL DESCRIPTION

To analyze the TFC and PEC and compare them to the ORC, the three cycles have been simulated using Microsoft Excel with Visual Basic for Applications (VBA). REFPROP 9 [5] is used for the thermodynamic properties of the working fluids and the Excel solver is used for the optimization.

3.1 Cycle simulations

Before the simulations, the working fluid and boundary conditions are specified. The mass flow, inlet temperature and pressure of the heat source are given, and the inlet temperature and pressure of the heat sink. The following parameters are then optimized during the simulations: working fluid mass flow, pump outlet pressure, vapor quality at expander inlet (only PEC), condensation temperature, heat sink outlet temperature and superheat at the expander inlet (only ORC). Heat source and sink specifications as well as component efficiencies are constant inputs which have to be chosen by the user. The only exception to this are the expander efficiencies for the TFC and PEC, which are calculated automatically. The heat transfer coefficients and pressure drops are calculated using the correlations specified in section 3.2.

The cycles are calculated based on enthalpy balances with a number of constraints to avoid unfeasible solutions: The minimum pinch point temperatures in the heat exchangers and the minimum superheat throughout the ORC expander are specified. Both are calculated by dividing the component into several small sections and ensuring the limits in each section. Also, the pump outlet pressure is limited to 95% of the working fluid's critical pressure and the condensation pressure is kept above 1 bar to avoid a sub-atmospheric system. The total heat exchanger area is constrained during the case studies to compare the performances of the cycles at different system sizes. The cooling of the heat source is not limited although some practical limitations can occur in reality.

The optimization target for the Excel solver is the net power output, which is set to be maximized. Using the net power output instead of cycle efficiency is recommended for waste heat sources, as explained in [6]. The net power output is defined as

$$P_{net} = P_{expander} \cdot \eta_{generator} - \frac{P_{pumps}}{\eta_{motor}} - \frac{P_{fan}}{\eta_{motor}}$$

with P_{pumps} being the sum of working fluid pump power and heat sink pump power, and P_{fan} being the heat source fan power, both in kW. To perform the optimization, the Excel solver is used with the GRG Nonlinear solving method with forward derivatives. A high number of starting points are used to ensure that the global maximum is found with a high probability.

To calculate the heat exchanger area, the well-known logarithmic mean temperature difference (LMTD) method is used. Although the assumptions made in this method are not fully fulfilled in all of our cases, it gives a good approximation. The area for each section of the heat exchangers are calculated individually with the following formula:

$$A = \frac{\dot{Q}}{U \cdot \Delta T_{lm}}$$

Here \dot{Q} is the heat flow in the heat exchanger section in kW, U is the heat transfer coefficient in W/m^2K , and ΔT_{lm} is the LMTD in K.

All component efficiencies are assumed constant except for the expander efficiency in the TFC and PEC. The two-phase expander is modeled as a VPT. The nozzle and rotor efficiencies are calculated separately. The nozzle efficiency is calculated as

$$\eta_{\text{nozzle}} = 0.865 + 0.00175 \cdot d_{4,\text{vapor}}$$

where $d_{4,\text{vapor}}$ is the vapor density in kg/m^3 of the working fluid at condensing pressure. The rotor efficiency is calculated as

$$\eta_{\text{rotor}} = 0.575 + 0.325 \cdot q_4$$

where q_4 is the vapor quality of the working fluid at the nozzle exit. These relationships are based on values given in [7] and [8] and personal communication with Lance Hays, author of [7]. They allow a more realistic comparison between different working fluids, as the main influencing properties (vapor density and vapor quality) are taken into account. However, these relationships are simplified and not validated and should therefore not be taken as accurate.

3.2 Heat exchanger models

Heat exchanger models have been made for both the heater and condenser. The heater is modelled as a plate-finned tube heat exchanger, and the condenser as a plate heat exchanger. For the simulations, some geometry specifications and the mass fluxes needs to be specified by the user, and the inlet and outlet conditions for all the sections are taken from the cycle calculations. Multiple iterations are performed such that the parameters are calculated under the correct conditions. The overall heat transfer coefficients are calculated by the methods of [9].

The heater is divided into a preheating section, an evaporating section (for ORC and PEC) and a superheating section (for ORC). The heat transfer coefficient and pressure drop is calculated separately for each section, using the following correlations:

Single phase (working fluid): The heat transfer coefficients and friction factors for the single phase sections (preheating and superheating) are calculated from the correlation by Gnielinski [10]. **Two-phase:** In the evaporating section for the ORC and PEC the heat transfer coefficient is found from the Liu and Winterton correlation [11]. The pressure loss is calculated from the correlation method of Friedel [12]. The pressure losses in the header and tube entrance is estimated using the method from [9] and the pressure losses in the bends are calculated using the method from [13]. **Air side:** The heat transfer coefficient and friction factor is calculated from the Gray and Webb correlations [14].

The condenser is divided into a desuperheating section and a condensing section. The heat transfer coefficient and pressure drop is calculated separately for each section, using the following correlations:

Single phase: The Martin correlations [15] are used to calculate the heat transfer coefficient and pressure drop for the desuperheating on the working fluid side and for the heating on the heat sink side. It is a semi-theoretical correlation for single phase flow in chevron type heat exchangers. **Two-phase:** The Han, Lee et al. correlations [16] are used to find the heat transfer coefficient and friction factor for the condensation of the working fluid. It uses corrugation pitch and chevron angle as parameters. The pressure losses for the inlet and outlet ports as well as the acceleration pressure drop are calculated using the method of [16].

4. CASE STUDIES

Most of the specifications and boundary conditions for the ORC and TFC are the same, as shown in Table 1. To define a case, all user input values have to be chosen which is explained below.

4.1 Case definitions

Three different heat sources were chosen as case studies. Air was selected as heat source fluid with a mass flow of 10 kg/s and the temperatures were set to 100, 150 and 200 °C for Case I, Case II and Case III, respectively. Water at 20 °C was chosen as heat sink.

To show how the power output changes with system size, the maximum total heat exchanger area was constrained during the calculations. All cases were calculated with seven different limitations: 1000, 1500, 2000, 2500, 3000, 3500 and 4000 m^2 . The maximum total heat exchanger area includes all calculated sections: heater, evaporator, superheater, desuperheater and condenser.

All pump efficiencies were set to 0.70, the ORC expander efficiency was set to 0.80, all motor and generator efficiencies were set to 0.90 and the fan efficiency was set to 0.92. All user input values are shown in Table 1.

Table 1: Input data for the ORC, TFC and PEC simulations

	Parameter	Value
Cycle	Working Fluid	R123, R134a, R245fa, R1234ze, butane, pentane, isopentane and propane
	Total area restriction	1000, 1500, 2000, 2500, 3000, 3500 and 4000 m ²
Heat source	Fluid	Air
	Mass flow	10 kg/s
	Inlet temperature	100, 150 and 200 °C
	Inlet pressure	0.3 MPa
	Fan efficiency	0.92
Heat sink	Pressure drop	Calculated in heat exchanger simulation
	Fluid	Water
	Inlet temperature	20 °C
	Inlet pressure	0.3 MPa
	Pump efficiency	0.70
Pump	Motor efficiency	0.95
	Isentropic efficiency	0.70
HRHE	Motor efficiency	0.95
	HTC heater	Calculated in heat exchanger simulation
	HTC evaporator (ORC and PEC)	Calculated in heat exchanger simulation
	HTC superheater (ORC)	Calculated in heat exchanger simulation
	Minimum pinch temperature	1 °C
Expander	Pressure drop	Calculated in heat exchanger simulation
	Isentropic efficiency (ORC)	0.80
	Isentropic efficiency, nozzle (TFC and PEC)	$0.865 + 0.00175 * vapor\ density$
Condenser	Isentropic efficiency, rotor (TFC and PEC)	$0.575 + 0.325 * vapor\ fraction$
	HTC condenser	Calculated in heat exchanger simulation
	HTC desuperheater	Calculated in heat exchanger simulation
Condenser	Pressure drop	Calculated in heat exchanger simulation

4.2 Working fluid selection

Many working fluid studies can be found in the literature, mostly presenting comparisons of thermodynamic performance. However, other aspects like safety (toxicity, flammability, etc.) and environmental impact (global warming potential (GWP) and ozone depletion potential (ODP)) should also be considered.

The standard fluids used in low temperature ORC plants today are R134a and R245fa [17] and are therefore chosen as reference. R123 was chosen as it is suitable for low temperature applications [18]. R1234ze(E) was chosen as it is a promising refrigerant for the future [19]. To compare the performance of these refrigerants to natural working fluids, four hydrocarbons with different critical temperatures were chosen. One of the biggest disadvantages of hydrocarbons is their high flammability.

5. RESULTS AND DISCUSSION

Selected result details for the two best working fluids for each cycle with maximum area are given in Table 2, Table 3 and Table 4 for Case I, II and III respectively.

Table 2: Case I – selected result details for the two best ORCs, TFCs and PECs

Case I, 100 °C		ORC		TFC		PEC	
Working fluid		R134a	R1234ze	R134a	Propane	R134a	R1234ze
Net power	kW	32.0	31.9	28.7	27.4	33.1	33.1
Heat input	kW	497	492	646	618	407	488
Heater area	m ²	800	789	2246	805	807	1091
Condenser area	m ²	200	211	255	195	193	213
Working fluid mass flow	kg/s	2.5	2.6	5.3	2.6	2.6	2.8
Volume flow expander outlet	m ³ /s	0.09	0.11	0.11	0.09	0.08	0.12

The ORC and PEC outperforms the TFC for Case I. The best PEC, with R134a, has a power production that is 15 % higher than that of the best TFC, with R134a, and 3 % higher than that of the best ORC, with R134a. The vapor quality at the expander inlet is 1.00 for the PEC, which makes it an ORC without superheating. Both the heat input and power produced in the expander are highest for the TFC, but the required working fluid pump power and heat source fan power are also much higher for the TFC resulting in the lowest net power production. The reason for the high pump power is that the working fluid mass flow is much higher than for the two other cycles, and that it needs to be pumped to a higher pressure. The fan power is higher because the higher heater area requirement leads to higher pressure losses in the heater (the front area of the heater is the same for all cycles).

The best TFC requires a 178 % larger heater, a 32 % larger condenser and a 110 % higher working fluid mass flow than the best PEC. The volume flow at the expander outlet is about 30 % higher for the best TFC compared to the PEC and ORC. The reason the difference in volume flow isn't higher is that the expander outlet temperature is much higher for the PEC and ORC. When comparing the average values for mass flow of working fluid, volume flow rate at the expander outlet and total heat exchanger area requirement over all the different working fluids, the TFC is estimated to have a significantly larger total system size than the ORC and PEC for Case I.

The total expander efficiency ranges from 0.59 to 0.71 for the TFC and 0.59 to 0.82 for the PEC. The expander efficiency is slightly better for the best PECs compared to the ORC because the variable two-phase efficiency is at its optimum for these cases.

Table 3: Case II – selected result details for the two best ORCs, TFCs and PECs

Case II, 150 °C		ORC		TFC		PEC	
Working fluid		R1234ze	R134a	Butane	R245fa	R1234ze	Butane
Net power	kW	114.1	110.1	107.3	90.0	111.1	107.1
Heat input	kW	1180	1150	1183	1114	1141	1094
Heater	m ²	3266	2551	2086	3812	3525	2578
Condenser	m ²	519	449	414	188	479	420
Working fluid mass flow	kg/s	5.8	5.3	3.4	5.9	6.3	3.3
Volume flow expander outlet	m ³ /s	0.25	0.19	0.47	0.48	0.25	0.47

The ORC has the highest power production for Case II. The best ORC, with R1234ze, has a power production that is 3 % higher than that of the best PEC, with R245fa and 6 % higher than that of the best TFC, with butane. The best PEC has a vapor quality of 1.00 at the expander inlet, which makes it an ORC. The best TFC requires 36 % less heater area and 20 % less condenser area compared to the best ORC, due to higher heat transfer coefficients. The working fluid mass flow is 42 % lower, and the volume flow at the expander outlet is 87 % higher for the best TFC compared to the ORC. When comparing the average values over all the different working fluids, the TFC still has a significantly larger estimated system size than the ORC, however not as much as for Case I. The estimated system size for the PEC is between the ORC and the TFC.

The total expander efficiency ranges from 0.67 to 0.74 for the TFC and 0.70 to 0.81 for the PEC.

Table 4: Case III – selected result details for the two best ORCs, TFCs and PECs

Case III, 200 °C		ORC		TFC		PEC	
		Butane	R245fa	Isopentane	Butane	Butane	R245fa
Working fluid							
Net power	kW	220.4	200.6	185.6	183.9	217.2	194.8
Heat input	kW	1696	1662	1622	1772	1680	1629
Heater	m ²	2011	3758	1930	2015	2428	3758
Condenser	m ²	491	242	70	486	573	243
Working fluid mass flow	kg/s	3.4	6.3	3.6	4.6	3.7	6.8
Volume flow expander outlet	m ³ /s	0.61	0.67	0.84	0.66	0.63	0.66

The ORC has the highest power production for Case III. The ORC with butane has a power production that is 19 % higher than that of the best TFC, with isopentane. The best PEC, with butane, has a vapor quality of 1.00 at the expander inlet and is an ORC. The required heater area are about the same for the best ORC and TFC, but the ORC requires 599 % more condenser area. The mass flow of working fluid is similar for the ORC and TFC and the volume flow at the expander outlet is 38 % higher for the TFC. When comparing the average values over all the working fluids, the TFC requires a significantly larger mass flow of working fluid, about the same volume flow at the expander outlet, and a slightly lower total heat exchanger area. This is also the case for the PEC, and both cycles are estimated to have a larger system size compared to the ORC.

The total expander efficiency ranges from 0.70 to 0.78 for the TFC and 0.77 to 0.81 for the PEC.

The calculated expander efficiency for the TFC is lower than the assumed 0.8 for the ORC expander for all cases. The efficiency increases with increasing heat source temperature and has a maximum of 0.78 for isopentane in the 200 °C case.

The pressure losses in the evaporator are significantly higher for the natural working fluids butane, pentane and isopentane compared to the standard refrigerants. Despite this, these working fluids are among the best for the 150 °C and 200 °C cases.

The results from this study deviates from the results found in our previous study [...]. Now that the pressure losses and heat transfer coefficients are included the TFC can no longer outperform the ORC. The reason is that the increase in pressure losses and associated increase in pump power outweighs the increase in heat input and higher expander power output obtained by increasing the heater area. The heat exchanger coefficient for the TFC heater was also overestimated in the previous study. The new heat exchanger models have shown that the heat transfer coefficients are lower than earlier predicted, and that there are big differences between the different working fluids used. This study deviates even more from other published studies on the TFC by being less promising. This is mainly due to the variable two-phase expander efficiency used here, and that none of the other studies considers pressure losses in the system or calculation of heat transfer coefficients for each working fluid.

To improve this model the massflux of working fluid should be optimized in the cycle simulations to get the optimal tradeoff between the heat transfer coefficient and pressure loss. To do this the calculations needs to be done in another software. The use of working fluid mixtures and more complex cycle configurations could also be investigated.

6. CONCLUSIONS

- The TFC has the lowest power production in all cases, and the total system size is estimated to be larger for the TFC compared to the other cycles, especially for the lower heat source temperature cases.
- The top three PECs are close to pure ORCs or TFCs in all cases, and does not show an advantage over the ORC for the cases studied here.

- The TFC system is estimated to have a lower cost than the ORC due to the elimination of the evaporator, separator drum, gear box, lube oil system and the fact that simpler heat exchangers can be used. The TFC can therefore be suitable in systems with a heat source in the 100 °C to 150 °C range when system size is not a critical factor.
- The calculated expander efficiency for the TFC is lower than the assumed 0.80 for the ORC expander for all cases. The efficiency increases with increasing heat source temperature.
- The results are much less promising for the TFC than the results from our previous study [...] and other published studies on the TFC now that the pressure losses, heat transfer coefficients for each working fluid and better two-phase expander model are included.
- The natural working fluids with low environmental impact can match standard refrigerants in terms of performance despite having significantly higher pressure losses in the evaporator. However, the flammability of the investigated hydrocarbons is a disadvantage that needs to be kept in mind.

REFERENCES

1. Lecompte, S., M. van den Broek, and M. De Paepe. *Thermodynamic analysis of the partially evaporating trilateral cycle*. in *2nd International Seminar on ORC Power Systems, Proceedings*. 2013.
2. Welch, P. and P. Boyle, *New Turbines to Enable Efficient Geothermal Power Plants*. Geothermal Resource Council Transactions, 2009. **33**: p. 765-772.
3. Smith, I.K., N. Stosic, and A. Kovacevic, *Screw Expanders Increase Output and Decrease the Cost of Geothermal Binary Power Plant Systems*. Geothermal Resource Council Transactions, 2005. **29**: p. 787-794.
4. Boyle, P. and L. Hays, *Variable Phase Cycle*. Journal of the Gas Turbine Society of Japan, 2013. **41**(6): p. 461-466.
5. Lemmon, E.W., M.L. Huber, and M.O. McLinden, *NIST Standard Reference Database 23: Reference Fluid Thermodynamic and Transport Properties-REFPROP, Version 9.1*, S.R.D.P. National Institute of Standards and Technology, Editor. 2013.
6. Quoilin, S., et al., *Thermo-economic optimization of waste heat recovery Organic Rankine Cycles*. Applied Thermal Engineering, 2011. **31**(14–15): p. 2885-2893.
7. Hays, L., *Demonstration of a Variable Phase Turbine Power System for Low Temperature Geothermal Resources*, in *Geothermal Technologies Program 2010*. 2010, U.S. Department of Energy.
8. Welch, P. and P. Boyle, *New Turbines to Enable Efficient Geothermal Power Plants*. Geothermal Resources Council Transactions, 2009. **33**: p. 765-772.
9. Bell, K.J. and A.C. Mueller, *Wolverine Engineering Data Book II*. 2001: Wolverine Tube, Inc.
10. Gnielinski, V., *New equations for heat and mass transfer in turbulent pipe and channel flow*. International Chemical Engineering, 1976. **16**(2): p. 359-368.
11. Liu, Z. and R.H.S. Winterton, *A general correlation for saturated and subcooled flow boiling in tubes and annuli, based on a nucleate pool boiling equation*. International Journal of Heat and Mass Transfer, 1991. **34**(11): p. 2759–2766.
12. Friedel, L., *Improved friction pressure drop correlations for horizontal and vertical two phase pipe flow*, in *European Two Phase Flow Group Meeting*. 1979.
13. White, F.M., *Fluid mechanics*. 6th ed., international ed. ed. 2009: McGraw-Hill.
14. Gray, D.L. and R.L. Webb, *Heat Transfer and Friction Correlations for Plate Finned-Tube Heat Exchangers having Plain Fins*, in *International Heat Transfer Conference*. 1986.
15. Martin, H., *A theoretical approach to predict the performance of chevron-type plate heat exchangers*. Chemical Engineering and Processing, 1996. **35**: p. 301 - 310.
16. Han, D.H., K.J. Lee, and Y.H. Kim, *The Characteristics of Condensation in Brazed Plate Heat Exchangers with Different Chevron Angles*. Journal of the Korean Physical Society, 2003. **43**(1): p. 66 -73.
17. Quoilin, S., et al., *Techno-economic survey of Organic Rankine Cycle (ORC) systems*. Renewable and Sustainable Energy Reviews, 2013. **22**(0): p. 168-186.
18. Li, M., et al., *Construction and preliminary test of a low-temperature regenerative Organic Rankine Cycle (ORC) using R123*. Renewable Energy, 2013. **57**(0): p. 216-222.
19. Zyhowski, G. and A. Brown, *Low Global Warming Fluids for Replacement of HFC-245fa and HFC-134a in ORC Applications*, in *First International Seminar on ORC Power Systems*. 2011: Delft, The Netherlands.

15 Appendix E: Important macros

```
Sub MaxNP()
```

```
Call Optimize("NP", True)
```

```
End Sub
```

```
Sub MaxEff()
```

```
Call Optimize("Eff", True)
```

```
End Sub
```

```
Sub Reset()
```

```
Application.ScreenUpdating = False
```

```
'Set start values
```

```
[MF] = 1.02 * [MFmin]
```

```
[HP] = 1.02 * [HPmin]
```

```
[CT] = 1.02 * [CTmin]
```

```
[OTSink] = [OTSinkmin] + 5
```

```
'Adjust condensation temperature
```

```
Do Until [DTCond] > 1.1 * [DTCondmin] And [DTCond] > 5 Or [CT] > 0.95 * [CTmax]
```

```
    [CT] = [CT] + 0.01 * ([CTmax] - [CTmin])
```

```
Loop
```

```
'Adjust superheat
```

```
If ActiveSheet.name = "ORC" Then
```

```
    [CA] = 1.02 * [CAmin]
```

```
    [SEin] = 1.02 * [SEinmin]
```

```
    Do Until [SEmin] > 1.02 * [SEminmin] Or [SEin] > 0.98 * [SEinmax] Or [DTHRHE] <  
1.5 * [DTHRHEmin]
```

```
        [SEin] = [SEin] + 0.01 * ([SEinmax] - [SEinmin])
```

```
    Loop
```

```
Else: End If
```

```
'Adjust pressure
```

```
Do
```

```
    [HP] = [HP] + 0.01 * ([HPmax] - [HPmin])
```

```
Loop Until [DTHRHE] < 1.02 * [DTHRHEmin] Or [DTHRHE] < 5 Or [HP] > 0.95 * [HPmax]  
Or [SEmin] < 1.02 * [SEminmin] Or [PR] > 0.95 * [PRmax]
```

```
    [HP] = [HP] - 0.01 * ([HPmax] - [HPmin])
```

```
'Adjust mass flow
```

```
Do
```

```
    [MF] = [MF] + 0.01 * ([MFmax] - [MFmin])
```

```
Loop Until [DTHRHE] < 1.02 * [DTHRHEmin] Or [DTHRHE] < 5 Or [MF] > 0.95 * [MFmax]
Or [TA] > [TAmix]
```

```
[MF] = [MF] - 0.01 * ([MFmax] - [MFmin])
```

```
Application.ScreenUpdating = True
```

```
End Sub
```

```
Sub Optimize(OptimizationTarget As String, ShowMessages As Boolean, Optional
TimeLimit As Integer)
```

```
Call Reset
```

```
Dim Result As Integer
```

```
Dim check As String
```

```
'Reset solver and add options
```

```
SolverReset
```

```
SolverOptions Precision:=0.001
```

```
SolverOptions Convergence:=Range("SolverConvergence").Value
```

```
SolverOptions MaxTime:=TimeLimit
```

```
SolverOptions RequireBounds:=True
```

```
SolverOptions Scaling:=True
```

```
SolverOptions MultiStart:=True
```

```
SolverOptions MaxSubproblems:=Range("SolverMaxSubproblems").Value
```

```
'Set optimization target and cells to be changed
```

```
If ActiveSheet.name = "ORC" Then
```

```
    If Range("IncludeRecuperator").Value = "yes" Then
```

```
        SolverOk SetCell:=[OptimizationTarget], MaxMinVal:=1, ByChange:="MF, HP,
CT, OTSink, SEin, CA", EngineDesc:="GRG Nonlinear"
```

```
        SolverAdd cellRef:=[CA], Relation:=1, FormulaText:="CAmax"
```

```
        SolverAdd cellRef:=[CA], Relation:=3, FormulaText:="CAmin"
```

```
        SolverAdd cellRef:=[DTRcup], Relation:=3, FormulaText:="DTRcupmin"
```

```
    Else
```

```
        SolverOk SetCell:=[OptimizationTarget], MaxMinVal:=1, ByChange:="MF, HP,
CT, OTSink, SEin", EngineDesc:="GRG Nonlinear"
```

```
    End If
```

```
        SolverAdd cellRef:=[SEin], Relation:=1, FormulaText:="SEinmax"
```

```
        SolverAdd cellRef:=[SEin], Relation:=3, FormulaText:="SEinmin"
```

```
        SolverAdd cellRef:=[SEmin], Relation:=3, FormulaText:="SEminmin"
```

```
Else
```

```
    SolverOk SetCell:=[OptimizationTarget], MaxMinVal:=1, ByChange:="MF, HP, CT,
OTSink", EngineDesc:="GRG Nonlinear"
```

```
End If
```

```
'Add constraints
```

Appendix E

```

SolverAdd cellRef:=[MF], Relation:=1, FormulaText:="MFmax"
SolverAdd cellRef:=[MF], Relation:=3, FormulaText:="MFmin"
SolverAdd cellRef:=[HP], Relation:=1, FormulaText:="HPmax"
SolverAdd cellRef:=[HP], Relation:=3, FormulaText:="HPmin"
SolverAdd cellRef:=[CT], Relation:=1, FormulaText:="CTmax"
SolverAdd cellRef:=[CT], Relation:=3, FormulaText:="CTmin"
SolverAdd cellRef:=[OTSink], Relation:=1, FormulaText:="OTSinkmax"
SolverAdd cellRef:=[OTSink], Relation:=3, FormulaText:="OTSinkmin"
If [OTSourcemax] > 0 Then SolverAdd cellRef:=[OTSource], Relation:=1,
FormulaText:="OTSourcemax"
If [OTSourcemin] > 0 Then SolverAdd cellRef:=[OTSource], Relation:=3,
FormulaText:="OTSourcemin"
If [TAmx] > 0 Then SolverAdd cellRef:=[TA], Relation:=1, FormulaText:="TAmx"
If [TAmin] > 0 Then SolverAdd cellRef:=[TA], Relation:=3, FormulaText:="TAmin"
SolverAdd cellRef:=[DTHRHE], Relation:=3, FormulaText:="DTHRHEmin"
SolverAdd cellRef:=[DTCond], Relation:=3, FormulaText:="DTCondmin"
SolverAdd cellRef:=[PR], Relation:=1, FormulaText:="PRmax"
SolverAdd cellRef:=[PR], Relation:=3, FormulaText:="PRmin"
'Solve and handle result
Result = SolverSolve(True, "SolverStop")
[SolverResult] = Result
If Result > 2 And Result <> 6 And Result <> 17 And ShowMessages = True Then
    If MsgBox("Solver error: " & Result & " - Reset variables?", vbYesNo +
vbQuestion, "Solver error") = vbYes Then Call Reset
ElseIf Result = 6 And ShowMessages = True Then
    If MsgBox("Solver reached maximum number of starting points for global
optimization - do you want to change the number?", vbYesNo + vbQuestion, "Limit
reached") = vbYes Then Range("SolverMaxSubproblems").Select
Else
    check = OptimizationTarget & "check"
    Range(check).Value = Range(OptimizationTarget).Value
End If
End Sub

Function SolverStop(Reason As Integer)
    SolverStop = 1
End Function

Sub SaveResults()
Application.ScreenUpdating = False

```

```

Dim cycle As String
Dim source, destination As Worksheet
Dim emptyColumn, Row, i, j As Integer
cycle = ActiveSheet.name
Set source = Sheets(cycle)
Set destination = Sheets("Results_" & cycle)
emptyColumn = 3
Row = 1
'Prepare column
destination.Activate
Columns(emptyColumn).Select
Selection.Copy
Selection.Insert Shift:=xlToRight
'General data
destination.Cells(Row, emptyColumn).Value = Now
Row = Row + 1
destination.Cells(Row, emptyColumn).Value = Now
Row = Row + 1
destination.Cells(Row, emptyColumn).Value = source.Range("SolverConvergence").Value
Row = Row + 1
destination.Cells(Row, emptyColumn).Value =
source.Range("SolverMaxSubproblems").Value
Row = Row + 1
destination.Cells(Row, emptyColumn).Value = source.Range("SolverResult").Value
Row = Row + 4
'Performance
destination.Cells(Row, emptyColumn).Value = source.Range("NP").Value
Row = Row + 1
destination.Cells(Row, emptyColumn).Value = source.Range("Eff").Value
Row = Row + 4
'Constants
source.Range("Constants").Copy
destination.Cells(Row, emptyColumn).PasteSpecial Paste:=xlPasteValues
Row = Row + source.Range("Constants").Rows.Count + 2
'Optimization variables
For i = 1 To source.Range("OptimizationVariables").Rows.Count
    For j = 1 To source.Range("OptimizationVariables").Columns.Count
        source.Range("OptimizationVariables")(i, j).Copy
        destination.Cells(Row, emptyColumn).PasteSpecial Paste:=xlPasteValues
    
```



```

        Row = Row + 1
    Next j
Next i
Row = Row + 2
'Constraints
For i = 1 To source.Range("Constraints").Rows.Count
    For j = 1 To source.Range("Constraints").Columns.Count
        If Not IsEmpty(source.Range("Constraints")(i, j)) Then
            source.Range("Constraints")(i, j).Copy
            destination.Cells(Row, emptyColumn).PasteSpecial Paste:=xlPasteValues
            Row = Row + 1
        Else: End If
    Next j
Next i
Row = Row + 2
'Cycle
For i = 1 To source.Range("Cycle").Columns.Count
    For j = 1 To source.Range("Cycle").Rows.Count
        If Not IsEmpty(source.Range("Cycle")(j, i)) Then
            source.Range("Cycle")(j, i).Copy
            destination.Cells(Row, emptyColumn).PasteSpecial Paste:=xlPasteValues
            Row = Row + 1
        Else: End If
    Next j
    Row = Row + 1
Next i
'Heat source
For i = 1 To source.Range("HeatSource").Columns.Count
    For j = 1 To source.Range("HeatSource").Rows.Count
        If Not IsEmpty(source.Range("HeatSource")(j, i)) Then
            source.Range("HeatSource")(j, i).Copy
            destination.Cells(Row, emptyColumn).PasteSpecial Paste:=xlPasteValues
            Row = Row + 1
        Else: End If
    Next j
    Row = Row + 1
Next i
'Heat sink

```

```

For i = 1 To source.Range("HeatSink").Columns.Count
    For j = 1 To source.Range("HeatSink").Rows.Count
        If Not IsEmpty(source.Range("HeatSink")(j, i)) Then
            source.Range("HeatSink")(j, i).Copy
            destination.Cells(Row, emptyColumn).PasteSpecial Paste:=xlPasteValues
            Row = Row + 1
        Else: End If
    Next j
    Row = Row + 1
Next i
source.Activate
Application.CutCopyMode = False
Application.ScreenUpdating = True
End Sub

```

```

Sub SetHTCdPandWFan()
[hel] = [hel] - 1
'htc
'heating
Cells(36, 3) = Cells(77, [hel].Value)
'Desup
Cells(37, 3) = Cells(81, [hel].Value)
'Cond
Cells(38, 3) = Cells(82, [hel].Value)
'dp
'HRHE
Cells(21, 3) = Cells(78, [hel].Value) / 1000
'Desup
Cells(22, 3) = Cells(83, [hel].Value) / 1000
'Cond
Cells(23, 3) = Cells(84, [hel].Value) / 1000
'Heat sink
Cells(24, 3) = Cells(85, [hel].Value) / 1000
'Heat source
Cells(25, 3) = Cells(79, [hel].Value) / 1000
'Fan work
Cells(47, 15) = Cells(87, [hel].Value) / 1000
End Sub

```

```

Sub AreaStudy()
Dim i As Integer
Dim ID As String
Dim ReachedMaxArea As Boolean
[TAmin] = 1
ReachedMaxArea = False
For i = 0 To [TAsteps] - 1
'Set maximum area constraint
    [TAmix] = [TAsstart] + i * ([TAend] - [TAsstart]) / ([TAsteps] - 1)
    Call SetHTCdpendWFan
'Check if case has been calculated before
    ID = [HeatSourceInletTemp] & "-" & [WorkingFluid] & "-" & [TAmix]
    If Not IsNumeric(Application.Match(ID, Sheets("Results_" &
ActiveSheet.name).Range("6:6"), 0)) Then
        If Not Sheets("Results_" & ActiveSheet.name).Range("C15").Value =
[WorkingFluid] Then Call Reset
            If ReachedMaxArea = False Then Call Optimize("NP", False)
            Call SaveResults
            Application.ActiveWorkbook.Save
            If [TA] < 0.98 * [TAmix] Then ReachedMaxArea = True
        Else: End If
    Next i
End Sub

```

```

Sub FluidStudy()
Dim i As Integer
For i = 1 To Range("Fluids").Rows.Count
    [WorkingFluid] = Range("Fluids")(i, 1)
    Call AreaStudy
Next i
End Sub

```

```

Sub HeatSourceCycleStudy()
Application.ScreenUpdating = False
Dim i As Integer
[hel] = "171"
'TFC
Sheets("TFC").Activate

```

```

For i = 100 To 200 Step 50
    [HeatSourceInletTemp] = i
    Call FluidStudy
Next i
'ORC
Sheets("ORC").Activate
For i = 100 To 200 Step 50
    [HeatSourceInletTemp] = i
    Call FluidStudy
Next i
Application.ScreenUpdating = True
End Sub

Sub Fluidloop()
Dim i As Integer
For i = 1 To Range("Fluids").Rows.Count
    [WorkingFluid] = Range("Fluids")(i, 1)
    Call Optimize("NP", False)
    Call SaveResults
    Application.ActiveWorkbook.Save
Next i
End Sub

```